On the Predictive Accuracy of Neural Temporal Point Process Models for Continuous-time Event Data

Anonymous authors
Paper under double-blind review

Abstract

The framework of Temporal Point Processes (TPPs) is the default paradigm used to model sequences of events occurring asynchronously in continuous time. Classical TPP models often rely on strong modeling assumptions which intrinsically limits their capacity in modeling complex real-world event dynamics. To address this limitation, neural network parametrizations of TPPs, referred to as Neural TPPs, have been proposed to allow more flexible and efficient modeling. Although recent research supports the effectiveness of neural TPPs, their analysis is often based on different baselines, datasets, and experimental setups. As a result, it is hard to pinpoint the source of empirical gains, which is a major limitation of research progress. To bridge this gap, we conduct a large-scale experimental study to assess the predictive accuracy of state-of-the-art neural TPP models on multiple real-world and synthetic event sequence datasets in a carefully designed unified setup. We study the influence of each major architectural component (event encoding, history encoder, decoder parametrization) for both time and mark prediction tasks. We also address the rarely discussed topic of probabilistic calibration for neural TPP models. Finally, we also draw meaningful conclusions from the analysis of our results, including the importance of the history size and the impact of the architectural components on predictive accuracy, as well as the poorly calibrated mark distributions of neural TPP models.

1 Introduction

From human social activity to natural phenomena, the evolution of a system of interest can often be characterized by a sequence of discrete events occurring at irregular time intervals. Online shopping activity (Cai et al., 2018), earthquake occurrences (Ogata, 1998), measurement of electronic health records (Wang et al., 2016), and users activity on social media (Farajtabar et al., 2015), are a few typical applications where such sequences can be frequently encountered. Given these streams of events, an important challenge is to predict *when* the next event is likely to happen. In scenarios where events are assigned a label, referred to as *marks*, we also need to predict *what* type of event is likely to happen. Intuitively, one may assume that events are dependent on one another and that a system's future evolution is directly driven by the occurrence of past events. For instance, an individual may be tempted to purchase a specific item at a particular time on an e-commerce platform, exclusively because a specific item purchased the week before made it necessary.

Consequently, understanding and modeling the complex dynamics of event occurrences is essential to predict future event occurrences from past observations.

Relying on strong theoretical foundations, the framework of Temporal Point Processes (TPPs) (Daley & Vere-Jones, 2007) has established itself as a natural choice for modeling these sequences of asynchronous and time-dependent data. A TPP can be fully characterized by the so-called conditional intensity function, which defines the instantaneous unit rate of events arrival, conditional on the history of the process (Rasmussen, 2018). A significant amount of previous works considered classical parametric forms of TPPs, such as the Hawkes process (Hawkes, 1971), for event sequence modeling in various fields, such as finance (Hawkes, 2018), crime (Egesdal et al., 2010) or epidemiology (Rizoiu et al., 2018). However, these classical parametrizations have been criticized for their lack of flexibility in modeling complex event dynamics (Mei & Eisner, 2016). Deep learning methods have been introduced in the TPP literature to provide more flexible models and capture more complex temporal dependencies. Examples include RNNs (Mei & Eisner, 2016; Shchur et al., 2019) and self-attention mechanisms (Zhang et al., 2020; Zuo et al., 2020; Enguehard et al., 2020). Since its introduction by Du et al. (2016), the topic of neural TPPs underwent rapid development with numerous new architectures and applications (Shchur et al., 2021).

Given a sequence of events, neural TPP models can be viewed as a combination of three main architectural components: 1) an event encoder, creating a fixed-sized embedding for each event in the sequence. 2) a history encoder, generating a summary of the history from past events' embeddings, and 3) a decoder parametrizing a function that fully characterizes the distribution of future events' arrival times and marks. Among other possibilities, improvements with respect to existing baselines are obtained by proposing alternatives to either of these components. For instance, one can replace an RNN-based history encoder with a self-attentive one, or choose to parametrize a certain TPP function that leads to useful properties, such as reduced computational costs or closed-form sampling. However, as pointed out by Shchur et al. (2021), "*new architectures often change all these components at once, which makes it hard to pinpoint the source of empirical gains*". Moreover, the baselines against which a newly proposed architecture is compared, as well as the datasets employed and the experimental setups, often differ from paper to paper, which renders a fair comparison even harder.

Additionally, modeling marked TPPs from data is a challenging problem from a statistical perspective in the sense that it requires joint modeling of discrete distributions over marks and continuous distributions over time. In practice, a model's ability to estimate the joint distribution of future arrival times and marks is often solely evaluated on its performance with respect to the negative log-likelihood (NLL). However, reporting a single NLL value encompasses the contributions of both arrival time and mark distributions, making it hard to evaluate model performance with respect to each prediction task separately. Moreover, even though the NLL allows the comparison of several baselines against each other, it actually gives very little insight into the shape of the modeled distributions and how the probability mass is spread across their respective domains. In real-world decision-making applications, a model should not only provide accurate predictions but also quantify how likely these predictions are going to happen. In other terms, neural TPP models should ideally provide a calibrated confidence measure associated with their predictions (Guo et al., 2017). However, assessing the calibration of the fitted models has been overlooked by the neural TPP community, both for the time and mark predictive distributions.

In summary, we aim to address the above concerns by proposing the following contributions:

- We perform a large-scale experimental study to assess the predictive accuracy of state-of-the-art neural TPP models on 15 real-world event sequence datasets in a carefully designed unified setup. Our study also includes classical parametric TPP models as well as synthetic datasets. In particular, we study the influence of each major architectural component (event encoding, history encoder, decoder parametrization) for both time and mark prediction tasks. To the best of our knowledge, this is the largest comprehensive study for neural TPPs to date. Our study is fully reproducible and implemented in a common code base that will be made publicly available after the reviewing process.

- We assess the calibration of neural TPP models by evaluating both the time and mark predictive distributions. To this end, we employ standard metrics and tools borrowed from the forecasting literature, namely the probabilistic calibration error and reliability diagrams. Assessing the calibration of probabilistic models is essential to evaluate their predictive ability. Yet, to the best of our knowledge, this has been generally overlooked by the neural TPP community.

- Among others, we found that neural TPP models often do not fully leverage the complete information contained in all historical events and that relying solely on a few of the last observed occurrences usually yields comparable performance to encoding a full history. We also show that several decoder parametrizations are highly sensitive to the event encoder, for which an appropriate choice can lead to large gains in predictive accuracy. Moreover, while the distribution of arrival times is often well-calibrated, we found that the mark distribution of classical parametric baselines is better calibrated compared to neural TPP models. Finally, we show that several event sequence datasets frequently employed in the TPP literature may not be appropriate to benchmark neural TPP baselines.

2 Background and Notations

Marked Temporal Point Processes are stochastic processes whose realizations consist in a sequence of n discrete events $\mathcal{S} = \{(t_1, k_1), ..., (t_n, k_n)\}$ observed within a fixed window $[0, T]$. For each event $e_i = (t_i, k_i)$, t_i corresponds to the **arrival time** of the i^{th} event, with $0 \leq t_1 < ... < t_n \leq T$, and $k_i \in \mathcal{K} = \{1, ..., K\}$ is the associated **mark**, or class to which the event belongs. Note that in this definition, the number of events n is itself a random variable. In an unmarked setting, events are only defined by their arrival times, i.e. $S = \{t_1, ..., t_n\}$. Without loss of generality, we will focus on the marked setting for the remainder of the section. Additionally, while we focus exclusively on discrete marks, it is worth noting that other alternatives exist, such as continuous marks, i.e. $k_i \in \mathbb{R}$ (Chen et al., 2021). An alternate way to represent the realization of a marked TPP is by the counting process $N(t) = \sum_{k=1}^{K} N_k(t)$, where $N_k(t) = |\{(t_i, k_i) \in \mathcal{S} | t_i < t\}|$ is the number of events of mark k that occurred before t.

Let $e_{i-1} = (t_{i-1}, k_{i-1})$ be the last observed event. The occurrence of a future event in $[t_{i-1}, \infty[$ can be characterized by the conditional joint distribution of arrival-times and marks $f(t, k|\mathcal{H}_t)$, where $\mathcal{H}_t = \{(t_i, k_i) \in \mathcal{S} \mid t_i < t\}$ denotes the observed process' history. The conditional joint distribution can be decomposed as $f(t, k|\mathcal{H}_t) = f(t|\mathcal{H}_t)p(k|t, \mathcal{H}_t)$, where $f(t|\mathcal{H}_t)$ corresponds to the conditional density of time t, while $p(k|t, \mathcal{H}_t)$ is the probability of observing mark k, conditional on both t and $\mathcal{H}_t$. Given the conditional cumulative distribution of arrival-times $F(t|\mathcal{H}_t)$, a marked TPP can be equivalently characterized by the *mark-wise conditional intensity function* (MCIF) $\lambda_k(t|\mathcal{H}_t)$, i.e:

$$\lambda_k(t|\mathcal{H}_t) = \frac{f(t,k|\mathcal{H}_t)}{1 - F(t|\mathcal{H}_t)}. \tag{1}$$

Furthermore, for $t > t_{i-1}$, we have (Rasmussen, 2018):

$$\begin{aligned}\lambda_k(t|\mathcal{H}_t) = \frac{f(t,k|\mathcal{H}_t)}{1 - F(t|\mathcal{H}_t)} &= \lambda(t|\mathcal{H}_t)p(k|t,\mathcal{H}_t) &(2)\\ &= \frac{\mathbb{E}\left[N_k[t,t+dt]|\mathcal{H}_t, t_i \notin [t_{i-1},t]\right]}{dt} &(3)\\ &\simeq \frac{\mathbb{P}\big[t_i \in [t,t+dt], k_i = k|\mathcal{H}_t, t_i \notin [t_{i-1},t]\big]}{dt}, &(4)\end{aligned}$$

where $\lambda(t|\mathcal{H}_t) = \sum_{k=1}^{K} \lambda_k(t|\mathcal{H}_t)$ is the ground conditional intensity function of the process (GCIF). In essence, the MCIF gives the expected instantaneous occurrence rate of an event of mark $k \in \mathcal{K}$ and can be heuristically interpreted as the probability of observing the next event of mark k in an infinitesimal interval around t, conditional on the past of the process up to but not including t. We will employ the notation '$*$' of Daley & Vere-Jones (2007) to indicate dependence on $\mathcal{H}_t$, i.e. $\lambda_k^*(t) = \lambda_k(t|\mathcal{H}_t)$. Also, for the remaining of the paper, all expressions will be defined for $t_{i-1} < t \leq t_i$, unless stated otherwise.

From the MCIF, we can compute the *cumulative MCIF*,

$$\Lambda_k^*(t) = \int_{t_{i-1}}^{t} \lambda_k^*(s)ds, \tag{5}$$

and the *conditional joint density* of time t and mark k,

$$f^*(t,k) = \lambda_k^*(t)\exp\big(-\sum_{k=1}^{K}\Lambda_k^*(t)\big). \tag{6}$$

The proof of (6) can be found in Appendix E. Lastly, note that a realization of a marked TPP can be equivalently represented by the sequence $\{(\tau_1,k_1),...,(\tau_n,k_n)\}$ where $\tau_i = t_i - t_{i-1}$ are the *inter-arrival times*. We will use both notations interchangeably throughout the paper.

Parametrization of TPP models and Learning. Defining a marked TPP model usually involves specifying a parametric form for any of the functions in (2), (5) or (6), provided that the chosen parametrization defines a valid joint distribution. In this regard, a distinct set of requirements need to be fulfilled depending on the chosen function. We consider exclusively the setting of *non-terminating* TPP, meaning that a future event will arrive eventually with probability one. For a non-terminating TPP, if one decides to parametrize the MCIF, then the following conditions must be satisfied (Rasmussen, 2018):

R_1^λ: $\lambda_k^*(t) \geq 0$.

R_2^λ: $\lim_{t\to\infty} \int_{t_{i-1}}^{t} \lambda_k^*(s)ds = \infty$.

Alternatively, parametrizing the conditional joint density implies:

R^f_1: $f(t,k) > 0$.

R^f_2: $\int_{t_{i-1}}^{\infty} \sum_{k=1}^{K} f(t,k)dt = 1$.

Specifying a parametrization of the cumulative MCIF involves four constraints (Enguehard et al., 2020):

R^Λ_1: $\Lambda^*_k(t) > 0$.

R^Λ_3: $\lim\limits_{t\to\infty} \Lambda^*_k(t) = \infty$.

R^Λ_2: $\Lambda^*_k(t_{i-1}) = \int_{t_{i-1}}^{t_{i-1}} \lambda^*_k(s)ds = 0$.

R^Λ_4: $d\Lambda^*_k(t)/dt \geq 0$,

where conditions R^Λ_1 and R^Λ_4 result from $\lambda^*_k(t) \geq 0$, while R^Λ_3 directly follows R^λ_2. In the setting of *terminating* TPP, where there is a probability π that the process stops after the last observed event, R^f_2, R^λ_2 and R^Λ_3 are no longer satisfied.

A common example of parametrization is the homogeneous Poisson process (Daley & Vere-Jones, 2007; De et al., 2019) that defines a constant MCIF:

$$\lambda^*_k(t) = \mu_k \geq 0, \tag{7}$$

and hence implicitly assumes an exponential distribution with rate $\mu = \sum_{k=1}^{K} \mu_k$ for the inter-arrival times τ:

$$f^*(\tau) = \mu \exp(-\mu\tau). \tag{8}$$

Another example is the well-known Hawkes process (Hawkes, 1971; Liniger, 2009), which defines the MCIF to account for the influence of previous events on the process' dynamics:

$$\lambda^*_k(t) = \mu_k + \sum_{k'=1}^{K} \sum_{\{(t_i,k'):t_i<t\}} \phi_{k,k'}(t - t_i), \tag{9}$$

where $\phi_{k,k'}$ is the so-called triggering kernel. For instance, choosing the exponential kernel $\phi_{k,k'}(t-t_i) = \alpha_{k,k'} \exp\big(-\beta_{k,k'}(t-t_i)\big)\mathbb{1}[t - t_i \geq 0]$ with $\alpha_{k,k'} > 0$ and $\beta_{k,k'} > 0$ allows to explicitly model self-excitation dynamics, for which the occurrence of an event increases the probability of observing future events, in a positive, additive and exponentially decaying fashion.

Let $\boldsymbol{\theta}$ be the set of learnable parameters for a valid parametrization of a marked TPP function. As an example, for the Hawkes process in (9), we have $\boldsymbol{\theta} = \{\boldsymbol{\mu}, \boldsymbol{\alpha}, \boldsymbol{\beta}\}$, where $\boldsymbol{\mu} \in \mathbb{R}^K$ and $\boldsymbol{\alpha}, \boldsymbol{\beta} \in \mathbb{R}^{K\times K}$. The most common approach to learning $\boldsymbol{\theta}$ is achieved by maximum likelihood estimation, i.e. by minimizing the negative log-likelihood (NLL). Given a parametric form of $\lambda^*_k(t;\boldsymbol{\theta})$, $f^*(t,k;\boldsymbol{\theta})$ or $\Lambda^*_k(t;\boldsymbol{\theta})$, and a sequence $\mathcal{S}$ of n events observed on $[0,T]$, the NLL objective writes:

$$\begin{aligned}\mathcal{L}(\boldsymbol{\theta};\mathcal{S}) &= -\sum_{i=1}^{n} \left[\log \lambda^*_k(t_i;\boldsymbol{\theta}) - \Lambda^*(t_i;\boldsymbol{\theta})\right] + \Lambda^*(T;\boldsymbol{\theta}) &(10)\\ &= -\sum_{i=1}^{n} \left[\log f^*(t_i;\boldsymbol{\theta}) + \log p^*(k_i|t_i;\boldsymbol{\theta})\right] + \Lambda^*(T;\boldsymbol{\theta}), &(11)\end{aligned}$$

where the term $\Lambda^*(T;\boldsymbol{\theta}) = \sum_{k=1}^{K} \Lambda^*_k(T;\boldsymbol{\theta})$ accounts for the fact that no event has been observed in the interval $]t_n, T]$.

Prediction tasks on Marked TPPs. The expression (11) shows that learning a marked TPP model from a sequence of events involves two estimation problems: (1) the conditional density of (inter-)arrival times $f^*(t)$, and (2) the conditional distribution of marks $p^*(k|t)$.

Once estimated, we can answer queries of the following type: *When is the next event likely to occur? What will be the type of the next event, given that it occurs at a certain time t ? How long until an event of type k occurs?* Throughout the paper, we will focus exclusively on tasks (1) and (2), which will be referred to as the *time prediction* and *mark prediction* tasks, respectively.

Given the conditional density of (inter-)arrival times, the next expected arrival time can be computed as follows:

$$\tilde{t} = \mathbb{E}[t] = \int_{t_{i-1}}^{\infty} t f^*(t;\boldsymbol{\theta}) dt. \tag{12}$$

Given the conditional distribution of marks, the mark of the event at time t can be computed as follows:

$$\tilde{k} = \underset{k}{\operatorname{argmax}}\ p^*(k|t;\boldsymbol{\theta}) = \underset{k}{\operatorname{argmax}}\ \frac{\lambda_k^*(t;\boldsymbol{\theta})}{\lambda^*(t;\boldsymbol{\theta})} = \underset{k}{\operatorname{argmax}}\ \lambda_k^*(t;\boldsymbol{\theta}). \tag{13}$$

For clarity of notations, we will drop the explicit dependency of the parametrizations on $\boldsymbol{\theta}$ in the remainder of the paper.

3 Neural Temporal Point Processes

While simple parametric forms of marked TPPs, such as the Hawkes process, have been used to model event sequences in a variety of real-world scenarios, they have been criticized for their lack of flexibility. For instance, events may inhibit the occurrences of future events rather than excite them, or their influence might not be strictly additive. While previous works proposed modifications of the Hawkes process to encompass such complementary effects, e.g. excitation and inhibition (Mei & Eisner, 2016; Costa et al., 2020; Duval et al., 2022), others relied on the expressiveness of neural networks to capture more complex event dynamics. The resulting framework, called *Neural* TPPs, defines models that can be characterized by three major components (Shchur et al., 2021). Recall that $\mathcal{S} = \{e_1, ..., e_n\}$, where $e_i = (t_i, k_i)$. A neural TPP model involves:

1. An **event encoder** which, for each $e_i \in \mathcal{S}$, generates a fixed size embedding[1] $\boldsymbol{e}_i \in \mathbb{R}^{d_e}$;
2. A **history encoder**, which for each $e_i \in \mathcal{S}$, generates a fixed size history embedding $\boldsymbol{h}_i \in \mathbb{R}^{d_h}$ from past event representations $\{\boldsymbol{e}_1, ..., \boldsymbol{e}_{i-1}\}$;
3. A **decoder**, which given a query time t and its associated embedding $\boldsymbol{e}^t$ for $t_{i-1} \leq t < t_i$, parametrizes a function characterizing the TPP (i.e. $\lambda_k^*(t)$, $\Lambda_k^*(t)$, or $f^*(t,k)$) using $\boldsymbol{e}^t$, and/or $\boldsymbol{h}_i$.

The general modeling pipeline is shown in Figure 1. In the following, we will give more details about each of its major components.

---

[1] Note that e_i is used to designate an event, while the bold notation $\boldsymbol{e}_i$ is used for the event representation.

3.1 Event encoding

The task of event encoding consists in generating a representation $\boldsymbol{e}_i \in \mathbb{R}^{d_e}$ for each event in $\mathcal{S}$, to be fed to the history encoder, and eventually to the decoder, at a later stage. This task essentially boils down to finding an embedding $\boldsymbol{e}_i^t \in \mathbb{R}^{d_t}$ for the (inter-)arrival time t_i, and an embedding $\boldsymbol{e}_i^k \in \mathbb{R}^{d_k}$ for the associated mark k_i. The event embedding $\boldsymbol{e}_i$ is finally obtained through some combination of $\boldsymbol{e}_i^t$ and $\boldsymbol{e}_i^k$, e.g. via concatenation:

$$\boldsymbol{e}_i = \begin{bmatrix} \boldsymbol{e}_i^t \\ \boldsymbol{e}_i^k \end{bmatrix} \tag{14}$$

Encoding the arrival times. A straightforward approach to obtain $\boldsymbol{e}_i^t$ is to select the raw inter-arrival times as time embeddings $\boldsymbol{e}_i^t = \tau_i$ or the inter-arrival times logarithms $\boldsymbol{e}_i^t = \log \tau_i$ (Omi et al., 2019; Shchur et al., 2019; Mei & Eisner, 2016; Du et al., 2016). Inspired by the positional encoding of Transformer architectures (Vaswani et al., 2017) and their extension to temporal data (Kazemi et al., 2019), other works exploit more expressive representations by encoding the arrival-times as vectors of sinusoïdals (Enguehard et al., 2020):

$$\boldsymbol{e}_i^t = \bigoplus_{j=0}^{d_t/2-1} \sin\left(\alpha_j t_i\right) \oplus \cos\left(\alpha_j t_i\right), \tag{15}$$

where $\alpha_j \propto 1000^{\frac{-2j}{d_t}}$ and $\oplus$ is the concatenation operator. Variants of sinusoïdal encoding can also be found in Zhang et al. (2020) and Zuo et al. (2020). Alternatively, learnable embeddings can be obtained by feeding the inter-arrival times to a fully connected layer (FC) (Enguehard et al., 2020):

$$\boldsymbol{e}_i^t = \mathrm{FC}\left(\tau_i\right), \tag{16}$$

where $\mathrm{FC} : \mathbb{R} \to \mathbb{R}^{d_t}$.

Encoding the mark: When marks are available, the most common approach to obtain the mark embeddings is by specifying a learnable embedding matrix $\mathbf{E}^k \in \mathbb{R}^{d_k \times K}$ (Du et al., 2016; Mei & Eisner, 2016; Shchur et al., 2019; Zhang et al., 2020; Zuo et al., 2020; Enguehard et al., 2020). Given the one-hot encoding $\boldsymbol{k}_i \in \{0,1\}^K$ of mark k_i, its embedding $\boldsymbol{e}_i^k \in \mathbb{R}^{d_k}$ is retrieved as:

$$\boldsymbol{e}_i^k = \mathbf{E}^k \boldsymbol{k}_i. \tag{17}$$

3.2 History encoding

The general principle behind history encoding in the context of neural TPP approaches is to construct a fixed-size embedding $\boldsymbol{h}_i \in \mathbb{R}^{d_h}$ for event e_i from its sequence of past events representations $\{\boldsymbol{e}_1, ..., \boldsymbol{e}_{i-1}\}$, using some form of auto-regressive mechanism. Naturally, the main goal when constructing $\boldsymbol{h}_i$ is to capture as closely as possible relevant patterns in the process history, in order to accurately estimate the distributions of arrival times and marks of future events.

Recurrent architectures. A natural choice to handle ordered sequences of tokens is achieved by employing a form of recurrent architecture, such as an LSTM or a GRU (Shchur et al., 2019; Du et al., 2016; Mei & Eisner, 2016). In this context, starting from an initial state $\boldsymbol{h}_1$ initialized

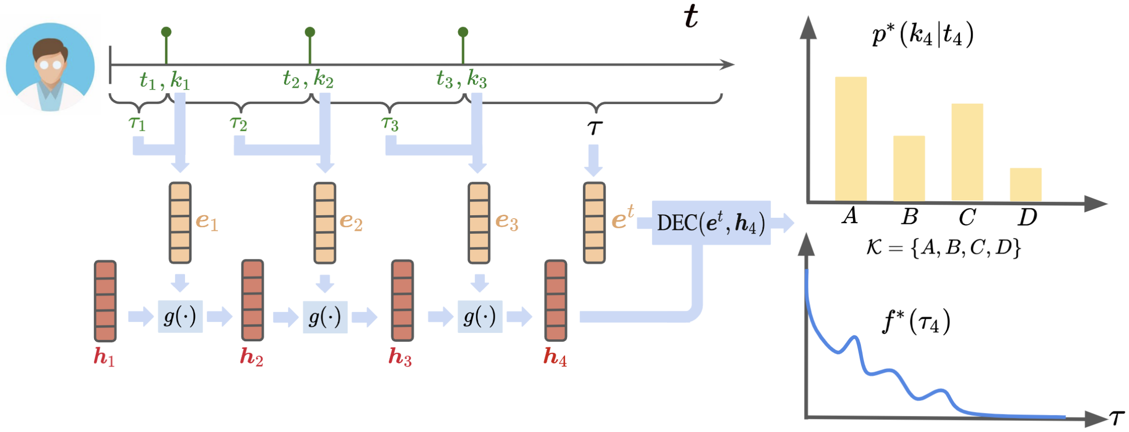

Figure 1: General workflow of neural parametrizations for marked TPPs. Events inter-arrival times τ_i and marks k_i are encoded into a vector $\boldsymbol{e}_i$, which is in turn used to generate the history embeddings $\boldsymbol{h}_i$ through some form of auto-regressive mechanisms $g(\cdot)$ (e.g. GRU). A query time embedding $\boldsymbol{e}^t$ and the history embeddings are then fed to the decoder to estimate the conditional density $f^*(\tau_{i+1})$ and conditional distribution $p^*(k_{i+1}|t_{i+1})$ of the next event.

randomly, the history embedding $\boldsymbol{h}_i$ of an event e_i is constructed by sequentially updating the history embeddings at the previous time steps by using the next event's representation:

$$\begin{aligned}\boldsymbol{h}_2 &= g\big(\boldsymbol{h}_1, \boldsymbol{e}_1\big),\\ &\dots\\ \boldsymbol{h}_i &= g\big(\boldsymbol{h}_{i-1}, \boldsymbol{e}_{i-1}\big),\end{aligned} \tag{18}$$

where $p_{\boldsymbol{h}}$ is a distribution from which the initial state $\boldsymbol{h}_1$ is drawn, and $g : \mathbb{R}^{d_h} \to \mathbb{R}^{d_h}$ refers to the update function of the chosen recurrent layer.

Self-attention encoders. As an alternative to recurrent architectures, the self-attention mechanism of Transformers (Vaswani et al., 2017) computes the $\boldsymbol{h}_i$'s for each i independently as follows (Zhang et al., 2020; Zuo et al., 2020; Enguehard et al., 2020):

$$\boldsymbol{h}_i = \mathrm{SA}(\boldsymbol{q}_i, \mathbf{K}_i, \mathbf{V}_i) = \mathbf{W}_2\sigma_R\big(\mathbf{W}_1\hat{\boldsymbol{h}}_i^\top + \boldsymbol{b}_1\big) + \boldsymbol{b}_2, \tag{19}$$

$$\hat{\boldsymbol{h}}_i = \mathrm{Softmax}\Big(\frac{\boldsymbol{q}_i^\top \mathbf{K}_i}{\sqrt{d_q}}\Big)\mathbf{V}_i^\top, \tag{20}$$

where $\mathrm{SA}(\cdot)$ refers to the self-attention mechanism between a *query* vector $\boldsymbol{q}_i$, a *key* matrix $\mathbf{K}_i$ and a *value* matrix $\mathbf{V}_i$ defined as

$$\boldsymbol{q}_i = \mathbf{W}_Q\boldsymbol{e}_{i-1}, \quad \mathbf{K}_i = \mathbf{W}_K[\boldsymbol{e}_1, ..., \boldsymbol{e}_{i-1}], \quad \mathbf{V}_i = \mathbf{W}_V[\boldsymbol{e}_1, ..., \boldsymbol{e}_{i-1}], \tag{21}$$

where $\mathbf{W}_Q, \mathbf{W}_K \in \mathbb{R}^{d_q \times d_e}$, $\mathbf{W}_V \in \mathbb{R}^{d_h \times d_e}$, $\mathbf{W}_2$, $\mathbf{W}_1 \in \mathbb{R}^{d_h \times d_h}$, $\boldsymbol{b}_1$, $\boldsymbol{b}_2 \in \mathbb{R}^{d_h}$, and σ_R is the ReLU activation function. In essence, the history embedding $\boldsymbol{h}_i$ is therefore constructed as a weighted sum of the past events representations, where the attention weights are obtained by measuring a similarity score (e.g. dot product) between the projection of $\boldsymbol{e}_{i-1}$, and the projections of $\{\boldsymbol{e}_1, ..., \boldsymbol{e}_{i-1}\}$.

As pointed out by Zuo et al. (2020), recurrent architectures may fail to capture long-term dependencies and are difficult to train due to vanishing and exploding gradients. Moreover, due to their inherently sequential nature, recurrent models forbid parallel processing and are usually trained using truncated backpropagation through time, which only returns an approximation of the true gradients. Conversely, architectures based on a self-attention mechanism can compute the history embeddings $\boldsymbol{h}_i$ for each i in parallel, leading to improved computational efficiency. However, since each $\boldsymbol{h}_i$ depends on all events preceding e_i, computing such embeddings for all L events of a sequence scales in $O(L^2)$ time for architectures based on a self-attention mechanism, while it scales in $O(L)$ time for their recurrent counterparts (Shchur et al., 2021).

3.3 Decoders

As mentioned in Section 2, fully characterizing a marked TPP can be achieved by parametrizing either of the functions $\lambda_k^*(t)$, $\Lambda_k^*(t)$ or $f^*(k,t)$, as any can be uniquely retrieved from the others. While being mathematically equivalent, a specific choice among these functions leads to particular advantages, challenges, and constraints, which will be discussed below. Nonetheless, given the encoding $\boldsymbol{e}$ of a query event $e = (t, k)$ with $t > t_i$ and its history embedding $\boldsymbol{h}_i$, the parametrization is almost systematically carried out by a neural network. We will consider the following state-of-the-art decoders in our study:

- The Exponential Constant decoder (**EC**) (Upadhyay et al., 2018) parametrizes a constant MCIF between two events using a feed-forward network on $\boldsymbol{h}_i$ as in (22).
- The MLP decoder (**MLP/MC**) (Enguehard et al., 2020) parametrizes the MCIF as in (26) using a feed-forward network on $\boldsymbol{e}$ and $\boldsymbol{h}_i$.
- The Self-Attention decoder (**SA/MC**) (Enguehard et al., 2020) parametrizes the MCIF as in (28) by letting $\boldsymbol{e}$ attend to all $\{\boldsymbol{h}_1, ..., \boldsymbol{h}_i\}$.
- The Neural Hawkes decoder (**NH**) (Mei & Eisner, 2016) parametrizes the MCIF as in (34) using a set of continuous-time LSTM equations.
- The RMTPP decoder (**RMTPP**) (Du et al., 2016) separately parametrizes the GCIF as in (30), and a distribution of marks independent of time given the history as in (31).
- The LogNormMix decoder (**LNM**) (Shchur et al., 2019) separately parametrizes the conditional density of inter-arrival times as a mixture of log-normals as in (44), and the distribution of marks similarly to RMTPP.
- The LogNorm decoder (**LN**) is defined similarly to LNM, but with a single mixture component.
- The FullyNN decoder (**FNN**) (Omi et al., 2019) parametrizes the cumulative MCIF as in (52) using a feed-forward network on $\boldsymbol{e}$ and $\boldsymbol{h}_i$.

- The Cumulative Self-Attention decoder (**SA/CM**) (Enguehard et al., 2020) parametrizes the cumulative MCIF as in (56) by letting $\boldsymbol{e}$ attend to all $\{\boldsymbol{h}_1, ..., \boldsymbol{h}_i\}$.
- A Hawkes decoder (**Hawkes**) with exponential kernels, which parametrizes the MCIF as in (9).
- A simple Poisson decoder (**Poisson**), which parametrizes a constant MCIF as in (7).

In the following, we will describe and discuss each of the above decoders, except the Poisson and Hawkes decoders which have already been introduced in Section 2.

EC decoder. The MCIF is assumed to be constant between two events and is parametrized using a feed-forward network on the history embedding, i.e.

$$\lambda_k^*(t) = \lambda_k^* = \sigma_{S,k}\left(\boldsymbol{w}_k^\mathsf{T}(\sigma_R\big(\mathbf{W}_1\boldsymbol{h}_i + \boldsymbol{b}_1\big) + b_k\right), \tag{22}$$

where $\mathbf{W}_1 \in \mathbb{R}^{d_{in}\times d_h}$ and $\boldsymbol{b}_1 \in \mathbb{R}^{d_{in}}$, and $\boldsymbol{w}_k \in \mathbb{R}^{d_{in}}$ and b_k are mark-specific weights and biases, respectively. $\sigma_{S,k}$ is a mark-specific Softplus activation function:

$$\sigma_{S,k}(x) = s_k \log\left(1 + \exp\left(\frac{x}{s_k}\right)\right), \tag{23}$$

with $s_k \in \mathbb{R}_+$ ensuring R_1^λ. The MCIF being independent of time between two events, its cumulative is given by

$$\Lambda_k^*(t) = (t - t_{i-1})\lambda_k^*(t), \tag{24}$$

and the distribution of inter-arrival times is exponential with rate $\lambda^*(t)$:

$$f^*(\tau) = \lambda^*(t)\ \exp(-\lambda^*(t)\tau). \tag{25}$$

MLP/MC decoder. Although the EC decoder can capture more general patterns than the Hawkes decoder, it does not allow evolving dynamics between consecutive events. To circumvent this limitation, the MLP/MC decoder takes as input the concatenation of $\boldsymbol{e}^t$ (which is a function of t) and $\boldsymbol{h}_i$. In contrast to the EC decoder, the MCIF is allowed to vary between consecutive events:

$$\lambda_k^*(t) = \mu_k + \sigma_{S,k}\big(\boldsymbol{w}_k^\mathsf{T}(\sigma_R\big(\mathbf{W}_1[\boldsymbol{h}_i, \boldsymbol{e}^t] + \boldsymbol{b}_1\big) + b_k\big). \tag{26}$$

where $\mu_k \in \mathbb{R}_+$ ensures that R_2^λ is met. The Softplus activation forbids the computation of the cumulative MCIF in closed form, requiring numerical integration techniques, such as Monte Carlo, to approximate its expression:

$$\Lambda_k^*(t) \simeq \frac{t - t_{i-1}}{n_s}\sum_{j=1}^{n_s}\lambda_k^*(s_j), \tag{27}$$

where $s_j \sim \mathcal{U}[t_{i-1}, t]$ and n_s is the number of Monte Carlo samples.

SA/MC decoder. The MCIF is parametrized by re-employing the same set of equations as (20), with the only difference being that the query vector is constructed using $\boldsymbol{e}^t$. By doing so, this allows the query event e to attend to previous event representations in $\mathcal{H}_t$:

$$\lambda_k^*(t) = \mu_k + \sigma_{S,k}\big(\boldsymbol{w}_k^\mathsf{T}(\mathrm{SA}\big(\boldsymbol{q}, \mathbf{K}_i, \mathbf{V}_i\big) + b_k\big), \tag{28}$$

$$\boldsymbol{q} = \mathbf{W}_Q \boldsymbol{e}^t, \quad \mathbf{K}_i = \mathbf{W}_K[\boldsymbol{h}_1, ..., \boldsymbol{h}_i], \quad \mathbf{W}_V = \mathbf{V}_i[\boldsymbol{h}_1, ..., \boldsymbol{h}_i], \tag{29}$$

where $\mathbf{W}_Q \in \mathbb{R}^{d_q \times d_t}$, $\mathbf{W}_K \in \mathbb{R}^{d_q \times d_h}$ and $\mathbf{W}_V \in \mathbb{R}^{d_h \times d_z}$, d_z being the output dimension of the attention mechanism. Similarly to the MLP/MC decoder, the cumulative MCIF must be approximated by numerical integration techniques, e.g. as in (27).

RMTPP decoder. Instead of specifying the MCIF, the RMTPP decoder separately parametrizes the GCIF $\lambda^*(t)$ and the mark distribution $p^*(k)$ as:

$$\lambda^*(t) = \exp\Big(w^t(t - t_{i-1}) + (\boldsymbol{w}^h)^\top \boldsymbol{h}_i + b\Big), \tag{30}$$

$$p^*(k) = \text{Softmax}\big(\mathbf{W}^h \boldsymbol{h}_i + \boldsymbol{b}\big)_k, \tag{31}$$

where $w^t \in \mathbb{R}_+$, $\boldsymbol{w}^h \in \mathbb{R}^{d_h}$, $b \in \mathbb{R}$, $\mathbf{W}^h \in \mathbb{R}^{K \times d_h}$, and $\boldsymbol{b} \in \mathbb{R}^K$. The exponential transformation in (30), along with the positivity of w^t, ensure that R_1^λ and R_2^λ are met. By assuming the distribution of marks to be independent of the time given the history of the process, the RMTPP decoder makes a strong simplifying assumption, which has been criticized in previous works (Enguehard et al., 2020). However, the exponential in (30) allows us to directly compute the cumulative GCIF in closed form:

$$\Lambda^*(t) = \frac{1}{w^t}\Big(\exp\big(w^t(t - t_{i-1}) + (\boldsymbol{w}^h)^\top \boldsymbol{h}_i + b\big) - \exp\big((\boldsymbol{w}^h)^\top \boldsymbol{h}_i + b\big)\Big). \tag{32}$$

Moreover, as pointed out by Shchur et al. (2019), the RMTPP decoder defines a Gompertz distribution (Wienke, 2010) on the inter-arrival times, with a density given by

$$f^*(\tau) = \beta\eta \exp\left(\beta\tau - \eta \exp(\beta\tau) + \eta\right), \tag{33}$$

with shape $\eta = \frac{\exp\big((\boldsymbol{w}^h)^\top \boldsymbol{h}_i + b\big)}{w^t}$ and scale $\beta = w^t$.

NH decoder. The MCIF is parametrized using a fully-connected layer on a history embedding $\boldsymbol{h}_i(t)$ that is allowed to vary between consecutive events, i.e:

$$\lambda_k^*(t) = \sigma_{S,k}\Big((\boldsymbol{w}_k)^\top \boldsymbol{h}_i(t)\Big). \tag{34}$$

In contrast to a classical discrete-time LSTM, which would only update the history embedding $\boldsymbol{h}_i$ when the event at time t_i is observed, a continuous-time LSTM allows the history embedding to exponentially decay in the interval $]t_{i-1}, t_i]$, making it a function of time. Once (t_i, k_i) is observed, the continuous-time LSTM will apply a discrete update to $\boldsymbol{h}_i(t_i)$, using a modified set of discrete-time LSTM equations (37)-(43). To put it concisely, the parametrization of the MCIF can be summarized as

$$\boldsymbol{h}_i(t) = \boldsymbol{o}_i \odot \Big(2\sigma_{Si}\big(2\boldsymbol{c}(t)\big) - 1\Big), \tag{35}$$

$$\boldsymbol{c}(t) = \bar{\boldsymbol{c}}_i + (\boldsymbol{c}_i - \bar{\boldsymbol{c}}_i)\exp\big(-\boldsymbol{\delta}_i(t - t_{i-1})\big), \tag{36}$$

$$\boldsymbol{i}_i = \sigma_{Si}(\mathbf{W}_i \boldsymbol{k}_{i-1} + \mathbf{U}_i \boldsymbol{h}_{i-1}(t_i) + \boldsymbol{b}_i), \tag{37}$$

$$\boldsymbol{f}_i = \sigma_{Si}(\mathbf{W}_f \boldsymbol{k}_{i-1} + \mathbf{U}_f \boldsymbol{h}_{i-1}(t_i) + \boldsymbol{b}_f), \tag{38}$$

$$\boldsymbol{z}_i = 2\sigma_{Si}(\mathbf{W}_z \boldsymbol{k}_{i-1} + \mathbf{U}_z \boldsymbol{h}_{i-1}(t_i) + \boldsymbol{b}_z) - 1, \tag{39}$$

$$\boldsymbol{o}_i = \sigma_{Si}(\mathbf{W}_o \boldsymbol{k}_{i-1} + \mathbf{U}_o \boldsymbol{h}_{i-1}(t_i) + \boldsymbol{b}_o), \tag{40}$$

$$\boldsymbol{c}_i = \boldsymbol{f}_i \odot \boldsymbol{c}(t_{i-1}) + \boldsymbol{i}_i \odot \boldsymbol{z}_i, \tag{41}$$

$$\bar{\boldsymbol{c}}_i = \boldsymbol{f}_i \odot \bar{\boldsymbol{c}}_{i-1} + \boldsymbol{i}_i \odot \boldsymbol{z}_i, \tag{42}$$

$$\boldsymbol{\delta}_i = \sigma_S(\mathbf{W}_d \boldsymbol{k}_{i-1} + \mathbf{U}_d \boldsymbol{h}_{i-1}(t_i) + \boldsymbol{b}_d), \tag{43}$$

where $\boldsymbol{k}_{i-1} \in \{0,1\}^K$ is the one-hot encoding of mark k_{i-1}, $\boldsymbol{w}_k \in \mathbb{R}^{d_h}$, $\mathbf{W}_i$, $\mathbf{W}_f$, $\mathbf{W}_z$, $\mathbf{W}_o$, $\mathbf{W}_d \in \mathbb{R}^{d_h \times K}$, $\mathbf{U}_i$, $\mathbf{U}_f$, $\mathbf{U}_z$, $\mathbf{U}_o$, $\mathbf{U}_d \in \mathbb{R}^{d_h \times d_h}$, and $\boldsymbol{b_i}$, $\boldsymbol{b_f}$, $\boldsymbol{b}_z$, $\boldsymbol{b}_o$, $\boldsymbol{b}_d \in \mathbb{R}^{d_h}$. σ_{Si} is the Sigmoïd activation function, and σ_S is the unmarked formulation of the Softplus activation, i.e. $\sigma_S(x) = s \log\left(1 + \exp\left(x/s\right)\right)$ with $s \in \mathbb{R}_+$. Here also, one must rely on numerical integration techniques to estimate the cumulative MCIF.

LNM decoder. The conditional density of inter-arrival times is parametrized as a mixture of log-normal distributions, i.e:

$$f^*(\tau) = \sum_{m=1}^{M} p_m \frac{1}{\tau \sigma_m \sqrt{2\pi}} \exp\Big(- \frac{(\log \tau - \mu_m)^2}{2\sigma_m^2} \Big), \tag{44}$$

where $p_m = \mathrm{Softmax}\big(\mathbf{W}_m \boldsymbol{h}_i + \boldsymbol{b}\big)$ corresponds to the probability that τ_i was generated by the m^{th} mixture component, and $\mu_m = \boldsymbol{w}_\mu \boldsymbol{h}_i + b_\mu$, $\sigma_m = \exp(\boldsymbol{w}_\sigma \boldsymbol{h}_i + b_\sigma)$ are the mean and standard deviation of the m^{th} mixture component, respectively. $\mathbf{W}_m \in \mathbb{R}^{M \times d_h}$, $\boldsymbol{b}_m \in \mathbb{R}^M$, M being the number of mixture components, $\boldsymbol{w}_\mu$, $\boldsymbol{w}_\sigma \in \mathbb{R}^{d_h}$ and b_μ, b_σ are scalars. Defined similarly to equation (31), the mark distribution $p^*(k)$ is assumed to be conditionally independent of the inter-arrival times given the history of the process. Although not available in closed-form, the cumulative distribution of a mixture of log-normals can be approximated with high precision (Abramowitz & Stegun, 1965):

$$F^*(\tau) = \sum_{m=1}^{M} \frac{1}{2} \Big[1 + \mathrm{erf}\Big(\frac{\log \tau - \mu_m}{\sigma_m \sqrt{2}} \Big) \Big], \tag{45}$$

where $\mathrm{erf}(x) = \frac{2}{\sqrt{\pi}} \int_0^x e^{-s^2} ds$ is the Gaussian error function. From $F^*(\tau)$, we can retrieve the cumulative GCIF as:

$$\Lambda^*(t) = -\log\, \Big(1 - F^*(\tau)\Big). \tag{46}$$

FNN decoder. A major bottleneck of models parametrizing the MCIF resides in its cumulative not always being available in closed-form, thus requiring expensive numerical integration techniques. An elegant way of addressing this challenge is to directly parametrize the cumulative MCIF , from which $\lambda_k^*(t)$ can be easily retrieved through differentiation. The original definition of FullyNN parametrized $\Lambda^*(t)$ using a fully-connected network on both the inter-arrival times and the history embeddings, which in a marked setting would write:

$$\Lambda_k^*(t) = \sigma_{S,k}\big(\boldsymbol{w}_k^\top (\tanh\big(\boldsymbol{w}^t (t - t_{i-1}) + \mathbf{W}^h \boldsymbol{h}_i + \boldsymbol{b}\big) + b_k\big), \tag{47}$$

where each weight is constrained to be positive, ensuring condition R_1^Λ and R_4^Λ, i.e. $\boldsymbol{w}_k \in \mathbb{R}_+^{d_{in}}$, $\boldsymbol{w}^t \in \mathbb{R}_+^{d_{in}}$, $\mathbf{W}^h \in \mathbb{R}_+^{d_{in} \times d_h}$, $\boldsymbol{b} \in \mathbb{R}_+^{d_{in}}$ and $b_k \in \mathbb{R}_+$. However, as pointed out by Shchur et al. (2019), equation (47) fails to satisfy R_2^Λ:

$$\Lambda_k^*(t_{i-1}) = \sigma_S\big(\boldsymbol{w}_k^\top (\tanh\big(\mathbf{W}^h \boldsymbol{h}_i + \boldsymbol{b}_1\big) + b_k\big) > 0, \tag{48}$$

which in turn yields $F^*(\tau = 0) > 0$. In other terms, the original FNN model attributes non-zero probability mass to null inter-arrival times. The original formulation also fails to satisfy R_3^Λ due to the saturation of the tanh activation function:

$$\lim_{t \to \infty} \Lambda_k^*(t) = \sigma_S \left(\sum_{d=1}^{d_{in}} w_{k,d} + b_k \right) < \infty. \tag{49}$$

To prevent both these shortcomings, Enguehard et al. (2020) proposed to replace the tanh activation function with a Gumbel-Softplus activation:

$$\sigma_{GS,k}(x) = \big[1 - \big(1 + \alpha_k \exp(x)\big)^{-\frac{1}{\alpha_k}}\big]\big[1 + \sigma_{S,k}(x)\big], \tag{50}$$

with $\alpha_k \in \mathbb{R}_+$. The Gumbel-Softplus activation function being non-saturating (i.e. $\lim_{x\to\infty} \sigma_{GS,k}(x) = \infty$), using it as a replacement for the tanh activation function in (52) indeed satisfies R_3^Λ. Finally, R_2^Λ can be satisfied by defining $\Lambda_k^*(t)$ as

$$\Lambda_k^*(t) = G_k^*(t) - G_k^*(t_{i-1}), \tag{51}$$

$$G_k^*(t) = \sigma_{S,k}\big(\boldsymbol{w}_k^\mathsf{T}(\sigma_{GS,k}\big(\mathbf{W}_1^t \boldsymbol{e}^t + \mathbf{W}_1^h \boldsymbol{h}_i + \boldsymbol{b}_1\big) + b_k\big), \tag{52}$$

which defines the generalized corrected version of FullyNN. Note that $G_k^*(t)$ takes now as input any encoding of a query time $\boldsymbol{e}^t$ with $\mathbf{W}_1^t \in \mathbb{R}^{d_{in}\times d_t}$. However, to ensure that R_4^Λ remains satisfied, $\boldsymbol{e}^t$ must be monotonic in its input. Therefore, when parametrizing a cumulative decoder, the temporal event encoding in (15) cannot be used, and the weights of encoding (16) must be constrained to be positive. From the cumulative MCIF, $\lambda_k^*(t)$ can finally be retrieved through differentiation:

$$\lambda_k^*(t) = \frac{d}{dt}\Lambda_k^*(t). \tag{53}$$

SA/CM decoder. The SA/CM decoder shares a similar set of equations as in (28) to parametrize the cumulative MCIF. However, alike FullyNN, several modifications of the latter are required to ensure that the decoder meets the various constraints imposed by $\Lambda_k^*(t)$. First, the Softmax activation is replaced by a Sigmoid to satisfy R_4^Λ. Then, the ReLU activation is replaced by a Gumbel-Softplus, which prevents

$$\frac{d^2\Lambda_k^*(t)}{dt^2} = \frac{d\lambda_k^*(t)}{dt} = 0. \tag{54}$$

In other terms, a cumulative model defined with a ReLU activation is equivalent to the EC decoder in (22) (Enguehard et al., 2020). Moreover, given the saturation of the Sigmoid function, a term $\mu_k(t - t_i)$ with $\mu_k \in \mathbb{R}_+$ is added to the cumulative MCIF to satisfy R_4^Λ. Note that including this term is equivalent to add μ_k directly to the MCIF. Finally, the Cumulative Self-Attention decoder is given by

$$\Lambda_k^*(t) = G_k^*(t) - G_k^*(t_{i-1}), \tag{55}$$

$$G_k^*(t) = \mu_k(t - t_{i-1}) + \sigma_{S,k}\big(\boldsymbol{w}_k^\mathsf{T}(\mathrm{SA}\big(\boldsymbol{q}, \mathbf{K}_i, \mathbf{V}_i\big) + b_k\big), \tag{56}$$

$$\mathrm{SA}(\boldsymbol{q}, \mathbf{K}_i, \mathbf{V}_i) = \mathbf{W}_2\sigma_{GS,k}\big(\mathbf{W}_1\hat{\boldsymbol{z}}_i^\mathsf{T} + \boldsymbol{b}_1\big) + \boldsymbol{b}_2, \tag{57}$$

$$\hat{\boldsymbol{z}}_i = \mathrm{Sigmoid}\Big(\frac{\boldsymbol{q}^\mathsf{T}\mathbf{K}_i}{\sqrt{d_q}}\Big)\mathbf{V}_i^\mathsf{T},$$

where $\mathbf{W}_1,\ \mathbf{W}_2 \in \mathbb{R}_+^{d_z\times d_z}$, $\boldsymbol{b}_1, \boldsymbol{b}_2 \in \mathbb{R}_+^{d_z}$, and where each entry of $\mathbf{W}_K$, $\mathbf{W}_V$, $\mathbf{W}_Q$, $\boldsymbol{w}_k$ and b_k is now constrained to be positive. The query $\boldsymbol{q}$, keys $\mathbf{K}_i$, and values $\mathbf{V}_i$ are given in (29). As before, the MCIF can be retrieved through differentiation.

4 Related Work

Neural Temporal Point Processes. Simple parametric forms of TPP models, such as the self-exciting Hawkes process (Hawkes, 1971), or the self-correcting process (Isham & Westcott, 1979), rely on strong modeling assumptions, which inherently limits their flexibility. To capture complex dynamics of real-world processes, the ML community eventually turned to the latest advances in neural modeling and proposed new TPP models based on various neural-network architectures. For instance, Du et al. (2016) proposed to model the inter-arrival time distribution as a Gompertz distribution with a history encoding based on a discrete-time RNN. On a similar line of work, Mei & Eisner (2016) extended this idea by parametrizing the MCIF using a modified continuous-time RNN that allows the history to evolve between consecutive events. Given their huge success as sequence encoders in NLP, Zuo et al. (2020) and Zhang et al. (2020) employed a self-attention mechanism to encode the process history. Since differentiation is often easier to carry out than integration, FullyNN (Omi et al., 2019) instead proposed to directly parametrize the cumulative GCIF using a feed-forward network, avoiding expensive numerical integration techniques. Inspired by FullyNN, Enguehard et al. (2020) corrected and extended the FullyNN model to the marked case, and proposed a generic self-attention decoder that can be employed to parametrize the cumulative MCIF, but also the MCIF itself. Instead of modeling the (cumulative) MCIF, Xiao et al. (2017b) directly modeled the conditional density of inter-arrival times with a Gaussian distribution, while Shchur et al. (2019) relies on a mixture of log-normals whose parameters are obtained from an RNN-encoded history. To further alleviate the strong assumption of independence of times and marks given the history, Waghmare et al. (2022) proposed to model conditional mixtures of log-normals for each mark separately. Finally, Ben Taieb (2022) proposed to parametrize the conditional quantile function using recurrent neural splines, enabling analytical sampling of inter-arrival times. Alternatives to NLL optimization techniques for training neural TPPs include $\beta-$VAE objectives (Boyd et al., 2020), CRPS (Ben Taieb, 2022), reinforcement learning (De et al., 2019), noise contrastive estimation (Guo et al., 2018; Mei et al., 2020) and adversarial learning (Xiao et al., 2017a; 2018). For surveys on recent advances in neural TPP modeling, refer to Shchur et al. (2021) and Yan (2019).

Experimental studies. Most papers in the neural TPP literature mainly focused on proposing methodological improvements for modeling streams of event data, often inspired by contemporary advances in neural network representation learning. While these contributions are paramount to driving future progress in the field of TPP, few studies have been carried out to identify real sources of empirical gains across neural architectures and highlight future interesting research directions. The empirical study of Lin et al. (2021) is the closest to our work. While they also compared the impact of various history encoders and decoders, they did not discuss the influence of different event encoding mechanisms. However, we found that specific choices for this architectural component can lead to drastic performance gains. Additionally, they did not include simple parametric models to their baselines, such as the Hawkes decoder. Considering these models in an experimental study allows however to fairly evaluate the true gains brought by neural architectures. We also assess the calibration of neural and non-neural TPP models on the distribution of arrival times and marks, and our experiments are conducted across a wider range of real-world datasets. Finally, our results are supported by rigorous statistical tests. Lin et al. (2022) also conducted empirical comparisons in the context of neural TPPs but their attention was focused on deep generative models which are orthogonal to our work.

5 Experimental study of neural TPP models

We carry out a large-scale experimental study to assess the predictive accuracy of state-of-the-art neural TPP models on 15 real-world event sequence datasets in a carefully designed unified setup. We also consider classical parametric TPP models as well as synthetic datasets. In particular, we study the influence of each major architectural component (event encoding, history encoder, decoder parametrization) for both time and mark prediction tasks. The next section summarizes the variations of the architectural components we have considered in our experimental study. Section 5.2 presents the datasets including summary statistics and pre-processing steps. Section 5.3 describes our experimental setup. Finally, Section 5.4 presents the evaluation metrics and statistical tools used to assess the accuracy of the considered models.

5.1 Models

To ease understanding of the following sections, a brief summary of the different architectures considered in our experiments is presented below. Table 1 summarizes the correspondence between all variations of event encoding, history encoder, and decoder, and their mathematical expressions.

Event encoding mechanisms. For the event encoding mechanism, we consider the raw inter-arrival times τ (**TO**), the logarithms of inter-arrival times (**LTO**), a temporal encoding of arrival times (**TEM**), and a learnable encoding of inter-arrival times (**LE**). Additionally, we include all their variants resulting from the concatenation of the mark embeddings $\boldsymbol{e}^k$, i.e. **CONCAT** (TO and $\boldsymbol{e}^k$), **LCONCAT** (LTO an $\boldsymbol{e}^k$), **TEMWL** (TEM and $\boldsymbol{e}^k$), and **LEWL** (LE and $\boldsymbol{e}^k$).

History encoders. To encode a process' history, we employ a **GRU**, and a self-attention mechanism (**SA**). Additionally, we consider a constant history encoder (**CONS**), which systematically outputs $\boldsymbol{h}_i = \mathbf{1}_{d_h}$. Note that a decoder equipped with this encoder parametrizes a function independent of the process' history and reduces essentially to a renewal process (Lindqvist et al., 2003).

Decoders. The decoders considered in this experimental study can be classified on the basis of the function that they parametrize, as well as on the assumptions they make regarding the distribution of inter-arrival times and marks. As described in Section 3.3, decoders that parametrize the MCIF are the **EC** , **MLP/MC** , **SA/MC**, **NH**, **Hawkes** and **Poisson** decoders. On the other hand, decoders that directly parametrize the cumulative MCIF are the **FNN** and **SA/CM** decoders. Finally, **RMTPP** separately parametrizes the GCIF and the distribution of marks, while **LNM** and its single mixture version, **LN**, separately parametrize the density of inter-arrival times and the distribution of marks. For these last three decoders, the distribution of marks is assumed to be independent of the time, conditional on the history of the process.

For the EC, LNM, and RMTPP decoders, we consider the setting where a constant baseline intensity term μ_k (**B**) is added to the MCIF. Recall that for LNM, the MCIF can be retrieved from (6). We define a model as a specific choice of event encoding mechanism, history encoder, and decoder, e.g. TO-GRU-MLP/MC corresponds to the MLP/MC decoder where $\boldsymbol{h}_i$ has been obtained with a GRU, using the TO event encoding. While in most cases, any variation of a component can be seamlessly associated with any other variation of other components, some combinations are either incorrect or meaningless. Indeed, all cumulative decoders (SA/CM and FullyNN) cannot be trained with the TEM or TEMWL event encodings, as both would violate the monotonicity constraint of

Table 1: Summary of the various architectures components considered in the comparative study.

Component	**Name**	**Acronym**	**Parametrization**
Event encoding	Times	TO	$\boldsymbol{e}_i = \tau_i$
	Log-times	LTO	$\boldsymbol{e}_i = \log \tau_i$
	Concatenate	CONCAT	$\boldsymbol{e}_i^t = \tau_i$, $\boldsymbol{e}_i^k$ as in (17), $\boldsymbol{e}_i$ as in (14)
	Log-concatenate	LCONCAT	$\boldsymbol{e}_i^t = \log \tau_i$, $\boldsymbol{e}_i^k$ as in (17, $\boldsymbol{e}_i$ as in (14
	Temporal	TEM	$\boldsymbol{e}_i$ as in (15)
	Temporal with labels	TEMWL	$\boldsymbol{e}_i^t$ as in (15), $\boldsymbol{e}_i^k$ as in (17), $\boldsymbol{e}_i$ as in (14)
	Learnable	LE	$\boldsymbol{e}_i$ as in (16)
	Learnable with labels	LEWL	$\boldsymbol{e}_i^t$ as in (16), $\boldsymbol{e}_i^k$ as in (17), $\boldsymbol{e}_i$ as in (14)
Encoder	GRU	GRU	$\boldsymbol{h}_i = \text{GRU}(\boldsymbol{e}_1, ..., \boldsymbol{e}_{i-1})$ as in (18)
	Self-attention	SA	$\boldsymbol{h}_i$ as in (20)
	Constant	CONS	$\boldsymbol{h}_i = \mathbf{1}_{d_h}$

Component	**Name**	**Acronym**	**Parametrization**	**Closed-form MLE**
Decoder	Exponential constant	EC	λ_k^* as in (22)	✓
	MLP	MLP/MC	$\lambda_k^*(t)$ as in (26)	✗
	FullyNN	FNN	$\Lambda_k^*(t)$ as in (52)	✓
	LogNormMix	LNM	$f^*(\tau)$ as in (44), $p^*(k)$ in (31)	✓
	LogNorm	LN	$f^*(\tau)$ as in (44) with $M = 1$, $p^*(k)$ in (31)	✓
	RMTPP	RMTPP	$\lambda^*(t)$ as in (30), $p^*(k)$ in (31)	✓
	Neural Hawkes	NH	$\lambda_k^*(t)$ as in (34)	✗
	Self-attention	SA/MC	$\lambda_k^*(t)$ as in (28)	✗
	Cumulative Self-attention	SA/CM	$\Lambda_k^*(t)$ as in (56)	✓
	Hawkes	Hawkes	$\lambda_k^*(t)$ as in (9)	✓
	Poisson	Poisson	$\lambda_k^*(t)$ as in (7)	✓

the cumulative MCIF. Moreover, as all event encodings are irrelevant with respect to the CONS history encoder, all CONS-EC models are equivalent. For the NH decoder, we stick to the original model definition, as it can be hardly disentangled into different components. A complete list of the considered combinations is given in Table 14 in Appendix C.

We further classify the different models into three categories: *parametric*, *semi-parametric*, and *non-parametric*. Parametric TPP models include classical (i.e. non neural) architectures, characterized by strong modeling assumptions and hence, low flexibility. We consider the Hawkes and Poisson decoders as parametric baselines. On the other hand, semi-parametric models include architectures that still make assumptions regarding the distribution of inter-arrival times, but their parameters are obtained from neural transformations. All models equipped with LNM, LN, RMTPP, or EC decoders are deemed semi-parametric. All remaining baselines, i.e. FNN, MLP/MC, SA/MC, SA/CM, and NH, are considered non-parametric models.

5.2 Datasets

Real-world datasets. A total of 15 real-world datasets containing sequences of various lengths are used in our experiments, among which 7 possess marked events. A brief description is presented below, while their general statistics are summarized in Tables 2 and 3.

- **Marked Datasets**

  - **LastFM** [2] (Kumar et al., 2019) : Records of users listening to songs. Each sequence corresponds to a user, and the artist of the song is the mark.
  - **MOOC** [2] (Kumar et al., 2019): Records of student's actions on an online course system. Each sequence corresponds to a user, and the type of action is the mark.
  - **Wikipedia** [2] (Kumar et al., 2019) : Records of Wikipedia pages' edits. Each sequence corresponds to a Wikipedia page, and marks relate to the user that edited the corresponding page.
  - **MIMIC2** [3] (Du et al., 2016) : Clinical records of patients of an intensive care unit for seven years. Each sequence corresponds to a patient, and marks describe the type of disease.
  - **Github** [4] (Trivedi et al., 2018) : Records of users' actions on the open-source platform Github during the year 2013. Each sequence corresponds to a user, and the marks describe the action performed (Watch, Star, Fork, Push, Issue, Comment Issue, Pull Request, Commit).
  - **Stack Overflow** [6] (Du et al., 2016) : Records of the time users received a specific badge on the question answering website Stack Overflow. Each sequence corresponds to a user, and the mark is the badge received.
  - **Retweets** [3] (Mei & Eisner, 2016) : Streams of retweet events following the creation of an original tweet. Each sequence corresponds to a tweet, and the category (i.e. "small", "medium", "large") to which a retweeter belongs corresponds to the mark.

- **Unmarked Datasets**
  - **Twitter** [5] (Shchur et al., 2020) : Records of tweets made by a user over several years.
  - **PUBG** [5] (Shchur et al., 2020) : Records of players' death in the online game PUBG. Each sequence corresponds to a user.
  - **Yelp Airport** [5], **Mississauga** [5] (Shchur et al., 2020), and **Toronto** [6] (Shchur et al., 2019) : Records of users' reviews on the platform Yelp for the McCarran airport, Toronto city and Mississauga city respectively. Each sequence corresponds to a user.
  - **Reddit Ask Comments** [5](Shchur et al., 2020) : Records of comments in reply to Reddit threads within 24hrs of the original post submission. Each sequence corresponds to a thread.
  - **Reddit Subs** [5](Shchur et al., 2020) : Records of submissions to a political sub-Reddit in the period from 01.01.2017 to 31.12.2019. Each sequence corresponds to a 24hrs window.
  - **Taxi** [5] (Shchur et al., 2020) : Records of taxi pick-ups in the South of Manhattan.

Pre-processing. Some marked datasets, such as Wikipedia and LastFM, originally presented a very large amount of marks, which distributions turn out to be highly spread across their respective domains. This observation raises two issues: (1) Some marks are therefore highly under-represented, rendering the task of learning their underlying distribution difficult, and (2), as each mark is

---

[2] https://github.com/srijankr/jodie/
[3] https://github.com/babylonhealth/neuralTPPs
[4] https://github.com/uoguelph-mlrg/LDG
[5] https://github.com/shchur/triangular-tpp
[6] https://github.com/shchur/ifl-tpp

Table 2: Marked datasets statistics after pre-processing. "Sequences (%)" and "Events (%)" respectively correspond to the number of sequences and events that remain in the dataset after the pre-processing step. "MSL" is the mean sequence length.

	Sequences	**Sequences (%)**	**Events**	**Events (%)**	**MSL**	**Max Len.**	**Min Len.**	**Marks**
Wikipedia	590	0.59	30472	0.19	51.6	1163	2	50
MOOC	7047	1.00	351160	0.89	49.8	416	2	50
LastFM	856	0.92	193441	0.15	226.0	6396	2	50
MIMIC2	599	0.84	1812	0.68	3.0	32	2	43
Github	173	1.00	20657	1.00	119.4	4698	3	8
Stack Overflow	7959	1.00	569688	0.99	71.6	735	40	22
Retweets	24000	1.00	2610102	1.00	108.8	264	50	3

Table 3: Unmarked datasets statistics after pre-processing. "MSL" is the mean sequence length.

	Sequences	**Events**	**MSL**	**Max Len.**	**Min Len.**
Reddit Subs.	1094	1235128	1129.0	2658	362
Reddit Ask Comments	1355	400933	295.9	2137	4
Taxi	182	17904	98.4	140	12
Twitter	1804	29862	16.6	169	2
Yelp Toronto	300	215146	717.2	2868	424
Yelp Airport	319	9716	30.5	55	9
Yelp Mississauga	319	17621	55.2	107	3
PUBG	3001	229703	76.5	97	26

associated to a MCIF, the computational requirements drastically increase with the number of marks, which is even more exacerbated when Monte Carlo samples need to be drawn. With the incentive to avoid either of these two bottlenecks, each marked dataset is filtered to only contain events belonging to the 50 most represented marks. The resulting sequences containing less than two events are further removed from the dataset, which makes the number of distinct marks in MIMIC2 drop from 75 to 43. Finally, to avoid numerical instabilities, the arrival times of events are scaled in the interval [0,10]. Specifically, we compute $t_{i,\text{scaled}} = 10t_i/t_{\max}$, where $t_{\max}$ is the largest observed timestamp in the dataset. Unmarked datasets do not go through any processing steps, at the exception of the scaling and removal of sequences containing less than two events.

As observed in Tables 2 and 3, the considered datasets are relatively diverse in their characteristics. Indeed, some datasets, such as Yelp Toronto or LastFM, possess a relatively short number of very long sequences, while others, such as Twitter or MOOC, show the exact opposite characteristics. Figure 2 shows the distributions of the inter-arrival times logarithms across all sequences for all real-world datasets, as well as the mark distribution for marked datasets. As observed, the distribution of (log) inter-arrival times differ significantly from one dataset to the other, in some cases presenting characteristics such as multimodality (LastFM, MOOC, Wikipedia, Yelp Toronto, PUBG) or large variance (MOOC, Wikipedia, Github, Yelp Toronto). The marks distributions also show different characteristics. While the marks look evenly spread across their domains on LastFM, MOOC and

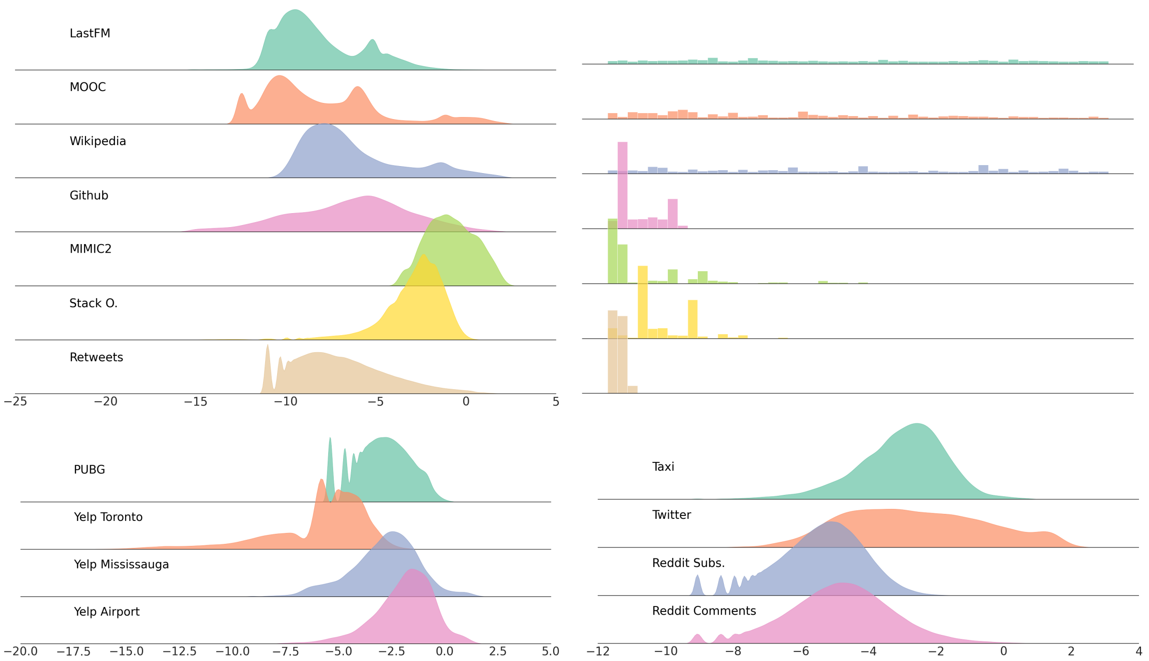

Figure 2: Distribution of log τ (top left) and mark distribution (top right) for marked datasets, after pre-processing. For unmarked datasets, only the distribution of log τ (bottom) is reported.

Wikipedia, their distribution appears sharper on Github, MIMIC2, Stack Overflow and Retweets. Such diversity should be empirically beneficial, as it would allow to assess the models' performance across a wider range of real-life applications. In Figures 12, 13 and 14 of Appendix D, we show the distribution of inter-arrival times and marks for some randomly sampled sequences in each dataset.

Synthetic datasets. We generate a synthetic dataset from the multidimensional Hawkes process with exponential kernel as in (9). We choose the following parameters:

$$\boldsymbol{\mu} = \begin{pmatrix} 0.2 \\ 0.6 \\ 0.1 \\ 0.7 \\ 0.9 \end{pmatrix} \qquad \boldsymbol{\alpha} = \begin{pmatrix} 0.25 & 0.13 & 0.13 & 0.13 & 0.13 \\ 0.13 & 0.35 & 0.13 & 0.13 & 0.13 \\ 0.13 & 0.13 & 0.2 & 0.13 & 0.13 \\ 0.13 & 0.13 & 0.13 & 0.3 & 0.13 \\ 0.13 & 0.13 & 0.13 & 0.13 & 0.25 \end{pmatrix} \qquad \boldsymbol{\beta} = \begin{pmatrix} 4.1 & 0.5 & 0.5 & 0.5 & 0.5 \\ 0.5 & 2.5 & 0.5 & 0.5 & 0.5 \\ 0.5 & 0.5 & 6.2 & 0.5 & 0.5 \\ 0.5 & 0.5 & 0.5 & 4.9 & 0.5 \\ 0.5 & 0.5 & 0.5 & 0.5 & 4.1 \end{pmatrix},$$

where the matrix α was scaled to have a spectral radius of approximately 0.8, this way guaranteeing stationarity of the process (Bacry et al., 2020). The process essentially corresponds to a marked process with $K = 5$ marks, from which we simulate 5 distinct datasets of 1000 sequences each using the library *tick* (Bacry et al., 2018).

5.3 Experimental Setup

For each real-world and synthetic datasets, we randomly split the sequences into 5 train/validation/test splits of sizes 60%/20%/20%, respectively. The models are trained to minimize the NLL in (11) on the training sequences using mini-batch gradient descent (Suvrit et al., 2011). The NLL on the validation sequences is evaluated at each epoch, and the training procedure is interrupted if the number of epochs reaches 500, or if no improvement is observed for 20 consecutive epochs. In the latter case, the model's parameters are reverted to their state of lowest validation loss. For all models, optimization is carried out using the Adam optimizer (Kingma & Ba, 2014) with an initial learning rate of 10^{-3}. If no improvement in validation loss is observed for 5 consecutive epochs, the learning rate is divided by a factor 2, and training continues.

We explore different values of event encoding dimension in $\{4, 8, 16, 32\}$ and different number of hidden units for fully-connected layers in $\{8, 16, 32\}$. For the GRU, SA encoder and SA/MC decoder, the number of hidden units is varied in $\{8, 16, 32, 64\}$, and the number of layers in $\{1, 2\}$. For the SA encoder and SA/MC decoder, we further consider the number of heads in $\{1, 2\}$. Finally, the number of mixtures in LNM is explored in $\{8, 16, 32, 64\}$. A model's hyper-parameters are selected as follows: For a given model and dataset split, 5 hyper-parameter configurations are randomly chosen. The model is trained on each of the 5 five configurations, and we retain the one displaying the lowest validation loss. These 5 best configurations (that might be different depending on the split) are then evaluated on the test set of their respective split. We finally report the average test metrics described in the next section.

5.4 Evaluation metrics

We report various metrics to evaluate a model's performance with respect to the time prediction task, i.e. its ability to estimate $f^*(\tau)$, and with respect to the mark prediction task, i.e. its ability to estimate $p^*(k|t)$, as well as to predict the next event's mark. As discussed in Section 2, reporting a single NLL metric gathers the contributions of both inter-arrival times and marks, and in effect, obscures how a model actually performs on fitting the two distributions separately. Consequently, we split the NLL into **NLL-T** and **NLL-M** terms, highlighting the contribution of each term to the total NLL metric. Given a set of test sequences $S = \{\mathcal{S}_1, ..., \mathcal{S}_L\}$, where each sequence $\mathcal{S}_l$ contains n_l events, the average test NLL is given by:

$$\mathcal{L}(\boldsymbol{\theta}; S) = \underbrace{-\frac{1}{L}\sum_{l=1}^{L}\sum_{i=1}^{n_l}\log f^*(t_{l,i};\boldsymbol{\theta}) + \Lambda^*(T;\boldsymbol{\theta})}_{\text{NLL-T}} \underbrace{-\frac{1}{L}\sum_{l=1}^{L}\sum_{i=1}^{n_l}\log p^*(k_{l,i}|t_{l,i};\boldsymbol{\theta})}_{\text{NLL-M}}. \tag{58}$$

On the other hand, a model's ability to predict the next event's mark is measured with the **F1-score**.

Calibration. In essence, TPPs are probabilistic models that aim to estimate distributions over future arrival times and marks. While the NLL score acts as a proper summary of a model's ability to fit a predictive distribution, it does not directly allow us to assess how the aforementioned model is actually calibrated. In forecasting theory, calibration refers to the statistical consistency between the predictive distribution and the actual observations (Gneiting et al., 2007). Formally, a model that outputs a predictive CDF $F^*(\tau)$ (which may be retrieved from $f^*(\tau)$, $\lambda^*(t)$ or $\Lambda^*(t)$)

is probabilistically (marginally) calibrated if (Dawid, 1984; Kuleshov et al., 2018):

$$\mathbb{P}\big(F^*(\tau) \leq p\big) = p, \quad \forall p \in [0,1], \tag{59}$$

where the probability is taken over all τ and all $\mathcal{H}_t$. In other words, for a calibrated model with respect to the distribution of inter-arrival times, a 90% prediction interval should contain τ on average 90% of the time. Similarly, in the context of mark prediction, probabilistic (marginal) calibration is defined as (Guo et al., 2017):

$$\mathbb{P}\big(\tilde{k} = \bar{k} \mid \ p^*(\tilde{k}|t) = p\big) = p, \quad \forall p \in [0,1], \tag{60}$$

where $\tilde{k}$ and $\bar{k}$ are the predicted and true mark at time t, respectively. Intuitively, this definition means that for a calibrated model with respect to the mark distribution, 90% of all predictions made with 0.9 confidence should correspond to the observed mark. Given discrete probability levels $p_m = \frac{m}{M} \in [0,1]$, we propose to evaluate models on the **Probabilistic Calibration Error** (PCE), defined as:

$$\text{PCE} = \frac{1}{M} \sum_{m=1}^{M} \left| \sum_{i=1}^{n} \frac{\mathbb{1}[F^*(\tau_i) \leq p_m]}{n} - p_m \right|, \tag{61}$$

where $n = \sum_{l=1}^{L} n_l$, and where we set $M = 50$. With respect to the mark distribution, we report the **Expected Calibration Error** (ECE) (Naeini et al., 2015) defined as:

$$\text{ECE} = \frac{1}{M} \sum_{j=1}^{M} \Big| \text{acc}(B_j) - \text{conf}(B_j) \Big|, \tag{62}$$

where each prediction $\tilde{k}$ is assigned to the j^{th} out of J bins (obtained by discretizing the interval $[0,1]$ in J equal-size bins) if $p^*(\tilde{k}|t)$ lies in the interval $[\frac{j-1}{J}, \frac{j}{J}]$. B_j is the set of predictions that fell within bin j, $\text{acc}(B_j)$ corresponds to the model's accuracy within bin j, and $\text{conf}(B_j)$ is the average confidence level of all predictions that fell within bin j. We set $J = 10$, and lower PCE and ECE are better.

Reliability diagrams. A disadvantage with PCE and ECE metrics is that information regarding the calibration error at individual probability levels $p_1, ..., p_M$, or within individual bins $B_1, ..., B_J$, is lost. Reliability diagrams are visual tools that can be used to assess the probabilistic calibration of a model at a fine-grained level for both continuous and discrete distributions. For the distribution of inter-arrival times, a reliability diagram is obtained by plotting the empirical CDF $\sum_{i=1}^{n} \frac{\mathbb{1}[F^*(\tau_i) \leq p_m]}{n}$ in (61) against all probability levels p_m. For the distribution of marks, it is obtained by plotting $\text{acc}(B_j)$ against $\text{conf}(B_j)$ for all B_j. In both cases, a probabilistically calibrated model should align with the diagonal line, and any deviation from it corresponds to miscalibration (Gneiting et al., 2007; Guo et al., 2017).

Statistical comparisons. We further conduct statistical pairwise comparisons between all decoders, for each metric separately. First, Friedman test (Friedman, 1937; 1940) is employed to assess of at least one statistical difference among all decoders. If the null hypothesis is rejected at the $\alpha = 0.05$ significance level, we proceed with comparing each decoder against each other, using Holm's posthoc test (Holm, 1979) to account for multiple hypothesis testing. The outcome of the pairwise comparisons is displayed on critical difference (CD) diagrams, which show the average rank of a model on a metric of interest across all datasets, as well as groups of models that are not statistically different from one another at a given significance level. Refer to Demšar (2006); García & Herrera (2008) for additional details.

5.5 Results Aggregation

Since any component variation can often be associated with any other component variation (e.g. TO-GRU-MLP/MC, TEM-GRU-MLP/MC), the number of possible combinations quickly rise to a high number, making individual model's comparisons across every dataset unmanageable. To overcome this challenge, we aggregate the model results for each metric separately across all datasets as follows. When comparing different event encodings, we first group all models that are equipped with a specific decoder variation (e.g. MLP/MC). Then, among this decoder group, we further group all models by event encoding variations (e.g. TO-Any history encoder-MLP/MC). We then compute the average score of that event encoding-decoder group on a given dataset with respect to each metric. Finally, for each metric, we rank this encoding-decoder group against other encoding-decoder groups based on their average score on the same dataset. We apply this operation for each dataset separately and report the average and median scores, as well as the average rank of that component variation group across all datasets.

Moreover, as the scale of the NLLs (NLL-T and NLL-M) vary significantly from one dataset to another, we standardize their values on each dataset separately prior to applying the aggregation procedure above. For each model, we compute its standardized NLL (-T or -M) as

$$\frac{\text{NLL}_d^m - m_d}{\text{IQR}}, \tag{63}$$

where NLL_d^m is the NLL score of model m on dataset d, while m_d and IQR are the median and inter-quartile ranges of NLL scores for all models on dataset d, respectively.

6 Results and Discussion

Tables 4 and 5 give the results averaged over all marked datasets for all decoders with different variations of event encoding and history encoders, respectively. Table 6 gives the results for the combination of architectural components that obtained the lowest NLL-T and NLL-M on average over all marked datasets for all decoders. The same results for the unmarked datasets as well as additional raw metrics (i.e. not aggregated) and standard errors for each dataset are given in Appendices A and B, respectively. Moreover, as discussed later in this section, we found that some datasets (MIMIC2, Stack Overflow, Taxi, Reddit Subs, Reddit Comments, Yelp Toronto and Yelp Mississauga) might not be appropriate for benchmarking neural TPP models, as most decoders achieve competitive performance on them. We invite researchers to exercise caution when using these datasets in future works. For completeness, we added the results of the aggregation procedure with the aforementioned datasets discarded in Appendix D. We found no significant differences in the results. For the following discussion, we focus on the 'Mean' column.

Impact of the event encoding. Comparing the results in Table 4, we aim to provide answers to the two following questions: (1) *Are vectorial representations of time better for estimating the inter-arrival time distribution?* (2) *What is the impact of jointly estimating the inter-arrival time and the mark distribution on the two distributions separately?*

(1) We observe that vectorial representations of time (i.e. TEM and LE in opposition to TO and LTO) yield lower NLL-T and PCE scores for the EC, LNM, and both SA decoders. Given that a model equipped with the EC and LNM decoders only uses the event encoding mechanism at the history encoding stage, this finding suggests that GRU and SA encoders rely on expressive transformations of time to capture patterns of event occurrences. However, we observed that the GRU encoder is rather stable with respect to the time encoding employed, while the performance of the SA encoder drastically decreases with TO or LTO encodings. Added to the fact that both SA decoders only perform well when using TEM and LE, we conclude that self-attention mechanisms must be combined with vectorial representations of time to yield good performance in the context of neural TPP models.

Furthermore, a log transformation of the inter-arrival times (i.e. LTO) drastically improves performance on the same metrics for the RMTPP, FNN and MLP/MC decoders. Using the LTO encoding in combination with the RMTPP decoder effectively defines an inverse Weibull distribution for the inter-arrival times (Kleiber & Kotz, 2003). It appears to be a better fit for the data than the Gompertz distribution from the original formulation of RMTPP.

Moreover, for FNN and MLP/MC decoders, we found that the last Softplus activation prevents the gradient of the GCIF to take large values for very short inter-arrival times. However, in many of the considered datasets, most events occur in packs during extremely short time spans, requiring the GCIF to change quickly between two events. The LTO encoding in combination with the Softplus activation allows steeper gradients for short inter-arrival times, and thus enables rapid changes in the GCIF. As a result, the FNN and MLP/MC decoders can reach lower NLL-T with the LTO encoding.

(2) Including a mark representation in the event encoding generally improves performance in terms of NLL-T and PCE when moving from TO to CONCAT and from LTO to LCONCAT. On the one hand, this observation suggests that information contained in previous marks does help the model to better estimate the arrival times of future events. However, we observe that in most cases, TEMWL and LEWL encodings show higher NLL-T compared to their TE and LE counterparts. Therefore, relevant information contained in previous marks appears less readily exploitable by the models when the mark embedding is concatenated to a vectorial representation of time.

All decoders improve substantially with respect to the NLL-M, ECE, and F1-score metrics when the mark is included in the event encoding. While expected, this finding confirms that expressive representations of past marks are paramount to predicting future marks.

Impact of the history encoder. From the results of Table 5, we observe that models equipped with a GRU history encoder yield better performance with respect to all time and mark-specific metrics compared to ones equipped with a SA encoder. While self-attention mechanisms have gained increasing popularity since their introduction by (Vaswani et al., 2017) for sequence modeling tasks, we found that they are on average less suited than their RNN counterparts in the context of TPPs. Specifically, the GRU encoder is more stable with respect to the choice of event encoding mechanism, while the SA encoder requires vectorial event representation to achieve good performance. Furthermore, the constant (CONS) history-independent encoder systematically achieves the worst results with respect to all metrics. This observation confirms the common assumption that future event occurrences associated with real-world TPPs indeed depend on past arrival times and marks, and hence better predictive accuracy can be achieved with better representations of the observed history.

Table 4: Average and median scores, as well as average ranks per decoder and variation of event encoding, for marked datasets. Refer to Section 5.5 for details on the aggregation procedure. Best results are highlighted in bold.

	Marked Datasets														
	NLL-T			PCE			NLL-M			ECE			F1-score		
	Mean	Median	Rank	Mean	Median	Rank	Mean	Median	Rank	Mean	Median	Rank	Mean	Median	Rank
EC-TO	0.43	0.44	6.38	0.2	0.23	6.25	0.14	0.14	6.75	0.44	0.44	7.5	0.19	0.17	6.88
EC-LTO	0.49	0.45	7.38	0.2	0.23	6.5	0.08	0.06	5.38	0.44	0.45	6.88	0.19	0.17	7.25
EC-CONCAT	0.15	0.15	**2.5**	**0.17**	**0.15**	**2.25**	-0.4	-0.6	2.88	0.34	0.31	**1.88**	0.3	0.28	2.12
EC-LCONCAT	0.24	0.27	4.38	0.19	0.2	4.88	-0.39	-0.54	3.5	0.34	0.3	2.75	0.28	0.27	3.0
EC-TEM	0.2	0.14	4.38	0.18	0.15	4.5	0.1	0.07	6.38	0.42	0.42	6.0	0.2	0.18	5.88
EC-TEMWL	0.25	0.24	4.12	0.19	0.17	4.5	**-0.63**	**-0.69**	**1.75**	**0.32**	**0.26**	2.38	**0.31**	**0.29**	**1.75**
EC-LE	**0.12**	**0.12**	3.0	0.18	0.15	3.0	0.08	0.09	5.38	0.41	0.42	5.25	0.2	0.18	5.75
EC-LEWL	0.2	0.16	3.88	0.18	0.15	4.12	-0.24	-0.5	4.0	0.35	0.35	3.38	0.29	0.28	3.38
LNM-TO	-0.2	**-0.41**	5.75	0.07	0.06	4.62	0.3	0.3	6.5	0.45	0.45	7.25	0.18	0.18	7.38
LNM-LTO	-0.15	-0.29	5.38	0.07	0.06	5.25	0.38	0.28	6.25	0.45	0.44	6.88	0.18	0.18	6.5
LNM-CONCAT	**-0.27**	-0.32	3.5	0.07	0.06	4.25	**-0.64**	**-0.47**	**2.0**	**0.36**	**0.34**	**1.62**	**0.28**	**0.25**	**1.38**
LNM-LCONCAT	-0.18	-0.22	**2.62**	0.07	0.06	**3.25**	-0.52	-0.32	3.12	0.38	0.35	3.0	0.26	0.25	2.88
LNM-TEM	-0.26	-0.41	4.12	**0.06**	**0.05**	3.62	0.27	0.31	6.12	0.44	0.44	6.12	0.19	0.19	6.0
LNM-TEMWL	-0.16	-0.21	5.0	0.07	0.06	4.88	-0.6	-0.37	2.0	0.37	0.34	2.38	0.27	0.25	2.25
LNM-LE	-0.26	-0.38	4.0	0.07	0.07	5.5	0.33	0.29	6.25	0.44	0.44	5.75	0.19	0.19	6.12
LNM-LEWL	-0.19	-0.18	5.62	0.08	0.06	4.62	-0.51	-0.31	3.75	0.38	0.38	3.0	0.24	0.24	3.5
FNN-TO	0.56	0.45	4.5	0.21	0.28	4.38	0.23	0.16	4.5	0.46	0.47	5.25	0.17	0.17	5.0
FNN-LTO	-0.33	-0.3	1.88	**0.03**	**0.02**	2.0	-0.02	-0.05	3.88	0.4	0.42	2.25	0.21	0.19	2.38
FNN-CONCAT	0.58	0.61	4.88	0.21	0.28	4.62	0.02	-0.02	3.25	0.45	0.47	4.62	0.18	0.17	4.25
FNN-LCONCAT	**-0.49**	**-0.56**	**1.75**	0.03	0.02	**1.38**	**-1.4**	**-0.84**	**1.62**	**0.28**	**0.3**	**1.12**	**0.29**	**0.31**	**1.12**
FNN-LE	0.53	0.63	4.12	0.21	0.29	3.75	0.2	0.15	4.12	0.46	0.47	4.25	0.17	0.16	4.38
FNN-LEWL	0.57	0.51	3.88	0.21	0.28	4.88	-0.01	-0.02	3.62	0.44	0.46	3.5	0.19	0.2	3.88
MLP/MC-TO	0.15	0.07	6.0	0.16	0.16	6.38	0.24	0.21	6.75	0.41	0.4	6.75	0.2	0.18	7.25
MLP/MC-LTO	-0.17	-0.08	4.12	**0.09**	**0.06**	**1.88**	0.35	0.17	6.5	0.39	0.42	6.25	0.21	0.18	6.12
MLP/MC-CONCAT	-0.02	0.01	4.38	0.15	0.12	5.25	-0.5	**-0.58**	**2.5**	0.29	0.26	2.5	**0.31**	0.31	**1.75**
MLP/MC-LCONCAT	**-0.27**	**-0.24**	**2.38**	0.09	0.07	2.25	**-0.82**	-0.51	3.12	**0.27**	0.26	**1.62**	0.31	**0.32**	2.12
MLP/MC-TEM	0.04	-0.02	5.75	0.15	0.13	6.12	0.18	0.14	5.5	0.4	0.41	6.38	0.2	0.18	6.5
MLP/MC-TEMWL	0.23	0.32	7.25	0.17	0.16	7.5	-0.35	-0.39	3.75	0.34	0.35	3.75	0.29	0.29	3.88
MLP/MC-LE	-0.1	-0.16	3.0	0.13	0.11	3.0	0.25	0.07	5.38	0.38	0.37	6.12	0.21	0.19	5.62
MLP/MC-LEWL	-0.09	-0.11	3.12	0.13	0.11	3.62	-0.34	-0.43	2.5	0.29	**0.24**	2.62	0.31	0.29	2.75
RMTPP-TO	0.16	0.23	6.75	0.16	0.16	6.75	0.04	0.05	6.25	0.42	0.43	7.12	0.19	0.18	7.12
RMTPP-LTO	-0.25	-0.18	4.62	0.06	0.05	3.25	0.01	0.0	6.25	0.42	0.42	7.0	0.19	0.18	6.38
RMTPP-CONCAT	0.01	-0.0	4.0	0.15	0.12	4.12	-1.36	-0.8	2.88	0.26	0.24	2.5	0.35	0.33	2.5
RMTPP-LCONCAT	**-0.41**	**-0.34**	**2.25**	**0.04**	**0.04**	**2.0**	-1.5	-0.97	3.0	0.25	**0.21**	2.12	0.37	0.34	2.0
RMTPP-TEM	0.04	-0.0	5.5	0.15	0.12	5.25	0.03	0.02	6.0	0.41	0.41	6.25	0.21	0.19	6.5
RMTPP-TEMWL	0.05	0.03	4.5	0.15	0.14	5.0	**-1.88**	**-1.19**	**1.5**	**0.24**	0.21	**1.88**	**0.4**	**0.37**	**1.62**
RMTPP-LE	-0.02	-0.01	3.88	0.15	0.13	4.75	0.04	0.04	6.25	0.4	0.41	5.62	0.21	0.19	6.0
RMTPP-LEWL	0.05	0.01	4.5	0.15	0.13	4.88	-1.09	-0.68	3.88	0.3	0.29	3.5	0.32	0.32	3.88
SA/CM-TO	4.43	-0.04	4.75	0.11	0.06	4.25	0.74	0.18	5.0	0.45	0.46	5.5	0.14	0.1	4.62
SA/CM-LTO	8.35	-0.13	3.75	0.1	0.05	3.0	0.33	0.03	4.5	0.43	0.44	3.38	0.18	0.1	3.38
SA/CM-CONCAT	-0.15	-0.16	4.5	0.1	0.1	4.75	-0.04	-0.02	3.38	0.43	0.44	3.5	0.2	0.21	3.62
SA/CM-LCONCAT	**-0.4**	**-0.43**	**2.0**	**0.03**	**0.03**	**2.0**	**-0.35**	**-0.3**	**1.5**	**0.38**	**0.41**	**1.62**	**0.24**	**0.24**	**1.5**
SA/CM-LE	-0.32	-0.32	2.25	0.05	0.04	2.88	0.05	0.01	4.0	0.42	0.44	3.38	0.19	0.17	4.5
SA/CM-LEWL	-0.2	-0.21	3.75	0.08	0.08	4.12	-0.2	-0.21	2.62	0.41	0.45	3.62	0.21	0.21	3.38
SA/MC-TO	0.81	0.85	7.62	0.23	0.31	7.62	0.17	0.14	6.25	0.47	0.47	7.5	0.17	0.16	7.88
SA/MC-LTO	0.7	0.79	6.88	0.22	0.29	6.88	0.2	0.22	6.62	0.46	0.47	7.0	0.17	0.16	7.12
SA/MC-CONCAT	-0.35	-0.35	3.5	0.1	0.08	4.0	**-0.61**	**-0.69**	**2.0**	0.3	0.28	2.38	**0.29**	**0.27**	2.38
SA/MC-LCONCAT	-0.45	**-0.44**	2.25	0.08	0.06	2.75	-0.45	-0.61	3.25	**0.27**	**0.23**	**1.62**	0.28	0.26	2.62
SA/MC-TEM	-0.33	-0.33	4.62	0.1	0.07	3.25	0.08	-0.01	6.12	0.39	0.4	5.88	0.2	0.18	5.88
SA/MC-TEMWL	-0.23	-0.23	5.62	0.11	0.09	5.88	-0.45	-0.5	3.25	0.32	0.32	3.25	0.28	0.26	2.75
SA/MC-LE	**-0.52**	-0.44	**2.0**	**0.07**	**0.04**	**1.62**	0.03	-0.07	5.75	0.37	0.38	5.0	0.21	0.19	5.12
SA/MC-LEWL	-0.37	-0.36	3.5	0.09	0.08	4.0	-0.59	-0.63	2.75	0.3	0.27	3.38	0.29	0.26	**2.25**

Impact of the decoder. On Table 6, we report for each decoder separately the combination that yielded the best performance with respect to the NLL-T (top rows) and the NLL-M (bottom rows), on average across all marked datasets. While we previously explained that some variations of event encoding and history encoders worked on average better for a given decoder, it does not necessarily mean that the best combination includes that variation. Regarding the EC decoder, for example, we find that the overall best combination is GRU-EC-TO, while Table 4 showed that the TO encoding

Table 5: Average and median scores, as well as average ranks per decoder and variation of history encoder, for marked datasets. Refer to Section 5.5 for details on the aggregation procedure. Best results are highlighted in bold.

	Marked Datasets														
	NLL-T			PCE			NLL-M			ECE			F1-score		
	Mean	Median	Rank	Mean	Median	Rank	Mean	Median	Rank	Mean	Median	Rank	Mean	Median	Rank
CONS-EC	1.14	1.05	3.0	0.24	0.33	2.88	0.57	0.54	2.75	0.48	0.47	3.0	0.16	0.15	3.0
SA-EC	0.44	0.35	2.0	0.2	0.22	2.12	-0.07	-0.13	1.88	0.41	0.39	2.0	0.24	0.23	1.75
GRU-EC	**0.08**	**0.1**	**1.0**	**0.17**	**0.14**	**1.0**	**-0.25**	**-0.37**	**1.38**	**0.36**	**0.32**	**1.0**	**0.25**	**0.24**	**1.25**
CONS-LNM	-0.08	-0.12	2.0	**0.03**	**0.03**	**1.0**	0.57	0.47	3.0	0.46	0.45	3.0	0.17	0.16	3.0
SA-LNM	-0.16	-0.2	2.5	0.07	0.05	2.5	-0.01	-0.01	1.88	0.42	0.41	1.88	0.22	0.22	1.88
GRU-LNM	**-0.25**	**-0.26**	**1.5**	0.07	0.07	2.5	**-0.24**	**-0.07**	**1.12**	**0.4**	**0.39**	**1.12**	**0.23**	**0.23**	**1.12**
CONS-FNN	0.72	0.65	3.0	0.16	0.23	2.75	0.44	0.24	2.88	0.45	0.46	2.88	0.19	0.18	2.62
SA-FNN	0.35	0.25	1.88	**0.15**	0.21	2.0	-0.06	-0.04	2.0	0.43	**0.43**	1.75	**0.2**	**0.2**	1.88
GRU-FNN	**0.12**	**0.08**	**1.12**	0.15	**0.18**	**1.25**	**-0.27**	**-0.16**	**1.12**	**0.4**	0.44	**1.38**	0.2	0.19	**1.5**
CONS-MLP/MC	0.47	0.41	3.0	0.15	0.17	2.88	0.31	0.35	2.5	0.38	0.37	2.25	0.24	0.23	2.5
SA-MLP/MC	0.07	-0.01	2.0	0.14	0.14	2.0	-0.05	-0.1	2.12	0.37	0.36	2.5	0.25	0.24	2.25
GRU-MLP/MC	**-0.18**	**-0.18**	**1.0**	**0.13**	**0.11**	**1.12**	**-0.17**	**-0.28**	**1.38**	**0.32**	**0.3**	**1.25**	**0.26**	**0.25**	**1.25**
CONS-RMTPP	0.7	0.67	3.0	0.14	0.16	2.5	0.86	0.63	2.88	0.47	0.47	3.0	0.15	0.15	3.0
SA-RMTPP	0.07	0.05	1.88	0.13	0.13	2.0	-0.43	-0.4	2.12	0.37	0.34	1.88	0.27	0.24	1.88
GRU-RMTPP	**-0.16**	**-0.14**	**1.12**	**0.12**	**0.1**	**1.5**	**-0.99**	**-0.52**	**1.0**	**0.31**	**0.29**	**1.12**	**0.29**	**0.27**	**1.12**
CONS-SA/CM	2.51	-0.02	3.0	0.09	0.12	2.62	0.51	0.36	2.75	0.43	0.44	2.25	0.19	**0.16**	2.12
SA-SA/CM	2.12	-0.2	1.88	**0.08**	**0.08**	2.0	0.09	-0.01	**1.62**	**0.42**	**0.43**	2.0	0.19	0.15	**1.5**
GRU-SA/CM	**1.78**	**-0.24**	**1.12**	0.08	0.08	**1.38**	**0.08**	**-0.06**	1.62	0.42	0.43	**1.75**	**0.2**	0.16	2.38
CONS-SA/MC	0.37	0.29	3.0	0.14	0.16	2.88	0.33	0.25	2.75	0.39	0.39	2.5	0.22	0.22	2.25
SA-SA/MC	-0.07	-0.11	1.75	**0.13**	**0.13**	1.75	-0.18	-0.26	**1.5**	0.37	0.36	**1.75**	**0.23**	**0.23**	2.12
GRU-SA/MC	**-0.11**	**-0.12**	**1.25**	0.13	0.13	**1.38**	**-0.23**	**-0.28**	1.75	**0.36**	**0.35**	1.75	0.23	0.23	**1.62**

performed poorly on average on the NLL-T. In this case, the high NLL-T score for TO was only due to the SA encoder performing particularly badly when equipped with this encoding. Moreover, we find that a single combination does not perform equally well on both metrics separately. In the following, we will thus focus our discussion on the top-row models for time-related metrics (NLL-T, PCE), and on bottom-row models for the mark-related ones (NLL-M, ECE, F1-score).

As a first observation, we note that LNM achieves the lowest NLL-T, outperforming all other baselines. The difference in performance with the LN decoder further suggests that the assumption of log-normality for the distribution of the inter-arrival times is not a sufficient inductive bias by itself and that the additional flexibility granted by the mixture is necessary to achieve a lower NLL-T. Specifically, some distributions of inter-arrival times displayed in Figure 2 show multi-modality (e.g. LastFM, MOOC, Wikipedia), a characteristic that the uni-modal LN decoder cannot capture. Most neural baselines achieve on average lower NLL-T than their parametric counterparts, indicating that high-capacity models are more amenable to capturing complex patterns in real-world event data.

Figure 3 shows $\lambda^*(t)$ (orange) and $f^*(t)$ (green) between two events in a test sequence in LastFM, for the combinations of Table 6 that performed the best on the NLL-T. The greater the gap between $\lambda^*(t)$ and $f^*(t)$, the higher the cumulative GCIF between two events. We observe that most decoders learn to assign a high probability to very low inter-arrival times, which allows them to reach low NLL-T on datasets where events are highly clustered, such as LastFM. This behavior is only possible if the GCIF is allowed to vary rapidly once a new event is observed. As discussed previously, for decoders employing a Softplus activation, such as MLP/MC, FNN, or SA/CM, a

Table 6: Average and median scores, and average ranks of the best combinations per decoder on the NLL-T (top rows) and NLL-M (bottom row) across all marked datasets. Best results are highlighted in bold.

	Marked Datasets														
	NLL-T			PCE			NLL-M			ECE			F1-score		
	Mean	Median	Rank	Mean	Median	Rank	Mean	Median	Rank	Mean	Median	Rank	Mean	Median	Rank
GRU-EC-TO	-0.06	-0.01	7.75	0.17	0.14	9.12	-0.14	-0.1	7.12	0.39	0.41	7.38	0.21	0.18	7.62
GRU-LNM-CONCAT	**-0.91**	**-0.79**	**1.12**	**0.02**	**0.01**	**1.38**	-2.35	-1.16	**2.25**	0.23	0.18	3.12	0.38	0.34	2.5
GRU-LN-LEWL	-0.37	-0.49	5.5	0.07	0.04	6.12	-1.42	-1.08	3.38	0.28	0.28	5.0	0.33	0.35	3.75
GRU-FNN-LCONCAT	-0.52	-0.57	3.75	0.03	0.02	2.75	-1.75	-0.87	4.12	0.28	0.3	4.0	0.28	0.26	4.62
GRU-MLP/MC-LTO	-0.35	-0.32	5.0	0.09	0.05	5.88	0.34	0.23	9.0	0.34	0.38	6.38	0.22	0.19	7.25
GRU-RMTPP-LCONCAT	-0.48	-0.44	4.75	0.04	0.03	5.0	-1.63	**-1.25**	2.62	0.22	0.15	3.12	0.4	0.35	**2.12**
GRU-SA/CM-LCONCAT	-0.43	-0.43	5.88	0.03	0.03	3.12	-0.34	-0.39	6.0	0.39	0.41	7.25	0.24	0.23	7.62
GRU-SA/MC-LE	-0.56	-0.45	4.38	0.08	0.05	5.5	0.01	-0.08	7.75	0.35	0.37	6.75	0.21	0.2	7.12
Hawkes	0.76	-0.11	7.62	0.11	0.1	6.5	**-4.02**	-0.71	4.5	**0.15**	**0.13**	**2.12**	**0.45**	**0.43**	2.62
Poisson	1.17	1.05	10.75	0.24	0.34	10.25	1.27	0.83	10.75	0.48	0.48	10.5	0.16	0.15	10.5
NH	0.87	0.9	9.5	0.24	0.32	10.38	0.15	0.26	8.5	0.48	0.47	10.38	0.17	0.16	11.0
GRU-EC-TEMWL	0.17	0.13	8.12	0.18	0.16	8.75	-1.21	-0.89	4.88	0.29	0.24	6.12	0.3	0.3	6.0
GRU-LNM-CONCAT	**-0.91**	**-0.79**	**1.12**	**0.02**	**0.01**	**1.5**	-2.35	**-1.16**	**2.5**	0.23	0.18	4.25	0.38	0.34	**2.75**
GRU-LN-CONCAT	-0.37	-0.49	4.62	0.07	0.04	5.38	-2.41	-1.07	3.12	0.25	0.25	4.5	0.33	0.34	3.88
GRU-FNN-LCONCAT	-0.52	-0.57	2.88	0.03	0.02	2.75	-1.75	-0.87	5.38	0.28	0.3	4.88	0.28	0.26	5.75
GRU-MLP/MC-LCONCAT	-0.33	-0.32	5.25	0.09	0.06	6.12	-1.2	-0.66	6.5	0.25	0.27	4.38	0.31	0.3	5.12
GRU-RMTPP-LCONCAT + B	-0.41	-0.44	5.0	0.05	0.04	5.0	-2.52	-1.07	3.38	0.2	0.16	3.62	0.38	0.37	3.25
SA-SA/CM-LCONCAT	-0.38	-0.43	5.88	0.04	0.03	3.5	-0.36	-0.24	8.12	0.37	0.41	8.12	0.24	0.25	8.5
SA-SA/MC-CONCAT	-0.29	-0.35	5.75	0.1	0.08	5.88	-0.66	-0.69	6.88	0.3	0.3	6.5	0.28	0.27	6.62
Hawkes	0.76	-0.11	7.62	0.11	0.1	6.38	**-4.02**	-0.71	5.38	**0.15**	**0.13**	**2.75**	**0.45**	**0.43**	3.12
Poisson	1.17	1.05	10.75	0.24	0.34	10.38	1.27	0.83	10.88	0.48	0.48	10.5	0.16	0.15	10.75
NH	0.87	0.9	9.0	0.24	0.32	10.38	0.15	0.26	9.0	0.48	0.47	10.38	0.17	0.16	11.0

steeper gradient for the GCIF can be obtained at low inter-arrival times by using the LTO or LCONCAT encodings.

With respect to the mark prediction task, we find that the Hawkes decoder achieves the overall best results, outperforming all baselines in terms of NLL-M, ECE, and F1-score. While the Hawkes decoder did not perform favorably on time-related metrics, its clear superiority compared to more complex models on the mark prediction task is rather intriguing. Likewise, the RMTPP and LN(M) decoders also show competitive performance on these metrics, despite their simplifying assumption of marks being independent of the time given the history of the process. The overall superiority of parametric and semi-parametric architectures on the mark prediction task suggests that non-parametric decoders may actually suffer from their high flexibility, making them hard to optimize in practice. This particularly stands out for the NH decoder which performs extremely badly on all metrics, only marginally outperforming the Poison decoder. Nonetheless, although LN, LNM, RMTPP, and Hawkes do better than their non-parametric counterparts, we find that all decoders perform rather poorly on the mark prediction task.

Figure 4 shows the CD diagrams between the average ranks of all decoders at the $\alpha = 0.1$ significance level, on each metric separately. The lower the rank (further to the left on the top horizontal axis), the better the performance of a decoder with respect to that metric, while a bold black line groups decoders that are not significantly different from one another. As can be seen, there are clear differences between the models' average ranks (e.g. LNM on the NLL-T for marked datasets). The fact that Holm's posthoc tests do not allow us to conclude statistically significant differences between them can be explained by a large number of pairwise comparisons compared to the few available samples (datasets), which results in high adjusted p-values.

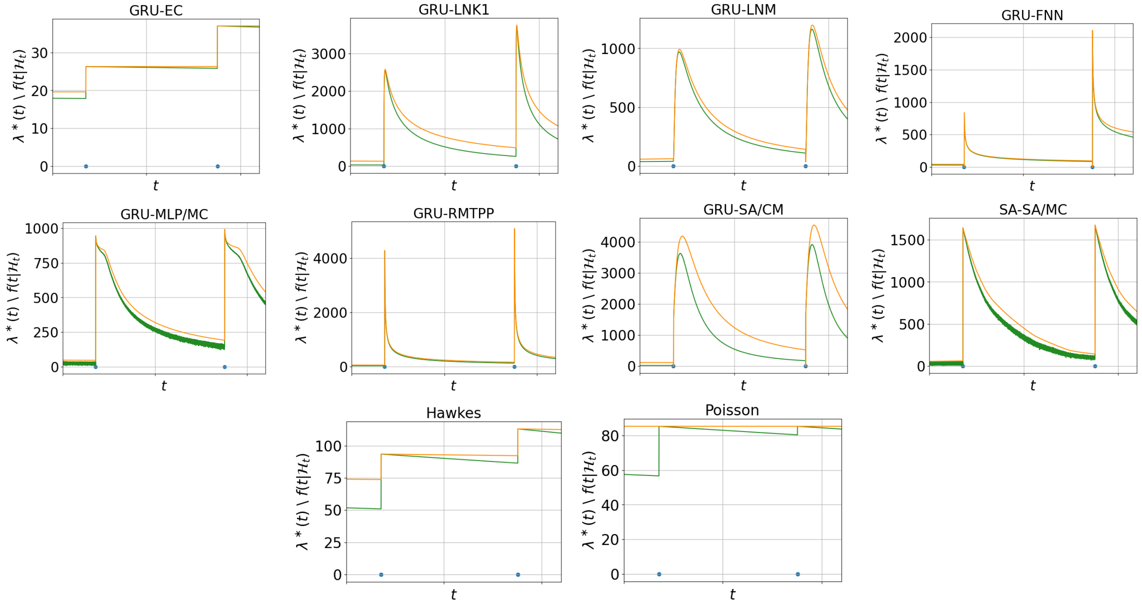

Figure 3: Evolution of $\lambda^*(t)$ (orange) and $f(t|\mathcal{H}_t)$ (green) between two events on the LastFM dataset. Arrival times correspond to 2.0975 and 2.0986, respectively.

On the calibration of TPP models. Figure 5 shows the reliability diagrams for the inter-arrival time predictive distributions associated with the combinations presented in Table 6, averaged over all marked datasets. We observe good marginal calibration of the LNM, FNN, MLP/MC, RMTPP, and SA/CM decoders, as demonstrated by their curves closely matching the diagonal. On the other hand, the other decoders present higher degrees of miscalibration. More precisely, their empirical CDF lays systematically above the diagonal line, which suggests that the distributions attribute little probability mass to low inter-arrival times. This observation supports our argument about the behavior of $f^*(\tau)$ on Figure 3, i.e. the conditional density of calibrated models attributes most probability to short inter-arrival times.

Figure 6 shows the reliability diagrams for the mark distributions associated with the best-performing combinations (in terms of the NLL-M) in Table 6, aggregated over all marked datasets. Overall, we observe that the calibration of these decoders mirrors their performance on the NLL-M and F1-scores, i.e. better scores with respect to these metrics correspond to better calibration. Indeed, the Hawkes decoder is the best-calibrated model among our baselines, followed by RMTPP and LNM. Nonetheless, we note that all decoders are usually over-confident in their predictions, as shown by the bin accuracies falling systematically below the diagonal line.

Impact of the history size. When training a neural TPP model, we usually assume that the *complete* history $\mathcal{H}_{t_i}$ from the first to the last observed event, could contain insightful information about the process dynamics. In other terms, the joint distribution of an event $e_i = (t_i, k_i)$ is by default modeled as being dependent on the complete history of the process up to e_i, i.e $f(e_i|\mathcal{H}_{t_i}) = f(e_i|e_{i-1}, ...e_1)$. However, in some real-world situations, it might be more appropriate to assume (explicitly) that the process actually possesses a Markovian property, i.e. only q of the last $i -$

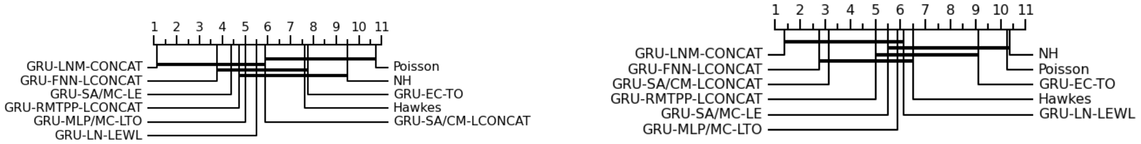

(a) NLL-T.

(b) PCE.

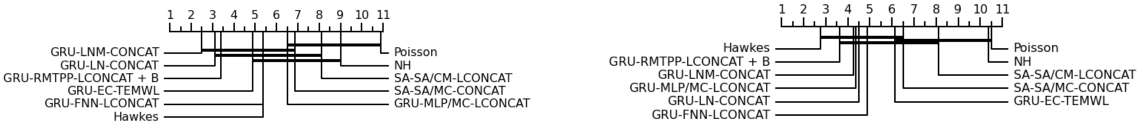

(c) NLL-M.

(d) ECE.

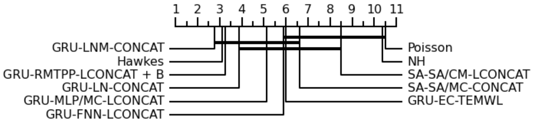

(e) F1-score.

Figure 4: Critical Distance (CD) diagrams per metric at the $\alpha = 0.10$ significance level for all decoders on marked datasets. The decoders' average ranks are displayed on top, and a bold line joins the decoders' variations that are not statistically different.

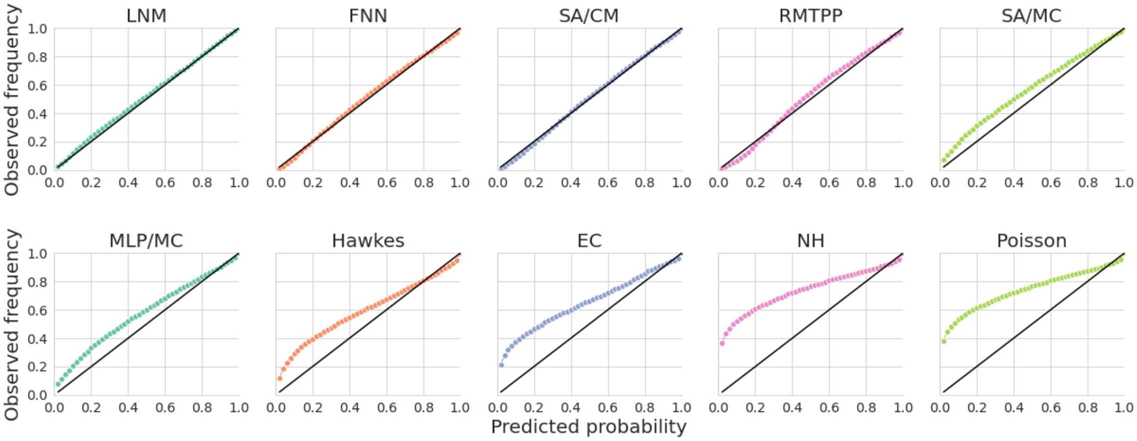

Figure 5: Reliability diagrams of the distribution of inter-arrival times for the decoder's combinations that performed the best on the NLL-T (top rows of Table 6), averaged over all marked datasets. The bold black line corresponds to perfect marginal calibration.

1 events preceding e_i have an actual influence on the distribution of e_i. When comparing the influence of the different encoders, we concluded that efficient encoding of a process' history is indeed paramount to modeling this joint distribution. However, it does not inform us of the number

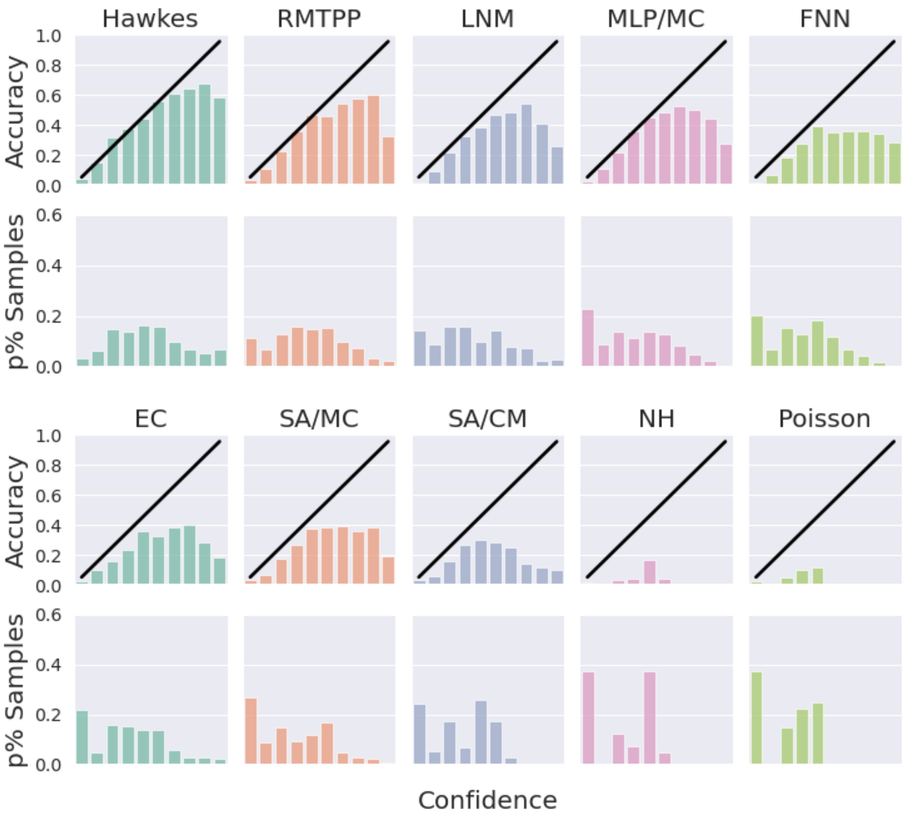

Figure 6: Reliability diagrams of the distribution of marks for various decoders, averaged over all marked datasets. Front rows depict a decoder's average accuracy per bin, while bottom rows show the average proportion of samples falling per bin. Bins aligning with the bold black line corresponds to perfect calibration.

of past events that truly contain useful information. To answer this question, we train the models by employing variations of both the GRU and self-attention history encoders, which generate a history embedding $\boldsymbol{h}_i$ for the event e_i only out of $\mathcal{H}^q_{t_i} = \{(t_j, k_j) \in \mathcal{H} | t_j < t_i,\ i - q \leq j < i\}$, i.e. $\boldsymbol{h}_i$ is constructed with at most q events preceding e_i.

In Figure 7, we show the evolution of the NLL-T and NLL-M (when relevant), by varying the maximal history size q to which the history encoder has access to during training. We report our observations for the GRU encoder operating on this fixed-size window (GRU-Fixed), but similar results were obtained for a fixed self-attentive encoder (SA-Fixed). Compared to a completely masked history, which is equivalent to training the model with the CONS encoder (i.e. $q = 0$), we observe a substantial improvement in NLL-T for most models when only the last event is made available to the encoder. This indicates a process' past does indeed contain useful information. However, as observed on most datasets, additional context does not yield significant improvement, with an NLL-T that often quickly stabilizes as q increases.

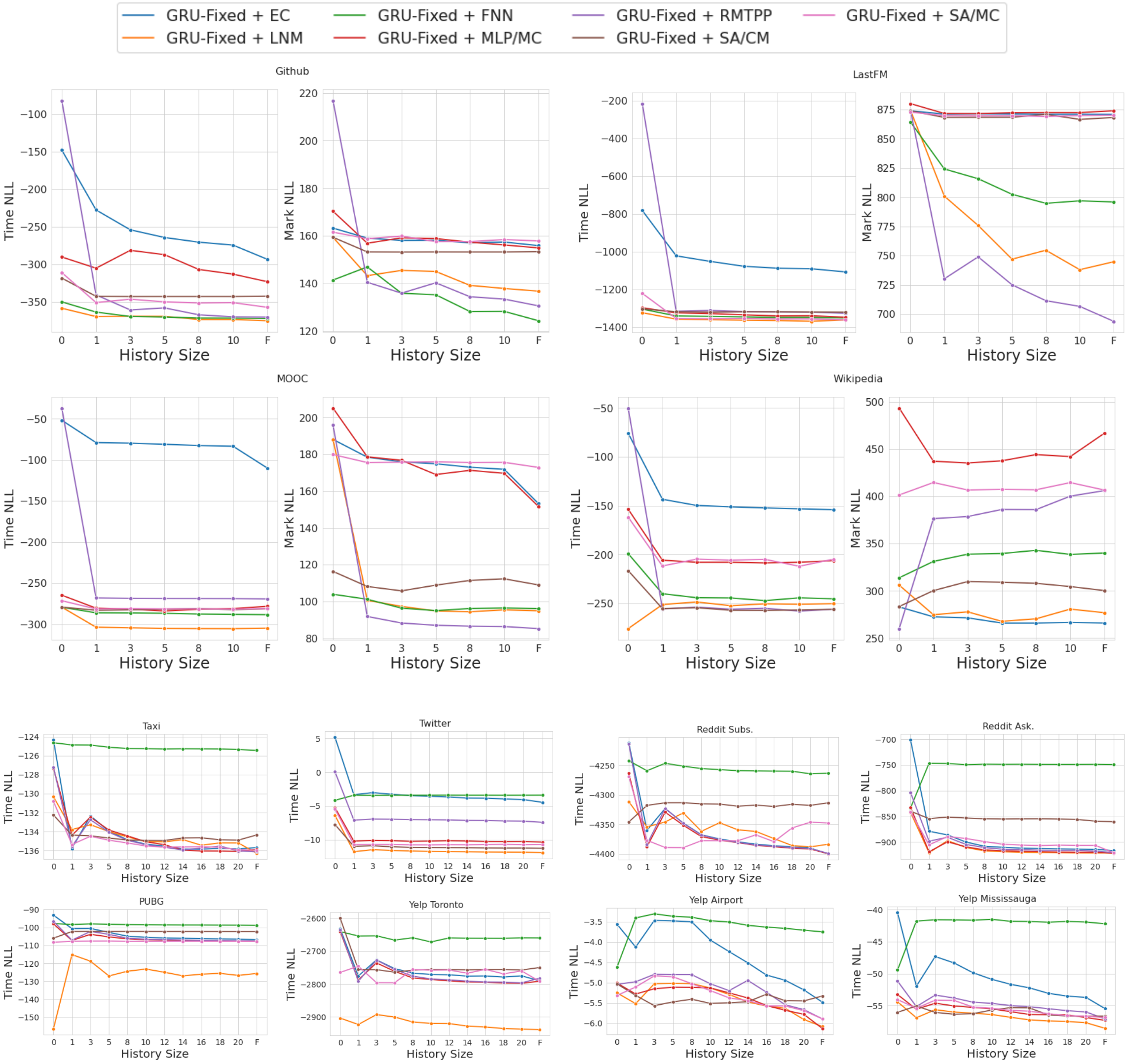

Figure 7: Evolution of models' performance with respect to the Time NLL, and the Mark NLL when available, as a function of the maximal number of events used to construct $\boldsymbol{h}_i$ when using a GRU operating on a fixed-size window. 'F' refers to the unconstrained GRU, i.e. the encoder having access to the full history.

On the one hand, this finding suggests that real-world processes do possess a Markovian property and that going far in history does not bring valuable additional insight regarding the arrival time of the next event. On the other hand, it could also indicate that RNNs (and self-attention mechanisms) fail to capture long-term dependencies among event occurrences in the context of TPPs and that more research is needed to design better alternatives to encode the history. Furthermore, the EC decoder appears to be more impacted on the NLL-T as q increases than other baselines. Considering

(a) Marked datasets.

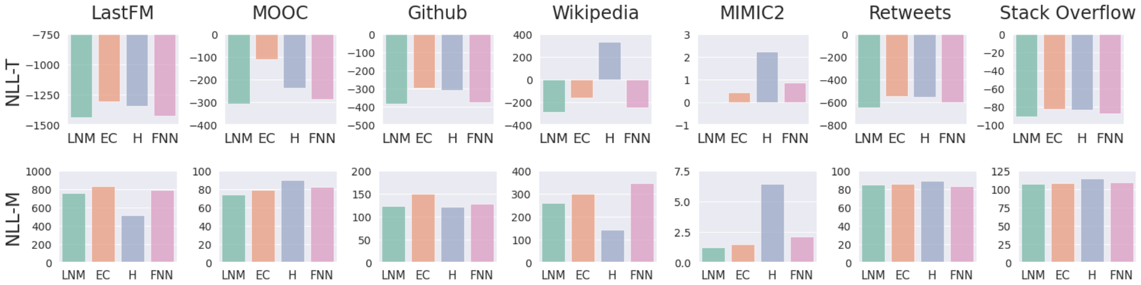

(b) Unmarked datasets.

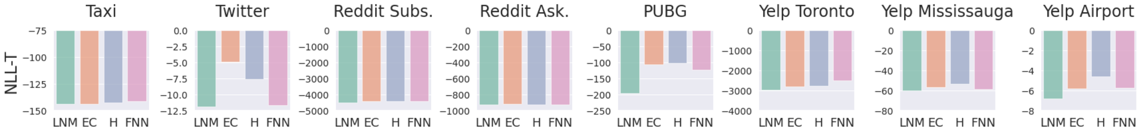

Figure 8: Performance OF LNM, EC, Hawkes (H), and SA/CM on the NLL-T and NLL-M for each dataset.

that this decoder can only leverage the history embedding to define the MCIF, we hypothesize that optimization may in this case force the encoder to extract as much information as possible from the patterns of previous marks occurrences.

A similar statement can be made for the NLL-M. However, we find continuous improvement as q increases for FNN, RMTPP, and LNM on Github and LastFM. As LNM and RMTPP parametrize the mark distribution solely from $\boldsymbol{h}_i$, they also require expressive representations of the history to perform well with respect to the NLL-M.

On the adequacy of TPPs datasets. A concern that is rarely addressed in the neural TPP literature relates to the validity of the current benchmark datasets for neural TPP models. Enguehard et al. (2020) raised some concerns regarding MIMIC2 and Stack Overflow as the simple time-independent EC decoder yielded competitive performance with more complex baselines on such datasets. Figure 8 reports both NLL-T and NLL-M (when available) for LNM, EC, Hawkes and FNN decoders[7] on all real-world datasets. We indeed observe that the EC decoder is competitive with LNM on the NLL-T and NLL-M for MIMIC2 and Stack Overflow, supporting their recommendation that future research should show a certain degree of caution when benchmarking new methods on these datasets. We further express additional concerns about Taxi, Reddit Subs and Reddit Ask Comments, Yelp Toronto, and Yelp Mississauga, on which all decoders achieve comparable performance. All remaining datasets appear to be appropriate benchmarks for evaluating neural TPP models, as higher variability is observed in the results.

---

[7] Here also, we employed the combinations on the top row of Table 6 to compute the NLL-T on marked datasets, and the combinations of Table 10 to compute the NLL-T on unmarked datasets. The NLL-M was computed using the combinations on the bottom row of Table 6.

Computational times. On Table 7, we report for each decoder the average computing time (in seconds) averaged over 10 epochs for a single forward and backward pass on the training sequences of MOOC dataset. All decoders were equipped with the GRU history encoder and the TEMWL event encoding, when relevant (i.e. not for Hawkes, Poisson and NH), with similar hyper-parameters configurations. Additionally, the batch size was 32, and the average running time was taken over 10 epochs on a NVIDIA RTX A5000. With respect to the results on both the time and mark prediction tasks, we find LNM to provide the best performance/runtime trade-off among all the decoders considered in the study. On the other hand, the NH decoder is extremely expensive to train, while generally performing worse than other neural baselines.

Table 7: Average execution time in seconds per decoder for a single forward and backward pass on the MOOC dataset.

EC	LNM	MLP/MC	FNN	RMTPP	SA/CM	SA/MC	Hawkes	Poisson	NH
1.67	2.05	2.34	3.31	1.83	5.41	3.48	18.17	0.95	319.74

7 Conclusion

We conducted a large-scale empirical study of state-of-the-art neural TPP models using multiple real-world and synthetic event sequence datasets in a carefully designed unified setup. Specifically, we studied the influence of major architectural components on predictive accuracy and highlighted that some specific combinations of architectural components can lead to significant improvements for both time and mark prediction tasks. Moreover, we assessed the rarely discussed topic of probabilistic calibration for neural TPP models and found that the mark distributions are often poorly calibrated despite time distributions being well calibrated. Additionally, while recurrent encoders are better at capturing a process' history, we found that solely encoding a few of the last observed events yielded comparable performance to an embedding of the complete history for most datasets and decoders. Finally, we confirmed the concerns of previous research regarding the commonly used datasets for benchmarking neural TPP models and raised concerns about others. We believe our findings will bring valuable insights to the neural TPP research community, and we hope will inspire future work.

References

Milton Abramowitz and Irene A. Stegun. Handbook of mathematical functions: With formulas, graphs, and mathematical tables, 1965. Courier Corporation.

Emmanuel Bacry, Martin Bompaire, Philip Deegan, Stéphane Gaïffas, and Søren V. Poulsen. tick: a python library for statistical learning, with an emphasis on hawkes processes and time-dependent models, 2018. 18:1-5, Journal of Machine Learning Research.

Emmanuel Bacry, Martin Bompaire, Stéphane Gaïffas, and Jean-François Muzy. Sparse and low-rank multivariate hawkes processes, 2020. 21:1817–1848, Journal of Machine Learning Research.

Souhaib Ben Taieb. Learning quantile functions for temporal point processes with recurrent neural splines, 2022. AISTATS.

Alex Boyd, Robert Bamler, Stephan Mandt, and Padhraic Smyth. User-dependent neural sequence models for continuous-time event data, 2020. Neurips.

Renqin Cai, Xueying Bai, Zhenrui Wang, Yuling Shi, Parikshit Sondhi, and Hongning Wang. Modeling sequential online interactive behaviors with temporal point process, 2018. CIKM.

Ricky T. Q. Chen, Brandon Amos, and Maximilian Nickel. Neural spatio-temporal point processes, 2021. ICLR.

Manon Costa, Carl Graham, Laurence Marsalle, and Viet Chi Tran. Renewal in hawkes processes with self-excitation and inhibition. 2020. 52(3):879–915, Advances in Applied Probability.

Daryl Daley and David Vere-Jones. An introduction to the theory of point processes volume ii: General theory and structure, 2007.

A. P. Dawid. Present position and potential developments: Some personal views: Statistical theory: The prequential approach., 1984. Journal of the Royal Statistical Society. Series A, 147:278-292.

A. De, U. Upadhyay, and M. Gomez-Rodriguez. Temporal point processes, 2019. Notes for Human-Centered ML, Saarland University.

Janez Demšar. Statistical comparisons of classifiers over multiple data sets., 2006. Journal of Machine Learning Research, 7:1-30.

Nan Du, Hanjun Dai, Rakshit Trivedi, Utkarsh Upadhyay, Manuel Gomez-Rodriguez, and Le Song. Recurrent marked temporal point processes: Embedding event history to vector, 2016. SIGKDD.

Céline Duval, Eric Luçon, and Christophe Pouzat. Interacting hawkes processes with multiplicative inhibition, 2022. 148:180-226, Stochastic Processes and their Applications.

Mike Egesdal, Chris Fathauer, Kym Louie, Jeremy Neuman, George Mohler, and Erik Lewis, 2010. SIAM Undergraduate Research Online.

Joseph Enguehard, Dan Busbridge, Adam Bozson, Claire Woodcock, and Nils Y. Hammerla. Neural temporal point processes for modelling electronic health records, 2020. ML4H.

Mehrdad Farajtabar, Yichen Wang, Manuel Gomez Rodriguez, Shuang Li, Hongyuan Zha, and Le Song. Coevolve: A joint point process model for information diffusion and network co-evolution, 2015. Neurips.

Milton Friedman. The use of ranks to avoid the assumption of normality implicit in the analysis of variance., 1937. Journal of the American Statistical Association, 32:675–701.

Milton Friedman. A comparison of alternative tests of significance for the prob lem of m rankings., 1940. Annals of Mathematical Statistics, 11:86–92.

Salvador García and Francisco Herrera. An extension on "statistical comparisons of classifiers over multiple data sets" for all pairwise comparisons, 2008. Journal of Machine Learning Research, 9:2677-2694.

Tilmann Gneiting, Fadoua Balabdaoui, and Adrian E. Raftery. Probabilistic forecasts, calibration and sharpness, 2007. Journal of the Royal Statistical Society: Series B (Statistical Methodology).

Chuan Guo, Geoff Pleiss, Yu Sun, and Kilian Q. Weinberger. On calibration of modern neural networks, 2017. ICML.

Ruocheng Guo, Jundong Li, and Huan Liu. Initiator: Noise-contrastive estimation for marked temporal point process, 2018. IJCAI.

Alan G Hawkes. Point spectra of some mu- tually exciting point processes, 1971. Journal of the Royal Statistical Society: Series B, 33(3).

Alan G. Hawkes. Hawkes processes and their applications to finance: a review, 2018. Quantitative Finance, 18:2, 193-198.

Sture Holm. A simple sequentially rejective multiple test procedure., 1979. Scandinavian Journal of Statistics, 6:65–70.

Valerie Isham and Mark Westcott. A self-correcting point process., 1979. Stochastic Processes and Their Applications, 8(3):335–347.

Seyed Mehran Kazemi, Rishab Goel, Sepehr Eghbali, Janahan Ramanan, Jaspreet Sahota, Sanjay Thakur, Stella Wu, Cathal Smyth, Pascal Poupart, and Marcus Brubaker. Time2vec: Learning a vector representation of time, 2019.

Diederik P. Kingma and Jimmy Ba. Adam: A method for stochastic optimization, 2014. ICLR.

Christian Kleiber and Samuel Kotz. Statistical size distributions in economics and actuarial sciences, 2003. Wiley, p. 179.

Volodymyr Kuleshov, Nathan Fenner, and Stefano Ermon. Accurate uncertainties for deep learning using calibrated regression, 2018. ICML.

Srijan Kumar, Xikun Zhang, and Jure Leskovec. Predicting dynamic embedding trajectory in temporal interaction networks. In *Proceedings of the 25th ACM SIGKDD international conference on Knowledge discovery and data mining*, 2019. KDD.

Haitao Lin, Cheng Tan, Lirong Wu, Zhangyang Gao, and Stan. Z. Li. An empirical study: Extensive deep temporal point process, 2021.

Haitao Lin, Lirong Wu, Guojiang Zhao, Pai Liu, and Stan Z. Li. Exploring generative neural temporal point process, 2022. TMLR.

B. H. Lindqvist, Elvebakk G., and K. Heggland. The trend-renewal process for statistical analysis of repairable systems., 2003. Technometrics 45, no. 1 (2003): 31–44.

Thomas Josef Liniger. Multivariate hawkes processes., 2009. Diss., Eidgenossische Technische Hochschule ETH Zurich.

Hongyuan Mei and Jason Eisner. The neural hawkes process: A neurally self-modulating multivariate point process, 2016. Neurips.

Hongyuan Mei, Tom Wan, and Jason Eisner. Noise-contrastive estimation for multivariate point processes, 2020. Neurips.

Mahdi Pakdaman Naeini, Gregory F. Cooper, and Milos Hauskrecht. Obtaining well calibrated probabilities using bayesian binning, 2015. AAAI.

Yosihiko Ogata. Space-time point-process models for earthquake occurrences, 1998. Annals of the Institute of Statistical Mathematics, 50(2):379–402.

Takahiro Omi, Naonori Ueda, and Kazuyuki Aihara. Fully neural network based model for general temporal point processes. 2019. Neurips.

Jakob Gulddahl Rasmussen. Lecture notes: Temporal point processes and the conditional intensity function, 2018.

Marian-Andrei Rizoiu, Swapnil Mishra, Quyu Kong, Mark Carman, and Lexing Xie. Sir-hawkes: Linking epidemic models and hawkes processes to model diffusions in finite populations, 2018. Proceedings of the 2018 World Wide Web Conference on World Wide Web.

Oleksandr Shchur, Marin Biloš, and Stephan Günnemann. Intensity-free learning of temporal point processes, 2019. ICLR.

Oleksandr Shchur, Nicholas Gao, Marin Biloš, and Stephan Günnemann. Fast and flexible temporal point processes with triangular maps, 2020. Neurips.

Oleksandr Shchur, Ali Caner Türkmen, Tim Januschowski, and Stephan Günnemann. Neural temporal point processes: A review, 2021. Proceedings of 13th Joint Conference on Artificial Intelligence.

Sra Suvrit, Nowozin Sebastian, and J. Wright Stephen. Optimization for machine learning, 2011. MIT Press.

Rakshit Trivedi, Mehrdad Farajtabar, Prasenjeet Biswal, and Hongyuan Zha. Representation learning over dynamic graphs, 2018. ICLR.

Utkarsh Upadhyay, Abir De, and Manuel Gomez-Rodriguez. Deep reinforcement learning of marked temporal point processes, 2018. Neurips.

Ashish Vaswani, Noam Shazeer, Niki Parmar, Jakob Uszkoreit, Llion Jones, Aidan N. Gomez, Lukasz Kaiser, and Illia Polosukhin. Attention is all you need, 2017. Neurips.

Govind Waghmare, Ankur Debnath, Siddhartha Asthana, and Aakarsh Malhotra. Modeling interdependence between time and mark in multivariate temporal point processes, 2022. CIKM.

Yichen Wang, Bo Xie, Nan Du, and Le Song. Isotonic hawkes processes, 2016. 33rd International Conference on Machine Learning.

Andreas Wienke. Frailty models in survival analysis, 2010. Chapman and Hall/CRC.

Shuai Xiao, Mehrdad Farajtabar, Xiaojing Ye, Junchi Yan, Le Song, and Hongyuan Zha. Wasserstein learning of deep generative point process models, 2017a. Neurips.

Shuai Xiao, Junchi Yan, Stephen M. Chu, Xiaokang Yang, and Hongyuan Zha. Modeling the intensity function of point process via recurrent neural networks, 2017b. AAAI.

Shuai Xiao, Honteng Xu, Junchi Yan, Mehrdad Farajtabar, Xiaokang Yang, Le Song, and Hongyuan Zha. Learning conditional generative models for temporal point processes, 2018. AAAI.

Junchi Yan. Recent advance in temporal point process : from machine learning perspective, 2019.

Qiang Zhang, Aldo Lipani, Omer Kirnap, and Emine Yilmaz. Self-attentive hawkes processes, 2020. ICML.

Simiao Zuo, Haoming Jiang, Zichong Li, Tuo Zhao, and Hongyuan Zha. Transformer hawkes process, 2020. ICML.

A Results on unmarked datasets.

We report the comparison of different event encoding mechanisms and history encoders for unmarked datasets in Table 8 and Table 9, respectively, where we also added the worst score of each component's variation. The results of the combinations that performed best with respect to the NLL-T can be found in Table 10. Overall, our findings regarding unmarked datasets align with the ones described in Section 6. However, we note that most decoders show a lower PCE, and hence, improved calibration with respect to the distribution of inter-arrival time compared to marked datasets. The reliability diagrams displayed on Figure 9 for unmarked datasets do indeed confirm this observation.

On Figure 10, we report the CD diagrams between all combinations of Table 10 for the NLL-T and PCE. As for marked datasets, not enough evidence in the data allows to conclude of statistical differences between decoders at the $\alpha = 0.1$ significance level, despite clear separation in the average ranks.

Table 8: Average, median, and worst scores, as well as average ranks per decoder and variation of event encoding, for unmarked datasets. Refer to Section 5.5 for details on the aggregation procedure. Best scores are highlighted in bold.

	Unmarked Datasets							
	NLL-T				PCE			
	Mean	Median	Worst	Rank	Mean	Median	Worst	Rank
EC-TO	0.25	0.24	0.6	3.5	0.07	0.06	0.16	3.25
EC-LTO	0.25	0.26	0.64	3.5	0.07	0.06	0.16	3.62
EC-TEM	**-0.21**	**-0.26**	**0.31**	**1.0**	**0.05**	**0.03**	**0.14**	**1.25**
EC-LE	-0.09	-0.04	0.46	2.0	0.05	0.03	0.15	1.88
LNM-TO	-1.15	-0.5	-0.26	3.0	**0.01**	**0.01**	**0.01**	3.12
LNM-LTO	-1.17	-0.57	-0.25	3.38	0.01	0.01	0.01	2.25
LNM-TEM	**-1.46**	**-0.79**	**-0.51**	**1.12**	0.01	0.01	0.01	**1.5**
LNM-LE	-0.98	-0.59	-0.44	2.5	0.01	0.01	0.01	3.12
FNN-TO	0.7	0.6	1.06	2.62	0.09	0.09	0.15	2.62
FNN-LTO	**-0.19**	**-0.25**	1.69	**1.25**	**0.02**	**0.01**	**0.06**	**1.0**
FNN-LE	0.56	0.5	**1.03**	2.12	0.08	0.07	0.15	2.38
MLP/MC-TO	-0.02	0.0	0.1	3.75	0.05	0.04	0.08	3.62
MLP/MC-LTO	-0.14	-0.17	0.06	2.5	**0.03**	0.03	0.08	**1.88**
MLP/MC-TEM	-0.23	-0.21	**-0.04**	2.12	0.04	0.03	0.09	2.62
MLP/MC-LE	**-0.3**	**-0.33**	-0.04	**1.62**	0.03	**0.02**	**0.07**	1.88
RMTPP-TO	-0.07	-0.07	0.11	3.75	0.04	0.03	0.08	3.75
RMTPP-LTO	-0.21	-0.13	0.2	2.75	**0.02**	**0.02**	**0.03**	2.0
RMTPP-TEM	**-0.37**	**-0.32**	**-0.25**	**1.25**	0.03	0.02	0.07	**1.88**
RMTPP-LE	-0.3	-0.28	-0.14	2.25	0.03	0.02	0.08	2.38
SA/CM-TO	0.71	0.24	4.19	2.38	0.05	0.03	0.14	2.62
SA/CM-LTO	1.08	0.23	4.93	2.12	0.05	0.03	0.14	2.25
SA/CM-LE	**-0.22**	**-0.18**	**0.19**	**1.5**	**0.02**	**0.01**	**0.05**	**1.12**
SA/MC-TO	0.78	0.66	1.17	3.5	0.09	0.08	0.16	3.38
SA/MC-LTO	0.68	0.69	1.09	3.5	0.09	0.1	0.15	3.38
SA/MC-TEM	-0.42	-0.39	**-0.18**	1.88	**0.02**	**0.01**	**0.07**	**1.62**
SA/MC-LE	**-0.5**	**-0.49**	0.17	**1.12**	0.03	0.02	0.08	1.62

Table 9: Average, median, and worst scores, as well as average ranks per decoder and variation of history encoder, for unmarked datasets. Refer to Section 5.5 for details on the aggregation procedure. Best scores are highlighted in bold.

	Unmarked Datasets							
	NLL-T				PCE			
	Mean	Median	Worst	Rank	Mean	Median	Worst	Rank
CONS-EC	1.03	0.87	2.14	3.0	0.1	0.09	0.2	3.0
SA-EC	0.48	0.54	0.85	2.0	0.08	0.07	0.17	2.0
GRU-EC	**-0.38**	**-0.4**	**0.25**	**1.0**	**0.04**	**0.02**	**0.14**	**1.0**
CONS-LNM	-0.83	-0.16	0.13	2.75	**0.01**	**0.01**	0.02	2.25
SA-LNM	-0.69	-0.26	-0.14	2.25	0.01	0.01	0.02	2.25
GRU-LNM	**-1.7**	**-0.92**	**-0.61**	**1.0**	0.01	0.01	**0.01**	**1.5**
CONS-FNN	0.63	0.53	1.26	2.62	**0.06**	**0.05**	0.13	2.12
SA-FNN	0.46	0.35	1.06	2.25	0.06	0.06	**0.1**	**1.62**
GRU-FNN	**0.25**	**0.16**	**0.94**	**1.12**	0.06	0.06	0.11	2.25
CONS-MLP/MC	0.46	0.5	0.74	2.88	0.06	0.06	0.11	2.88
SA-MLP/MC	0.15	0.17	0.33	2.12	0.05	0.04	0.09	2.0
GRU-MLP/MC	**-0.49**	**-0.47**	**-0.33**	**1.0**	**0.03**	**0.02**	**0.06**	**1.12**
CONS-RMTPP	0.31	0.26	0.79	2.88	0.04	0.03	**0.06**	2.38
SA-RMTPP	0.04	0.01	0.29	2.12	0.04	0.03	0.07	2.38
GRU-RMTPP	**-0.52**	**-0.54**	**-0.33**	**1.0**	**0.02**	**0.01**	0.06	**1.25**
CONS-SA/CM	1.03	0.68	2.87	2.88	0.05	0.04	0.11	2.62
SA-SA/CM	0.53	0.26	**2.7**	1.62	**0.04**	**0.03**	**0.1**	1.88
GRU-SA/CM	**0.51**	**0.2**	3.0	**1.5**	0.04	0.03	0.1	**1.5**
CONS-SA/MC	0.52	0.49	0.86	2.88	0.07	**0.06**	0.11	2.62
SA-SA/MC	0.17	0.21	**0.34**	1.75	**0.06**	0.07	**0.08**	**1.5**
GRU-SA/MC	**0.1**	**0.14**	0.38	**1.38**	0.06	0.07	0.08	1.88

Table 10: Average, median, worst scores, and average ranks of the best combinations per decoder on the NLL-T across all unmarked datasets. Best results are highlighted in bold.

	Unmarked Datasets							
	NLL-T				PCE			
	Mean	Median	Worst	Rank	Mean	Median	Worst	Rank
GRU-EC-TEM + B	-0.41	-0.46	0.16	5.5	0.04	0.02	0.13	7.12
GRU-LNM-TEM	**-1.96**	**-0.95**	**-0.62**	**1.25**	**0.01**	**0.01**	**0.01**	**2.12**
GRU-LNK1-TEM	-0.25	-0.25	0.41	7.0	0.03	0.03	0.07	7.75
GRU-FNN-LTO + B	-0.48	-0.59	1.48	4.12	0.01	0.01	0.05	3.38
GRU-MLP/MC-LTO + B	-0.57	-0.56	-0.44	4.25	0.02	0.01	0.05	5.5
GRU-RMTPP-LTO	-0.6	-0.55	-0.28	4.25	0.01	0.01	0.03	4.12
SA-SA/CM-LE + B	-0.23	-0.15	0.0	7.38	0.02	0.01	0.04	4.5
GRU-SA/MC-LE + B	-0.56	-0.55	0.4	4.12	0.03	0.02	0.1	5.25
Hawkes	-0.22	-0.16	0.16	7.12	0.02	0.01	0.06	5.25
Poisson	4.23	2.54	12.29	11.0	0.25	0.26	0.47	11.0
NH	2.29	1.11	8.2	10.0	0.16	0.15	0.3	10.0

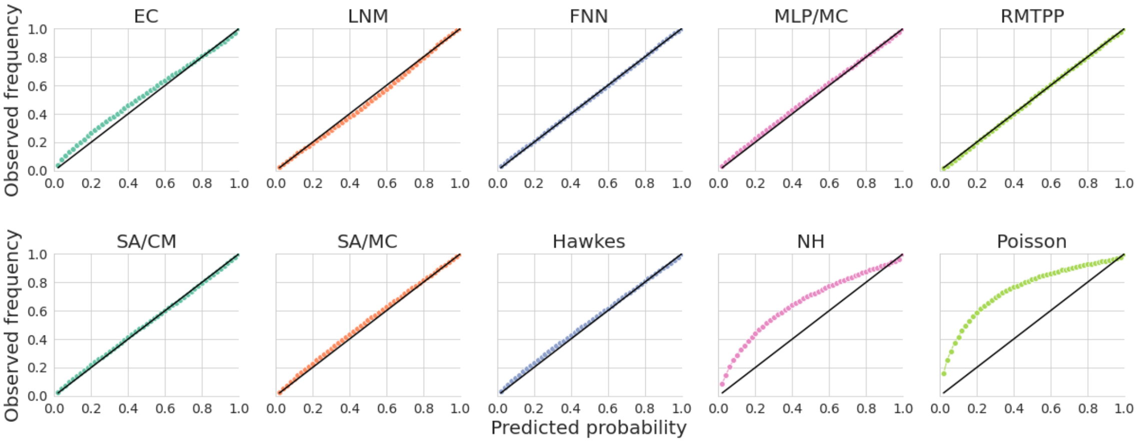

Figure 9: Reliability diagrams of the distribution of inter-arrival times for the decoder's combinations that performed the best on the NLL-T averaged over all unmarked datasets. The bold black line corresponds to perfect marginal calibration.

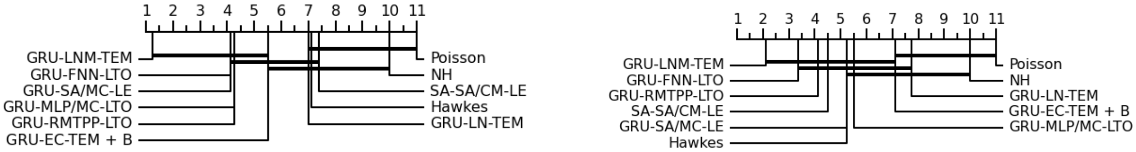

(a) NLL-T.

(b) PCE.

Figure 10: Critical Distance (CD) diagrams per metric at the $\alpha = 0.10$ significance level for all decoders on unmarked datasets. The decoders' average rank are displayed on top, and a bold line joins decoders variations that are not statistically different.

B Additional results

In Table 11, we report the results with respect to all time related metrics (NLL-T, PCE) for all models of Table 6 on marked datasets, while results with respect to marked related metrics (NLL-M, ECE, F1-score) are given in Table 12. In turn, results with respect to time related metrics for models of Table 10 on unmarked datasets are reported in Table 13. Finally, we report on Figure 11 the standardized NLL-T and NLL-M for all models of Table 6 for all marked datasets.

Table 11: Results with respect to the NLL-T and PCE for the combinations of models presented in Table 6 on all marked datasets. Standard error across all splits is reported in parenthesis.

				NLL-T				
	LastFM	MOOC	Wikipedia	Github	MIMIC2	Hawkes	SO	Retweets
GRU-LNM-CONCAT	-1366.61 (59.19)	-304.56 (3.84)	-285.0 (25.98)	-383.36 (59.71)	-0.08 (0.06)	-78.57 (0.78)	-90.45 (1.42)	-646.9 (14.15)
GRU-FNN-LCONCAT	-1350.4 (59.73)	-287.34 (3.34)	-244.96 (31.7)	-372.57 (57.96)	1.75 (0.11)	-78.22 (0.74)	-87.68 (1.31)	-596.29 (2.65)
GRU-SA/CM-LCONCAT	-1329.79 (55.49)	-282.93 (3.98)	-255.19 (30.86)	-348.16 (54.23)	1.77 (0.1)	-77.95 (0.79)	-86.78 (1.38)	-526.73 (1.82)
GRU-RMTPP-LCONCAT	-1331.75 (58.87)	-268.91 (3.25)	-267.41 (24.59)	-382.4 (61.05)	1.66 (0.08)	-78.49 (0.79)	-83.99 (1.47)	-570.73 (2.18)
GRU-SA/MC-LE	-1349.8 (60.0)	-277.66 (3.03)	-207.39 (51.79)	-348.82 (56.8)	0.47 (0.12)	-78.5 (0.76)	-85.17 (1.33)	-581.05 (2.59)
GRU-MLP/MC-LTO	-1355.3 (59.34)	-274.13 (3.8)	-173.31 (41.69)	-332.47 (59.63)	1.67 (0.1)	-78.55 (0.79)	-85.51 (1.28)	-575.5 (2.36)
Hawkes	-1189.48 (55.2)	-235.9 (3.09)	332.83 (93.92)	-308.42 (57.77)	4.49 (0.24)	-78.66 (0.82)	-83.18 (1.4)	-554.6 (2.15)
GRU-EC-TO	-1114.93 (50.98)	-109.66 (1.09)	-158.65 (16.2)	-294.6 (57.97)	0.9 (0.05)	-78.05 (0.78)	-82.27 (1.4)	-547.3 (1.99)
NH	-788.33 (33.0)	-76.64 (1.21)	-102.72 (12.9)	-168.39 (29.39)	1.73 (0.11)	-72.54 (0.67)	-73.79 (1.06)	-236.29 (4.38)
Poisson	-782.72 (33.38)	-51.74 (1.01)	-57.32 (16.36)	-142.58 (26.06)	2.98 (0.12)	-71.6 (0.7)	-73.6 (1.11)	-234.81 (0.5)
Hawkes	-1189.48 (55.2)	-235.9 (3.09)	332.83 (93.92)	-308.42 (57.77)	4.49 (0.24)	-78.66 (0.82)	-83.18 (1.4)	-554.6 (2.15)
GRU-RMTPP-LCONCAT + B	-1330.82 (58.7)	-269.63 (3.37)	-230.91 (39.01)	-382.93 (60.88)	1.84 (0.11)	-78.45 (0.79)	-84.02 (1.39)	-570.59 (2.14)
GRU-LNM-CONCAT	-1366.61 (59.19)	-304.56 (3.84)	-285.0 (25.98)	-383.36 (59.71)	-0.08 (0.06)	-78.57 (0.78)	-90.45 (1.42)	-646.9 (14.15)
GRU-MLP/MC-LCONCAT	-1341.48 (58.22)	-276.11 (2.82)	-169.11 (46.92)	-331.71 (57.1)	1.87 (0.13)	-78.5 (0.79)	-86.76 (1.45)	-577.8 (1.7)
GRU-FNN-LCONCAT	-1350.4 (59.73)	-287.34 (3.34)	-244.96 (31.7)	-372.57 (57.96)	1.75 (0.11)	-78.22 (0.74)	-87.68 (1.31)	-596.29 (2.65)
GRU-EC-TEMWL	-1002.13 (37.43)	-97.11 (1.01)	-144.57 (14.46)	-269.0 (51.2)	1.82 (0.11)	-78.0 (0.76)	-82.78 (1.42)	-535.75 (1.39)
SA-SA/MC-CONCAT	-1301.45 (57.5)	-266.72 (3.58)	-120.84 (29.03)	-342.25 (53.6)	1.74 (0.14)	-78.15 (0.76)	-87.51 (1.42)	-571.5 (1.87)
SA-SA/CM-LCONCAT	-1316.38 (58.15)	-279.82 (3.63)	-222.83 (24.78)	-349.26 (55.73)	1.77 (0.11)	-77.71 (0.78)	-86.32 (1.52)	-541.09 (5.36)

				PCE				
	LastFM	MOOC	Wikipedia	Github	MIMIC2	Hawkes	SO	Retweets
GRU-LNM-CONCAT	0.02 (0.01)	0.0 (0.0)	0.05 (0.01)	0.03 (0.0)	0.02 (0.0)	0.0 (0.0)	0.0 (0.0)	0.01 (0.0)
GRU-FNN-LCONCAT	0.03 (0.0)	0.02 (0.0)	0.06 (0.0)	0.02 (0.0)	0.06 (0.0)	0.0 (0.0)	0.0 (0.0)	0.01 (0.0)
GRU-SA/CM-LCONCAT	0.03 (0.01)	0.02 (0.0)	0.06 (0.01)	0.03 (0.01)	0.05 (0.0)	0.0 (0.0)	0.0 (0.0)	0.01 (0.0)
GRU-RMTPP-LCONCAT	0.06 (0.0)	0.07 (0.0)	0.1 (0.01)	0.02 (0.0)	0.04 (0.0)	0.01 (0.0)	0.01 (0.0)	0.03 (0.0)
GRU-SA/MC-LE	0.06 (0.01)	0.13 (0.0)	0.24 (0.04)	0.12 (0.01)	0.04 (0.01)	0.01 (0.0)	0.01 (0.0)	0.01 (0.0)
GRU-MLP/MC-LTO	0.07 (0.01)	0.12 (0.01)	0.29 (0.02)	0.14 (0.01)	0.04 (0.0)	0.01 (0.0)	0.01 (0.0)	0.02 (0.0)
Hawkes	0.21 (0.0)	0.2 (0.0)	0.19 (0.01)	0.15 (0.01)	0.06 (0.0)	0.0 (0.0)	0.01 (0.0)	0.03 (0.0)
GRU-EC-TO	0.27 (0.0)	0.37 (0.0)	0.34 (0.0)	0.18 (0.01)	0.09 (0.01)	0.02 (0.0)	0.02 (0.0)	0.09 (0.0)
NH	0.35 (0.01)	0.4 (0.0)	0.35 (0.01)	0.3 (0.02)	0.07 (0.0)	0.04 (0.0)	0.05 (0.0)	0.36 (0.0)
Poisson	0.35 (0.01)	0.4 (0.0)	0.34 (0.01)	0.33 (0.02)	0.07 (0.0)	0.04 (0.0)	0.04 (0.0)	0.36 (0.0)
Hawkes	0.21 (0.0)	0.2 (0.0)	0.19 (0.01)	0.15 (0.01)	0.06 (0.0)	0.0 (0.0)	0.01 (0.0)	0.03 (0.0)
GRU-RMTPP-LCONCAT + B	0.06 (0.0)	0.07 (0.0)	0.13 (0.05)	0.02 (0.0)	0.04 (0.01)	0.01 (0.0)	0.02 (0.0)	0.03 (0.0)
GRU-LNM-CONCAT	0.02 (0.01)	0.0 (0.0)	0.05 (0.01)	0.03 (0.0)	0.02 (0.0)	0.0 (0.0)	0.0 (0.0)	0.01 (0.0)
GRU-MLP/MC-LCONCAT	0.07 (0.0)	0.13 (0.01)	0.29 (0.02)	0.15 (0.01)	0.06 (0.01)	0.01 (0.0)	0.01 (0.0)	0.02 (0.0)
GRU-FNN-LCONCAT	0.03 (0.0)	0.02 (0.0)	0.06 (0.0)	0.02 (0.0)	0.06 (0.0)	0.0 (0.0)	0.0 (0.0)	0.01 (0.0)
GRU-EC-TEMWL	0.29 (0.01)	0.39 (0.0)	0.35 (0.01)	0.19 (0.01)	0.06 (0.0)	0.02 (0.0)	0.02 (0.0)	0.12 (0.01)
SA-SA/MC-CONCAT	0.13 (0.01)	0.16 (0.0)	0.33 (0.01)	0.11 (0.01)	0.04 (0.01)	0.01 (0.0)	0.01 (0.0)	0.03 (0.0)
SA-SA/CM-LCONCAT	0.04 (0.01)	0.03 (0.0)	0.13 (0.02)	0.03 (0.01)	0.05 (0.0)	0.0 (0.0)	0.0 (0.0)	0.01 (0.01)

Table 12: Results with respect to the NLL-M, ECE and F1-score for the combinations of models presented in Table 6 on all marked datasets. Standard error across all splits is reported in parenthesis.

	NLL-M							
	LastFM	MOOC	Wikipedia	Github	MIMIC2	Hawkes	SO	Retweets
GRU-LNM-CONCAT	762.03 (22.43)	92.47 (1.85)	259.12 (21.41)	124.34 (18.24)	2.51 (0.14)	110.15 (0.6)	107.09 (0.6)	85.16 (0.83)
GRU-FNN-LCONCAT	791.0 (31.28)	103.16 (4.6)	346.6 (47.58)	128.11 (19.55)	4.34 (0.15)	110.72 (0.61)	109.83 (0.87)	83.38 (0.23)
GRU-SA/CM-LCONCAT	864.68 (29.32)	110.49 (1.87)	292.59 (29.1)	152.63 (21.43)	4.37 (0.15)	111.6 (0.54)	115.49 (0.69)	90.19 (0.17)
GRU-RMTPP-LCONCAT	834.05 (40.33)	89.92 (1.67)	327.16 (77.34)	122.9 (16.42)	2.29 (0.23)	110.34 (0.56)	107.33 (0.34)	82.63 (0.18)
GRU-SA/MC-LE	869.85 (30.36)	177.49 (2.28)	407.99 (74.55)	156.81 (22.86)	4.55 (0.17)	111.71 (0.54)	117.3 (0.91)	88.5 (0.21)
GRU-MLP/MC-LTO	875.01 (31.01)	163.62 (4.1)	476.0 (136.36)	166.51 (23.07)	4.61 (0.2)	111.67 (0.54)	118.33 (0.73)	90.93 (2.61)
Hawkes	514.13 (16.19)	112.14 (1.26)	144.79 (11.89)	122.44 (15.5)	12.84 (0.23)	110.83 (0.54)	114.99 (0.75)	89.5 (0.14)
GRU-EC-TO	870.76 (29.88)	152.98 (1.71)	289.66 (41.0)	154.62 (21.3)	4.4 (0.16)	111.66 (0.55)	120.25 (0.69)	89.96 (0.25)
NH	869.55 (30.47)	184.55 (2.35)	272.66 (21.64)	161.84 (21.59)	4.66 (0.11)	111.99 (0.54)	131.2 (0.74)	91.1 (0.15)
Poisson	873.82 (30.24)	188.13 (2.37)	534.95 (131.14)	168.37 (21.04)	11.25 (0.46)	113.46 (0.54)	132.93 (0.74)	92.11 (0.15)
Hawkes	514.13 (16.19)	112.14 (1.26)	144.79 (11.89)	122.44 (15.5)	12.84 (0.23)	110.83 (0.54)	114.99 (0.75)	89.5 (0.14)
GRU-RMTPP-LCONCAT + B	722.89 (18.13)	86.32 (0.95)	461.49 (117.39)	123.67 (16.18)	3.75 (0.25)	110.31 (0.58)	108.45 (0.99)	82.74 (0.21)
GRU-LNM-CONCAT	762.03 (22.43)	92.47 (1.85)	259.12 (21.41)	124.34 (18.24)	2.51 (0.14)	110.15 (0.6)	107.09 (0.6)	85.16 (0.83)
GRU-MLP/MC-LCONCAT	800.68 (22.15)	117.88 (5.34)	520.5 (162.31)	147.26 (21.75)	3.69 (0.34)	110.85 (0.49)	112.62 (0.9)	83.37 (0.3)
GRU-FNN-LCONCAT	791.0 (31.28)	103.16 (4.6)	346.6 (47.58)	128.11 (19.55)	4.34 (0.15)	110.72 (0.61)	109.83 (0.87)	83.38 (0.23)
GRU-EC-TEMWL	830.42 (33.2)	98.53 (1.65)	298.61 (38.42)	150.4 (21.71)	3.06 (0.18)	110.06 (0.53)	108.8 (0.93)	85.55 (0.9)
SA-SA/MC-CONCAT	862.04 (28.39)	130.75 (2.06)	281.81 (34.96)	148.24 (23.17)	3.14 (0.31)	111.12 (0.5)	111.44 (0.6)	87.58 (0.46)
SA-SA/CM-LCONCAT	860.87 (30.33)	111.51 (3.0)	321.69 (41.29)	152.42 (20.93)	4.43 (0.16)	111.6 (0.51)	116.43 (0.44)	89.67 (0.34)

	ECE							
	LastFM	MOOC	Wikipedia	Github	MIMIC2	Hawkes	SO	Retweets
GRU-LNM-CONCAT	0.37 (0.03)	0.18 (0.02)	0.35 (0.07)	0.17 (0.02)	0.12 (0.02)	0.4 (0.0)	0.11 (0.03)	0.11 (0.02)
GRU-FNN-LCONCAT	0.42 (0.03)	0.22 (0.04)	0.49 (0.0)	0.13 (0.02)	0.46 (0.0)	0.39 (0.02)	0.03 (0.0)	0.06 (0.0)
GRU-SA/CM-LCONCAT	0.49 (0.0)	0.33 (0.03)	0.49 (0.0)	0.37 (0.02)	0.46 (0.0)	0.44 (0.0)	0.12 (0.04)	0.39 (0.01)
GRU-RMTPP-LCONCAT	0.43 (0.03)	0.06 (0.01)	0.36 (0.06)	0.15 (0.01)	0.16 (0.02)	0.4 (0.0)	0.15 (0.02)	0.08 (0.02)
GRU-SA/MC-LE	0.5 (0.0)	0.42 (0.01)	0.49 (0.0)	0.22 (0.02)	0.33 (0.01)	0.44 (0.0)	0.15 (0.01)	0.27 (0.02)
GRU-MLP/MC-LTO	0.5 (0.0)	0.42 (0.01)	0.5 (0.0)	0.19 (0.02)	0.34 (0.03)	0.44 (0.0)	0.11 (0.03)	0.2 (0.04)
Hawkes	0.03 (0.0)	0.14 (0.0)	0.11 (0.03)	0.07 (0.02)	0.19 (0.01)	0.34 (0.01)	0.09 (0.02)	0.19 (0.0)
GRU-EC-TO	0.5 (0.0)	0.44 (0.01)	0.48 (0.0)	0.27 (0.01)	0.38 (0.01)	0.44 (0.0)	0.25 (0.01)	0.38 (0.01)
NH	0.5 (0.0)	0.5 (0.0)	0.5 (0.0)	0.47 (0.01)	0.46 (0.0)	0.48 (0.0)	0.46 (0.0)	0.45 (0.01)
Poisson	0.5 (0.0)	0.5 (0.0)	0.5 (0.0)	0.49 (0.01)	0.47 (0.0)	0.48 (0.0)	0.46 (0.0)	0.46 (0.0)
Hawkes	0.03 (0.0)	0.14 (0.0)	0.11 (0.03)	0.07 (0.02)	0.19 (0.01)	0.34 (0.01)	0.09 (0.02)	0.19 (0.0)
GRU-RMTPP-LCONCAT + B	0.16 (0.04)	0.04 (0.0)	0.35 (0.08)	0.16 (0.01)	0.27 (0.05)	0.39 (0.01)	0.13 (0.0)	0.08 (0.02)
GRU-LNM-CONCAT	0.37 (0.03)	0.18 (0.02)	0.35 (0.07)	0.17 (0.02)	0.12 (0.02)	0.4 (0.0)	0.11 (0.03)	0.11 (0.02)
GRU-MLP/MC-LCONCAT	0.33 (0.03)	0.23 (0.02)	0.43 (0.06)	0.13 (0.02)	0.31 (0.04)	0.41 (0.01)	0.08 (0.02)	0.06 (0.0)
GRU-FNN-LCONCAT	0.42 (0.03)	0.22 (0.04)	0.49 (0.0)	0.13 (0.02)	0.46 (0.0)	0.39 (0.02)	0.03 (0.0)	0.06 (0.0)
GRU-EC-TEMWL	0.48 (0.01)	0.21 (0.03)	0.49 (0.0)	0.27 (0.04)	0.17 (0.02)	0.4 (0.0)	0.21 (0.01)	0.12 (0.02)
SA-SA/MC-CONCAT	0.49 (0.01)	0.3 (0.03)	0.46 (0.03)	0.19 (0.0)	0.3 (0.05)	0.43 (0.01)	0.03 (0.0)	0.17 (0.02)
SA-SA/CM-LCONCAT	0.49 (0.01)	0.27 (0.02)	0.49 (0.0)	0.34 (0.02)	0.45 (0.01)	0.44 (0.0)	0.12 (0.05)	0.37 (0.01)

	F1-score							
	LastFM	MOOC	Wikipedia	Github	MIMIC2	Hawkes	SO	Retweets
GRU-LNM-CONCAT	0.08 (0.03)	0.36 (0.01)	0.24 (0.09)	0.52 (0.02)	0.64 (0.01)	0.26 (0.0)	0.33 (0.0)	0.58 (0.01)
GRU-FNN-LCONCAT	0.05 (0.01)	0.27 (0.04)	0.01 (0.0)	0.5 (0.02)	0.22 (0.02)	0.24 (0.01)	0.33 (0.0)	0.6 (0.0)
GRU-SA/CM-LCONCAT	0.01 (0.0)	0.24 (0.01)	0.01 (0.0)	0.4 (0.03)	0.22 (0.02)	0.17 (0.01)	0.32 (0.0)	0.52 (0.0)
GRU-RMTPP-LCONCAT	0.03 (0.01)	0.38 (0.01)	0.31 (0.11)	0.52 (0.01)	0.74 (0.01)	0.25 (0.01)	0.33 (0.0)	0.6 (0.0)
GRU-SA/MC-LE	0.0 (0.0)	0.03 (0.0)	0.01 (0.0)	0.4 (0.03)	0.24 (0.03)	0.16 (0.01)	0.31 (0.0)	0.55 (0.0)
GRU-MLP/MC-LTO	0.01 (0.0)	0.09 (0.0)	0.01 (0.0)	0.4 (0.03)	0.22 (0.02)	0.15 (0.01)	0.31 (0.0)	0.55 (0.01)
Hawkes	0.3 (0.0)	0.29 (0.0)	0.66 (0.02)	0.54 (0.01)	0.63 (0.0)	0.28 (0.0)	0.32 (0.0)	0.56 (0.0)
GRU-EC-TO	0.0 (0.0)	0.06 (0.0)	0.02 (0.0)	0.4 (0.03)	0.22 (0.02)	0.13 (0.01)	0.29 (0.0)	0.52 (0.0)
NH	0.0 (0.0)	0.01 (0.0)	0.0 (0.0)	0.4 (0.03)	0.22 (0.02)	0.11 (0.0)	0.26 (0.0)	0.33 (0.0)
Poisson	0.0 (0.0)	0.01 (0.0)	0.01 (0.0)	0.4 (0.03)	0.2 (0.02)	0.11 (0.0)	0.26 (0.0)	0.33 (0.0)
Hawkes	0.3 (0.0)	0.29 (0.0)	0.66 (0.02)	0.54 (0.01)	0.63 (0.0)	0.28 (0.0)	0.32 (0.0)	0.56 (0.0)
GRU-RMTPP-LCONCAT + B	0.15 (0.04)	0.41 (0.0)	0.25 (0.11)	0.52 (0.02)	0.51 (0.08)	0.26 (0.01)	0.32 (0.0)	0.6 (0.0)
GRU-LNM-CONCAT	0.08 (0.03)	0.36 (0.01)	0.24 (0.09)	0.52 (0.02)	0.64 (0.01)	0.26 (0.0)	0.33 (0.0)	0.58 (0.01)
GRU-MLP/MC-LCONCAT	0.07 (0.01)	0.28 (0.01)	0.04 (0.03)	0.41 (0.03)	0.54 (0.08)	0.22 (0.02)	0.32 (0.0)	0.6 (0.0)
GRU-FNN-LCONCAT	0.05 (0.01)	0.27 (0.04)	0.01 (0.0)	0.5 (0.02)	0.22 (0.02)	0.24 (0.01)	0.33 (0.0)	0.6 (0.0)
GRU-EC-TEMWL	0.02 (0.0)	0.28 (0.01)	0.01 (0.0)	0.41 (0.03)	0.53 (0.03)	0.27 (0.0)	0.32 (0.0)	0.58 (0.01)
SA-SA/MC-CONCAT	0.01 (0.0)	0.16 (0.02)	0.06 (0.03)	0.4 (0.03)	0.53 (0.06)	0.22 (0.02)	0.33 (0.0)	0.56 (0.0)
SA-SA/CM-LCONCAT	0.01 (0.0)	0.28 (0.02)	0.01 (0.0)	0.4 (0.03)	0.22 (0.02)	0.18 (0.01)	0.31 (0.0)	0.53 (0.0)
NH	0.0 (0.0)	0.01 (0.0)	0.0 (0.0)	0.4 (0.03)	0.22 (0.02)	0.11 (0.0)	0.26 (0.0)	0.33 (0.0)
Poisson	0.0 (0.0)	0.01 (0.0)	0.01 (0.0)	0.4 (0.03)	0.2 (0.02)	0.11 (0.0)	0.26 (0.0)	0.33 (0.0)

Table 13: Results with respect to the NLL-T and PCE for the combinations of models presented in Table 10 on all unmarked datasets. Standard error across all splits is reported in parenthesis.

	NLL-T							
	Taxi	Twitter	Reddit Subs	Reddit Ask	PUBG	Yelp T.	Yelp A.	Yelp M.
GRU-EC-TEM + B	-136.78 (3.91)	-6.21 (0.46)	-4403.97 (24.0)	-917.48 (13.1)	-106.99 (0.21)	-2803.23 (85.58)	-5.76 (0.18)	-56.18 (0.76)
GRU-LNM-TEM	-137.02 (3.87)	-11.89 (0.62)	-4496.27 (37.01)	-926.36 (12.67)	-194.39 (18.07)	-2957.96 (92.81)	-6.8 (0.19)	-59.61 (0.9)
GRU-FNN-LTO	-132.51 (4.01)	-11.66 (0.53)	-4424.06 (24.21)	-926.25 (12.87)	-121.88 (0.18)	-2486.32 (80.2)	-5.72 (0.16)	-58.52 (0.78)
GRU-MLP/MC-LTO	-136.25 (3.95)	-10.4 (0.32)	-4403.41 (24.25)	-921.58 (12.77)	-110.44 (1.21)	-2808.32 (84.78)	-5.75 (0.26)	-58.21 (0.79)
GRU-RMTPP-LTO	-136.15 (3.98)	-9.96 (0.53)	-4407.58 (24.0)	-919.08 (12.91)	-107.04 (0.2)	-2906.91 (87.45)	-5.85 (0.14)	-58.31 (0.79)
SA-SA/CM-LE	-134.2 (4.13)	-10.54 (0.51)	-4320.9 (23.17)	-856.8 (12.31)	-104.81 (1.31)	-2739.73 (81.7)	-5.29 (0.15)	-55.49 (0.88)
GRU-SA/MC-LE	-124.53 (5.1)	-12.11 (0.5)	-4387.88 (19.64)	-922.39 (13.07)	-109.3 (0.9)	-2901.79 (92.0)	-6.83 (0.23)	-57.35 (0.84)
Hawkes	-134.09 (3.93)	-7.62 (0.51)	-4395.2 (23.74)	-919.51 (12.92)	-102.69 (0.2)	-2773.63 (87.1)	-4.62 (0.18)	-53.33 (0.8)
NH	-48.21 (24.44)	-1.94 (0.22)	-4158.41 (58.74)	-714.92 (11.7)	-94.95 (0.14)	-2084.84 (291.26)	-3.23 (0.14)	-39.19 (0.6)
Poisson	-41.71 (1.02)	5.18 (0.11)	-3706.3 (17.61)	-676.53 (10.2)	-93.11 (0.15)	-673.76 (17.22)	-2.11 (0.1)	-25.2 (0.29)

	PCE							
	Taxi	Twitter	Reddit Subs	Reddit Ask	PUBG	Yelp T.	Yelp A.	Yelp M.
GRU-EC-TEM + B	0.01 (0.0)	0.13 (0.0)	0.01 (0.0)	0.02 (0.0)	0.02 (0.0)	0.05 (0.0)	0.02 (0.0)	0.05 (0.0)
GRU-LNM-TEM	0.01 (0.0)	0.01 (0.0)	0.01 (0.0)	0.0 (0.0)	0.01 (0.0)	0.01 (0.0)	0.01 (0.0)	0.01 (0.0)
GRU-FNN-LTO	0.02 (0.0)	0.01 (0.0)	0.0 (0.0)	0.0 (0.0)	0.0 (0.0)	0.05 (0.0)	0.01 (0.0)	0.01 (0.0)
GRU-MLP/MC-LTO	0.01 (0.0)	0.03 (0.01)	0.01 (0.0)	0.01 (0.0)	0.01 (0.0)	0.05 (0.0)	0.01 (0.0)	0.02 (0.0)
GRU-RMTPP-LTO	0.01 (0.0)	0.03 (0.0)	0.01 (0.0)	0.01 (0.0)	0.01 (0.0)	0.03 (0.0)	0.01 (0.0)	0.01 (0.0)
SA-SA/CM-LE	0.01 (0.0)	0.01 (0.0)	0.01 (0.0)	0.01 (0.0)	0.01 (0.0)	0.04 (0.0)	0.01 (0.0)	0.02 (0.0)
GRU-SA/MC-LE	0.1 (0.03)	0.02 (0.0)	0.01 (0.0)	0.01 (0.0)	0.01 (0.0)	0.03 (0.0)	0.01 (0.0)	0.02 (0.0)
Hawkes	0.01 (0.0)	0.01 (0.0)	0.0 (0.0)	0.01 (0.0)	0.01 (0.0)	0.06 (0.0)	0.02 (0.0)	0.05 (0.0)
NH	0.3 (0.06)	0.17 (0.0)	0.1 (0.02)	0.17 (0.0)	0.06 (0.0)	0.28 (0.06)	0.04 (0.0)	0.13 (0.0)
Poisson	0.35 (0.0)	0.2 (0.0)	0.27 (0.0)	0.25 (0.0)	0.07 (0.0)	0.47 (0.0)	0.12 (0.0)	0.27 (0.0)

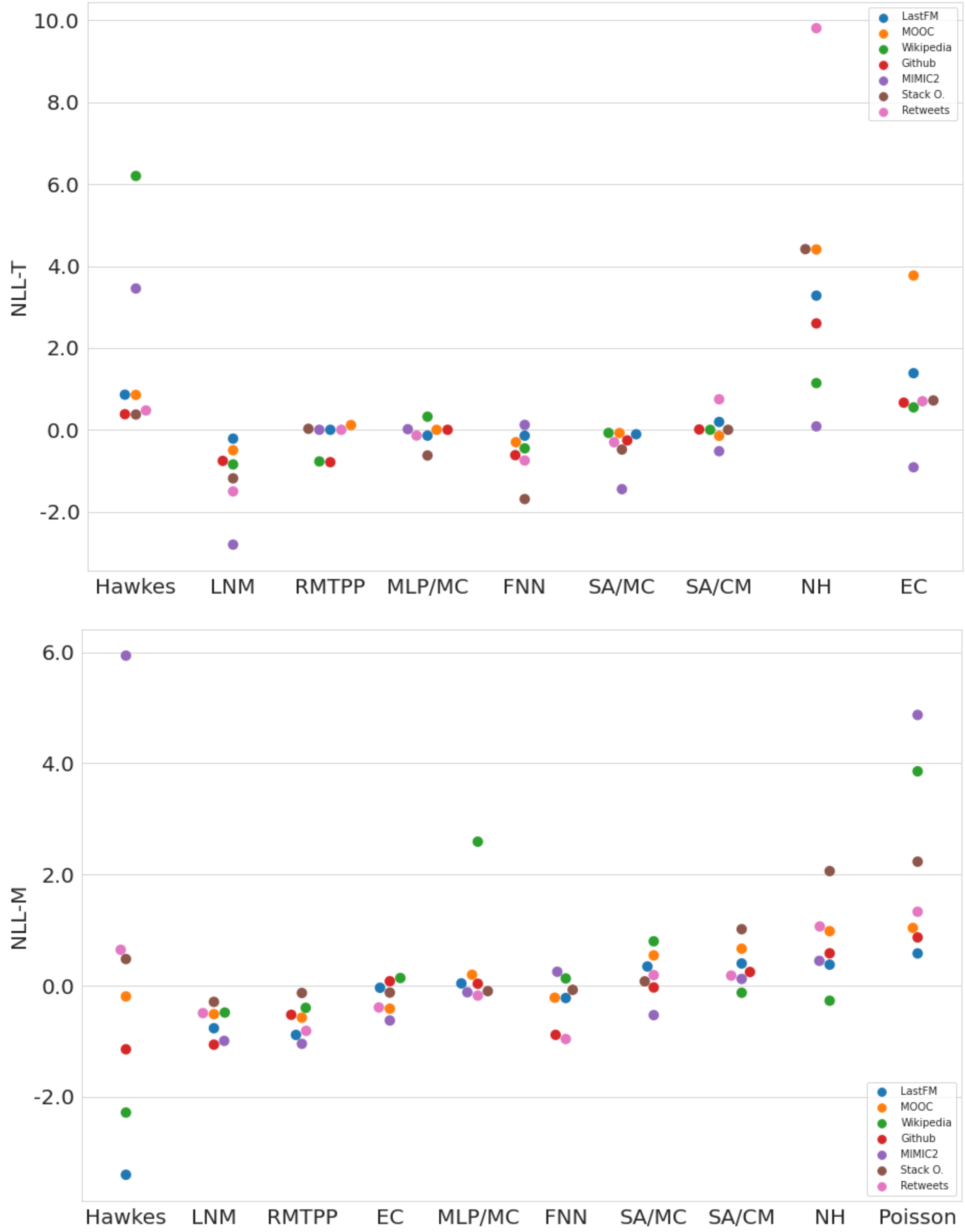

Figure 11: Standardized NLL-T and NLL-M for various decoders per dataset. The NLL-T was computed using the top row models of Table 6, while the NLL-M was computed using the bottom row models of Table 6. Lower NLL-T and NLL-M is better.

C Methods considered

Table 14: Combinations included in the experimental study. "Unmarked" refers to whether the method is adapted for unmarked datasets. For EC, LNM and RMTPP, the setting where a baseline intensity term (B) is also considered.

Decoder	Encoder	Event encoding	Name	Unmarked
EC	CONS	\	CONS-EC	✓
	GRU	TO	GRU-EC-TO	✓
		LTO	GRU-EC-LTO	✓
		CONCAT	GRU-EC-CONCAT	✗
		LCONCAT	GRU-EC-LCONCAT	✗
		TEM	GRU-EC-TEM	✓
		TEMWL	GRU-EC-TEMWL	✗
		LE	GRU-EC-LE	✓
		LEWL	GRU-EC-LEWL	✗
	SA	TO	SA-EC-TO	✓
		LTO	SA-EC-LTO	✓
		CONCAT	SA-EC-CONCAT	✗
		LCONCAT	SA-EC-LCONCAT	✗
		TEM	SA-EC-TEM	✓
		TEMWL	SA-EC-TEMWL	✗
		LE	SA-EC-LE	✓
		LEWL	SA-EC-LEWL	✗
LNM	CONS	\	CONS-LNM	✓
	GRU	TO	GRU-LNM-TO	✓
		LTO	GRU-LNM-LTO	✓
		CONCAT	GRU-LNM-CONCAT	✗
		LCONCAT	GRU-LNM-LCONCAT	✗
		TEM	GRU-LNM-TEM	✓
		TEMWL	GRU-LNM-TEMWL	✗
		LE	GRU-LNM-LE	✓
		LEWL	GRU-LNM-LEWL	✗
	SA	TO	SA-LNM-TO	✓
		LTO	SA-LNM-LTO	✓
		CONCAT	SA-LNM-CONCAT	✗
		LCONCAT	SA-LNM-LCONCAT	✗
		TEM	SA-LNM-TEM	✓
		TEMWL	SA-LNM-TEMWL	✗
		LE	SA-LNM-LE	✓
		LEWL	SA-LNM-LEWL	✗
RMTPP	CONS	\	CONS-RMTPP	✓
	GRU	TO	GRU-RMTPP-TO	✓
		LTO	GRU-RMTPP-LTO	✓
		CONCAT	GRU-RMTPP-CONCAT	✗
		LCONCAT	GRU-RMTPP-LCONCAT	✗
		TEM	GRU-RMTPP-TEM	✓
		TEMWL	GRU-RMTPP-TEMWL	✗
		LE	GRU-RMTPP-LE	✓
		LEWL	GRU-RMTPP-LEWL	✗
	SA	TO	SA-RMTPP-TO	✓
		LTO	SA-RMTPP-LTO	✓
		CONCAT	SA-RMTPP-CONCAT	✗
		LCONCAT	SA-RMTPP-LCONCAT	✗
		TEM	SA-RMTPP-TEM	✓
		TEMWL	SA-RMTPP-TEMWL	✗
		LE	SA-RMTPP-LE	✓
		LEWL	SA-RMTPP-LEWL	✗
FNN	CONS	TO	CONS-FNN-TO	✓
		LTO	CONS-FNN-LTO	✓
		CONCAT	CONS-FNN-CONCAT	✗
		LCONCAT	CONS-FNN-LCONCAT	✗
		LE	CONS-FNN-LE	✓
		LEWL	CONS-FNN-LEWL	✗
	GRU	TO	GRU-FNN-TO	✓
		LTO	GRU-FNN-LTO	✓
		CONCAT	GRU-FNN-CONCAT	✗
		LCONCAT	GRU-FNN-LCONCAT	✗
		LE	GRU-FNN-LE	✓
		LEWL	GRU-FNN-LEWL	✗
	SA	TO	SA-FNN-TO	✓
		LTO	SA-FNN-LTO	✓
		CONCAT	SA-FNN-CONCAT	✗
		LCONCAT	SA-FNN-LCONCAT	✗
		LE	SA-FNN-LE	✓
		LEWL	SA-FNN-LEWL	✗
MLP/MC	CONS	TO	CONS-MLP/MC-TO	✓
		LTO	CONS-MLP/MC-LTO	✓
		CONCAT	CONS-MLP/MC-CONCAT	✗
		LCONCAT	CONS-MLP/MC-LCONCAT	✗
		TEM	CONS-MLP/MC-TEM	✓
		TEMWL	CONS-MLP/MC-TEMWL	✗
		LE	CONS-MLP/MC-LE	✓
		LEWL	CONS-MLP/MC-LEWL	✗
	GRU	TO	GRU-MLP/MC-TO	✓
		LTO	GRU-MLP/MC-LTO	✓
		CONCAT	GRU-MLP/MC-CONCAT	✗
		LCONCAT	GRU-MLP/MC-LCONCAT	✗
		TEM	GRU-MLP/MC-TEM	✓
		TEMWL	GRU-MLP/MC-TEMWL	✗
		LE	GRU-MLP/MC-LE	✓
		LEWL	GRU-MLP/MC-LEWL	✗
	SA	TO	SA-MLP/MC-TO	✓
		LTO	SA-MLP/MC-LTO	✓
		CONCAT	SA-MLP/MC-CONCAT	✗
		LCONCAT	SA-MLP/MC-LCONCAT	✗
		TEM	SA-MLP/MC-TEM	✓
		TEMWL	SA-MLP/MC-TEMWL	✗
		LE	SA-MLP/MC-LE	✓
		LEWL	SA-MLP/MC-LEWL	✗
SA/CM	CONS	TO	CONS-SA/CM-TO	✓
		LTO	CONS-SA/CM-LTO	✓
		CONCAT	CONS-SA/CM-CONCAT	✗
		LCONCAT	CONS-SA/CM-LCONCAT	✗
		LE	CONS-SA/CM-LE	✓
		LEWL	CONS-SA/CM-LEWL	✗
	GRU	TO	GRU-SA/CM-TO	✓
		LTO	GRU-SA/CM-LTO	✓
		CONCAT	GRU-SA/CM-CONCAT	✗
		LCONCAT	GRU-SA/CM-LCONCAT	✗
		LE	GRU-SA/CM-LE	✓
		LEWL	GRU-SA/CM-LEWL	✗
	SA	TO	SA-SA/CM-TO	✓
		LTO	SA-SA/CM-LTO	✓
		CONCAT	SA-SA/CM-CONCAT	✗
		LCONCAT	SA-SA/CM-LCONCAT	✗
		LE	SA-SA/CM-LE	✓
		LEWL	SA-SA/CM-LEWL	✗
SA/MC	CONS	TO	CONS-SA/MC-TO	✓
		LTO	CONS-SA/MC-LTO	✓
		CONCAT	CONS-SA/MC-CONCAT	✗
		LCONCAT	CONS-SA/MC-LCONCAT	✗
		TEM	CONS-SA/MC-TEM	✓
		TEMWL	CONS-SA/MC-TEMWL	✗
		LE	CONS-SA/MC-LE	✓
		LEWL	CONS-SA/MC-LEWL	✗
	GRU	TO	GRU-SA/MC-TO	✓
		LTO	GRU-SA/MC-LTO	✓
		CONCAT	GRU-SA/MC-CONCAT	✗
		LCONCAT	GRU-SA/MC-LCONCAT	✗
		TEM	GRU-SA/MC-TEM	✓
		TEMWL	GRU-SA/MC-TEMWL	✗
		LE	GRU-SA/MC-LE	✓
		LEWL	GRU-SA/MC-LEWL	✗
	SA	TO	SA-SA/MC-TO	✓
		LTO	SA-SA/MC-LTO	✓
		CONCAT	SA-SA/MC-CONCAT	✗
		LCONCAT	SA-SA/MC-LCONCAT	✗
		TEM	SA-SA/MC-TEM	✓
		TEMWL	SA-SA/MC-TEMWL	✗
		LE	SA-SA/MC-LE	✓
		LEWL	SA-SA/MC-LEWL	✗
Neural Hawkes	\	\	NH	✓
Hawkes	\	\	Hawkes	✓
Poisson	\	\	Poisson	✓

D Sequence distribution plots

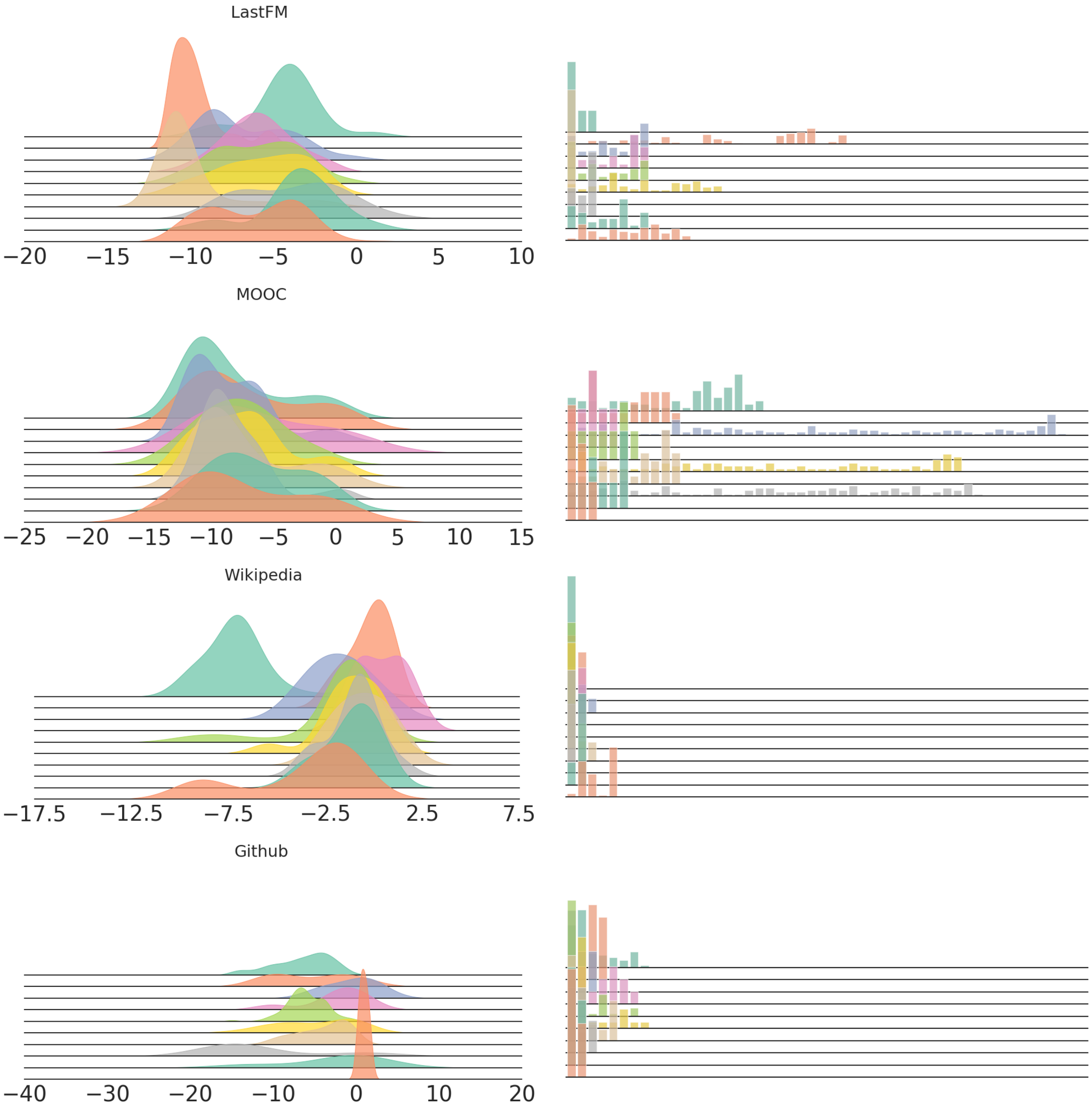

Figure 12: Distribution of log τ_i (left) and mark distribution (right) for 10 randomly sampled sequences in LastFM, MOOC, Wikipedia, and Github, after preprocessing.

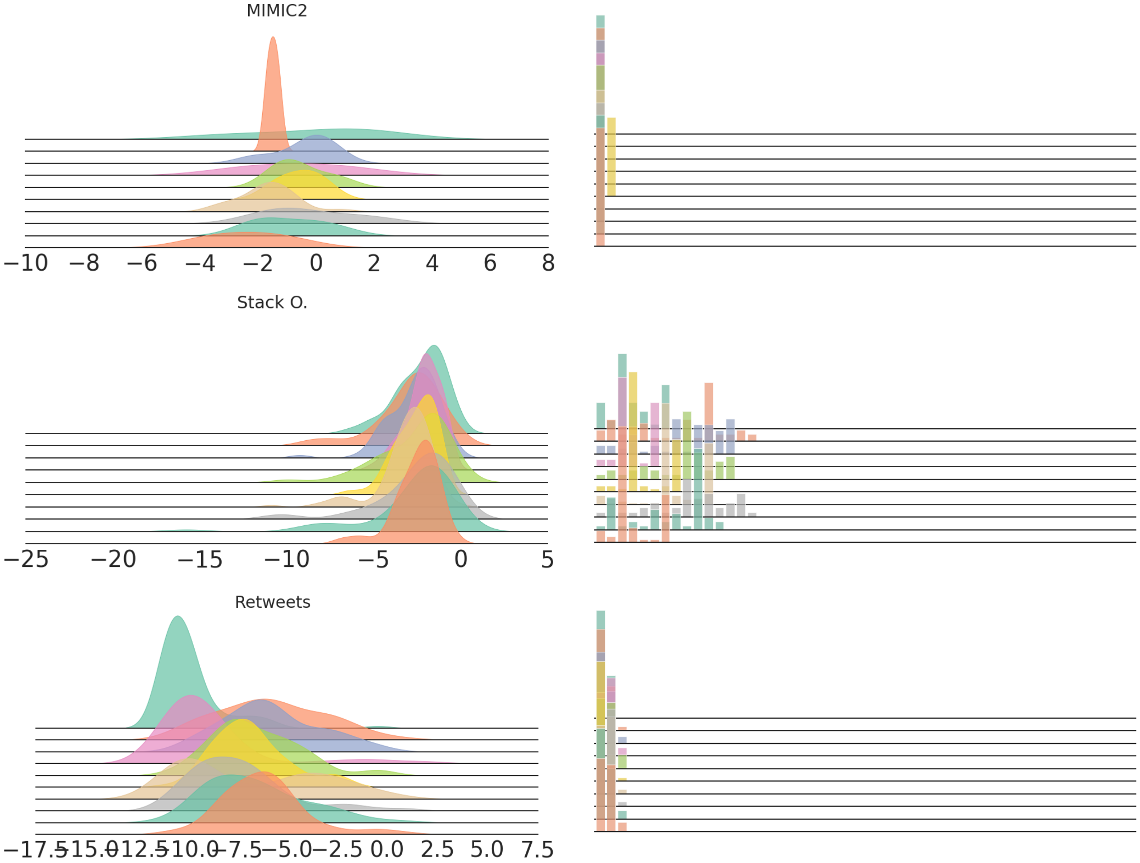

Figure 13: Distribution of $\log \tau_i$ (left) and mark distribution (right) for 10 randomly sampled sequences in MIMIC2, Stack Overflow, and Retweets, after preprocessing.

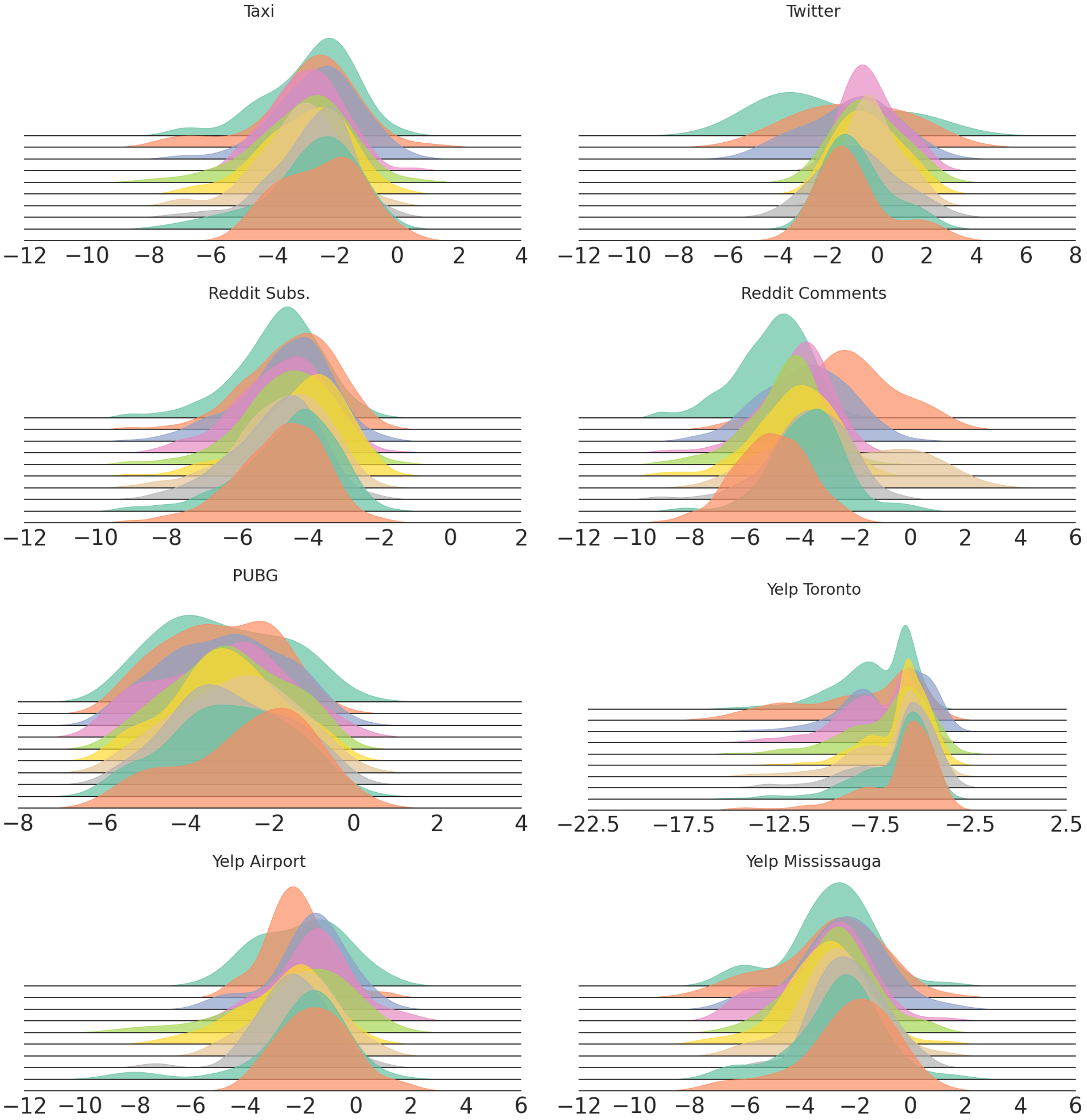

Figure 14: Distribution of $\log \tau_i$ for 10 randomly sampled sequences in unmarked datasets, after preprocessing.

E Proofs

1) Proof of Equation (6) in Section 2. By definition of $\lambda^*(t)$ Rasmussen (2018), we have:

$$\lambda^*(t) = \frac{f^*(t)}{1 - F^*(t)} \tag{64}$$

$$= \frac{f^*(t)}{1 - F^*(t)} \tag{65}$$

$$= -\frac{d}{dt}\log\left(1 - F^*(t)\right). \tag{66}$$

Integrating both sides from t_{i-1} to t, we get

$$\Lambda^*(t) = \int_{t_{i-1}}^{t} \lambda^*(s)ds = \int_{t_{i-1}}^{t} -d\log\left(1 - F^*(s)\right) \tag{67}$$

$$= -\log\left(1 - F^*(t)\right) + \log\left(1 - \underbrace{F^*(t_{i-1})}_{=0}\right), \tag{68}$$

where $F^*(t_{i-1}) = 0$ results from the point process being simple, i.e. two events cannot occur simultaneously. Rearranging the terms, we find:

$$F^*(t) = 1 - \exp\left(-\Lambda^*(t)\right) = 1 - \exp\left(-\sum_{k=1}^{K} \Lambda_k^*(t)\right). \tag{69}$$

Differentiating with respect to t gives

$$f^*(t) = \frac{d}{dt}F^*(t) = \lambda^*(t)\exp\left(-\Lambda^*(t)\right). \tag{70}$$

Given that $\lambda_k^*(t) = \lambda^*(t)p^*(k|t)$, we finally find

$$f^*(t,k) = f^*(t)p^*(k|t) = \lambda_k^*(t)\exp\left(-\Lambda^*(t)\right) \tag{71}$$

2) Expected number of events. Denoting the last observed event t_{i-1}, the expected number of events to occur at time t conditional on the observed history $\mathcal{H}_t$ is given by:

$$\mathbb{E}[N(t)|\mathcal{H}_t] = \int_0^t \lambda^*(t)dt \tag{72}$$

$$= \int_0^{t_1} \lambda^*(s)ds + \int_{t_1}^{t_2} \lambda^*(s)ds + ... + \int_{t_{i-2}}^{t_{i-1}} \lambda^*(s)ds + \int_{t_{i-1}}^{t} \lambda^*(s)ds \tag{73}$$

$$\overset{?}{=} i - 1 + \mathbb{P}(t_i \in [t_{i-1}, t]|\mathcal{H}_t) \tag{74}$$

For a Poisson process with rate λ, this expression simplifies to:

$$\begin{aligned}
\mathbb{E}[N(t)|\mathcal{H}_t] &= \int_0^t \lambda^*(t)dt && (75)\\
&= \int_0^{t_1} \lambda^*(s)ds + \int_{t_1}^{t_2} \lambda^*(s)ds + ... + \int_{t_{i-2}}^{t_{i-1}} \lambda^*(s)ds + \int_{t_{i-1}}^{t} \lambda ds && (76)\\
&= \int_0^{t_1} \lambda ds + \int_{t_1}^{t_2} \lambda ds + ... + \int_{t_{i-2}}^{t_{i-1}} \lambda ds + \int_{t_{i-1}}^{t} \lambda ds && (77)\\
&= \lambda t && (78)\\
&= \mathbb{E}[N(t)] && (79)
\end{aligned}$$

F Results on relevant datasets only

The discussion in Section 6 highlighted that some datasets (MIMIC2, Stack Overflow, Taxi, Reddit Subs, Reddit Ask Comments, Yelp Toronto and Yelp Mississauga) might potentially be inappropriate for benchmarking neural TPP models. For completeness, we report in Tables 15, 16, 22, 20, 18 and 19 the results of the aggregation procedure discussed in Section 5.5 without these borderline inadequate datasets included. We found no significance differences with respect to the conclusions of Section 6.

Table 15: Average and median scores, and average ranks of the best combinations per decoder on the NLL-T (top rows) and NLL-M (bottom row) across all relevant marked datasets. Best results are highlighted in bold.

	Marked Datasets														
	NLL-T			PCE			NLL-M			ECE			F1-score		
	Mean	Median	Rank	Mean	Median	Rank	Mean	Median	Rank	Mean	Median	Rank	Mean	Median	Rank
GRU-EC-TO	0.08	-0.04	8.33	0.21	0.22	9.0	-0.09	-0.02	6.83	0.42	0.44	7.17	0.19	0.1	7.67
GRU-LNM-CONCAT	**-0.87**	**-0.87**	**1.5**	**0.02**	**0.01**	**1.5**	-2.38	-1.57	**2.17**	0.26	0.27	3.17	0.34	0.31	2.5
GRU-LN-LTO	-0.41	-0.67	4.5	0.06	0.04	5.0	-0.23	-0.2	6.83	0.4	0.4	7.67	0.21	0.14	7.67
GRU-FNN-LCONCAT	-0.63	-0.73	4.33	0.02	0.02	2.17	-1.85	-1.54	3.83	0.29	0.3	3.33	0.28	0.26	3.83
GRU-MLP/MC-LTO	-0.4	-0.41	5.33	0.11	0.09	6.83	0.53	0.31	9.5	0.37	0.43	7.0	0.2	0.12	7.5
GRU-RMTPP-LCONCAT	-0.6	-0.52	4.5	0.05	0.04	5.0	-1.67	**-1.85**	2.83	0.25	0.26	2.67	0.35	0.34	2.17
GRU-SA/CM-LCONCAT	-0.4	-0.44	6.0	0.03	0.03	3.0	-0.3	-0.35	5.83	0.42	0.41	7.33	0.22	0.21	7.33
GRU-SA/MC-LCONCAT	-0.54	-0.53	3.67	0.1	0.08	6.17	-0.43	-0.32	6.17	0.31	0.32	4.83	0.24	0.2	5.0
Hawkes	0.6	-0.14	7.17	0.13	0.17	6.5	**-4.68**	-1.43	3.0	**0.15**	**0.13**	**1.83**	**0.44**	**0.42**	**1.83**
Poisson	1.78	1.34	10.83	0.3	0.35	10.5	1.1	0.9	10.83	0.49	0.49	10.5	0.14	0.06	10.17
NH	1.6	1.18	9.83	0.3	0.35	10.33	0.18	0.37	8.17	0.48	0.49	10.5	0.14	0.06	11.0
GRU-EC-TEMWL	0.26	0.17	8.33	0.23	0.24	9.17	-1.22	-1.11	5.33	0.33	0.33	6.33	0.26	0.27	5.83
GRU-LNM-CONCAT	**-0.87**	**-0.87**	**1.17**	**0.02**	**0.01**	**1.67**	-2.38	-1.57	**3.0**	0.26	0.27	4.67	0.34	0.31	3.33
GRU-LN-CONCAT	-0.37	-0.62	4.33	0.08	0.04	5.0	-2.38	-1.48	3.5	0.28	0.3	4.0	0.3	0.31	3.83
GRU-FNN-LCONCAT	-0.63	-0.73	2.67	0.02	0.02	1.83	-1.85	-1.54	5.17	0.29	0.3	4.67	0.28	0.26	6.0
GRU-MLP/MC-LCONCAT	-0.39	-0.4	4.83	0.11	0.1	6.33	-1.1	-0.88	6.67	0.26	0.28	4.17	0.27	0.25	5.5
GRU-RMTPP-LCONCAT + B	-0.54	-0.51	4.33	0.05	0.04	5.0	-2.55	**-1.86**	3.0	0.2	0.16	2.83	0.37	0.33	**2.17**
SA-SA/CM-LCONCAT	-0.37	-0.43	6.0	0.04	0.03	3.33	-0.31	-0.24	8.0	0.4	0.41	8.5	0.23	0.23	8.33
SA-SA/MC-CONCAT	-0.27	-0.34	6.5	0.13	0.12	6.5	-0.57	-0.58	7.5	0.34	0.37	7.33	0.24	0.19	7.33
Hawkes	0.6	-0.14	7.17	0.13	0.17	6.5	**-4.68**	-1.43	4.0	**0.15**	**0.13**	**2.5**	**0.44**	**0.42**	2.67
Poisson	1.78	1.34	10.83	0.3	0.35	10.5	1.1	0.9	11.0	0.49	0.49	10.5	0.14	0.06	10.67
NH	1.6	1.18	9.83	0.3	0.35	10.17	0.18	0.37	8.83	0.48	0.49	10.5	0.14	0.06	11.0
MRC	\	\	\	\	\	\	\	\	\	\	\	\	0.14	0.06	11.33

Table 16: Average and median scores, as well as average ranks per decoder and variation of event encoding, for relevant marked datasets. Refer to Section 5.5 for details on the aggregation procedure. Best results are highlighted in bold.

	Marked Datasets														
	NLL-T			PCE			NLL-M			ECE			F1-score		
	Mean	Median	Rank	Mean	Median	Rank	Mean	Median	Rank	Mean	Median	Rank	Mean	Median	Rank
EC-TO	0.87	0.69	7.0	0.25	0.27	5.83	0.21	0.18	6.5	0.45	0.46	7.67	0.17	0.08	7.0
EC-LTO	0.88	0.69	7.5	0.26	0.27	6.67	0.15	0.14	5.5	0.45	0.46	6.5	0.17	0.08	**7.5**
EC-CONCAT	0.26	0.21	**2.5**	**0.22**	**0.23**	2.5	-0.27	-0.61	3.0	0.37	0.39	**1.67**	0.25	0.23	2.17
EC-LCONCAT	0.45	0.33	4.0	0.24	0.24	4.83	-0.31	-0.57	3.5	0.36	**0.35**	2.67	0.24	0.22	3.17
EC-TEM	0.29	0.18	4.0	0.23	0.24	4.5	0.16	0.16	6.0	0.44	0.45	6.0	0.19	0.09	5.67
EC-TEMWL	0.37	0.29	4.17	0.23	0.25	5.0	**-0.53**	**-0.78**	**1.83**	**0.35**	0.35	2.0	**0.27**	**0.24**	**1.33**
EC-LE	**0.25**	**0.14**	3.0	0.22	0.24	**2.0**	0.13	0.1	5.17	0.43	0.45	5.33	0.19	0.09	5.5
EC-LEWL	0.31	0.3	3.83	0.23	0.25	4.67	-0.06	-0.29	4.5	0.39	0.41	4.17	0.24	0.22	3.67
LNM-TO	-0.56	-0.58	6.5	**0.02**	0.02	5.0	0.05	0.1	6.83	0.45	0.46	6.83	0.17	0.09	7.5
LNM-LTO	-0.57	-0.62	6.17	0.02	0.02	5.5	0.03	0.04	6.5	0.45	0.46	7.17	0.17	0.1	6.67
LNM-CONCAT	**-0.81**	-0.82	**1.67**	0.02	0.02	4.0	**-2.01**	-1.32	**1.5**	**0.28**	**0.26**	2.0	**0.35**	**0.35**	**1.5**
LNM-LCONCAT	-0.8	**-0.85**	2.0	0.02	**0.01**	**2.33**	-1.61	-1.11	3.0	0.31	0.33	2.83	0.29	0.27	3.33
LNM-TEM	-0.75	-0.81	4.5	0.02	0.01	4.0	0.02	0.03	6.5	0.44	0.45	6.0	0.19	0.1	5.83
LNM-TEMWL	-0.71	-0.74	4.83	0.03	0.02	4.0	-1.75	**-1.34**	2.17	0.3	0.32	**1.83**	0.32	0.29	2.0
LNM-LE	-0.71	-0.79	5.67	0.03	0.02	6.83	-0.0	0.02	6.17	0.43	0.44	6.0	0.19	0.1	6.0
LNM-LEWL	-0.72	-0.78	4.67	0.02	0.02	4.33	-1.69	-1.09	3.33	0.32	0.31	3.33	0.29	0.26	3.17
FNN-TO	1.21	0.74	4.5	0.26	0.31	4.67	0.36	0.33	4.33	0.48	0.48	5.5	0.14	0.07	4.83
FNN-LTO	-0.43	-0.48	1.83	**0.03**	**0.02**	**1.5**	0.08	0.09	3.5	0.42	0.42	2.0	0.2	0.12	2.0
FNN-CONCAT	1.26	0.76	5.0	0.27	0.31	4.67	0.19	0.21	3.5	0.48	0.48	4.67	0.15	0.08	4.5
FNN-LCONCAT	**-0.59**	**-0.68**	**1.17**	0.03	0.02	1.5	**-1.49**	**-1.36**	**1.67**	**0.3**	**0.3**	**1.0**	**0.28**	**0.28**	**1.0**
FNN-LE	1.2	0.87	4.33	0.27	0.32	4.17	0.31	0.3	3.83	0.48	0.48	4.0	0.15	0.06	4.33
FNN-LEWL	1.25	0.72	4.17	0.27	0.32	4.5	0.2	0.15	4.17	0.47	0.47	3.83	0.15	0.08	4.33
MLP/MC-TO	0.28	0.2	6.5	0.19	0.25	5.83	0.34	0.29	6.33	0.43	0.43	6.67	0.18	0.09	7.17
MLP/MC-LTO	-0.17	-0.16	3.33	**0.11**	0.1	**1.83**	0.51	0.3	6.83	0.41	0.45	6.5	0.19	0.1	5.83
MLP/MC-CONCAT	0.05	0.08	4.67	0.19	0.22	5.67	-0.39	-0.49	**2.83**	0.33	0.34	2.67	**0.27**	0.27	1.83
MLP/MC-LCONCAT	**-0.3**	**-0.23**	**1.83**	0.11	**0.09**	1.83	**-0.72**	**-0.81**	3.0	**0.29**	**0.27**	**1.17**	0.27	**0.28**	**1.67**
MLP/MC-TEM	0.08	0.13	5.83	0.19	0.23	6.17	0.27	0.2	5.17	0.41	0.41	5.83	0.19	0.1	6.5
MLP/MC-TEMWL	0.34	0.41	7.5	0.22	0.24	7.83	-0.24	-0.25	3.83	0.36	0.38	3.5	0.25	0.25	4.0
MLP/MC-LE	-0.07	-0.05	3.0	0.16	0.19	3.33	0.39	0.24	5.17	0.4	0.42	6.5	0.19	0.1	5.83
MLP/MC-LEWL	-0.04	0.0	3.33	0.17	0.21	3.5	-0.22	-0.26	2.83	0.34	0.33	3.17	0.25	0.25	3.17
RMTPP-TO	0.37	0.33	7.33	0.2	0.24	6.83	0.09	0.13	6.17	0.44	0.45	7.17	0.17	0.09	7.33
RMTPP-LTO	-0.27	-0.35	3.83	0.06	0.07	2.17	0.08	0.07	6.5	0.44	0.44	6.67	0.18	0.11	6.33
RMTPP-CONCAT	0.04	0.08	4.17	0.19	0.22	4.33	-1.33	-1.17	3.0	0.29	0.34	2.33	0.31	0.3	2.5
RMTPP-LCONCAT	**-0.52**	**-0.46**	**1.5**	**0.05**	**0.05**	**1.0**	-1.52	**-1.47**	3.0	**0.26**	**0.27**	**1.83**	0.34	0.32	**1.67**
RMTPP-TEM	0.07	0.05	5.33	0.19	0.22	5.83	0.08	0.1	5.67	0.43	0.44	6.5	0.19	0.11	6.33
RMTPP-TEMWL	0.12	0.16	4.83	0.19	0.22	5.83	**-1.82**	-1.33	**1.67**	0.27	0.29	2.17	**0.35**	**0.37**	1.83
RMTPP-LE	0.05	0.04	4.17	0.19	0.22	4.5	0.09	0.1	6.0	0.43	0.44	5.67	0.19	0.11	6.0
RMTPP-LEWL	0.1	0.14	4.83	0.19	0.23	5.5	-0.98	-0.85	4.0	0.32	0.38	3.67	0.28	0.28	4.0
SA/CM-TO	-0.04	-0.01	4.5	0.08	0.06	4.17	0.72	0.21	4.83	0.46	0.46	5.33	0.14	0.1	4.17
SA/CM-LTO	-0.21	-0.11	3.17	0.05	0.05	2.5	0.17	0.14	4.17	0.44	0.44	3.17	0.19	0.1	3.0
SA/CM-CONCAT	-0.07	-0.17	4.83	0.12	0.12	5.0	0.09	0.08	3.83	0.45	0.44	3.67	0.17	0.09	4.17
SA/CM-LCONCAT	**-0.39**	**-0.44**	**1.83**	**0.03**	**0.03**	**1.83**	**-0.3**	**-0.3**	**1.17**	**0.41**	**0.41**	**1.33**	**0.23**	**0.22**	**1.17**
SA/CM-LE	-0.29	-0.31	2.5	0.06	0.04	3.0	0.14	0.09	4.17	0.45	0.45	3.67	0.18	0.08	4.67
SA/CM-LEWL	-0.17	-0.16	4.17	0.1	0.13	4.5	-0.09	-0.13	2.83	0.43	0.45	3.83	0.19	0.09	3.83
SA/MC-TO	1.47	1.08	8.0	0.29	0.34	7.67	0.25	0.32	6.33	0.48	0.49	7.33	0.14	0.06	7.83
SA/MC-LTO	1.3	0.92	7.0	0.28	0.32	7.33	0.27	0.36	6.5	0.47	0.48	7.0	0.15	0.06	7.17
SA/MC-CONCAT	-0.32	-0.39	3.83	0.12	0.12	4.0	**-0.51**	**-0.61**	**1.83**	0.35	0.38	2.33	**0.24**	0.18	**2.0**
SA/MC-LCONCAT	**-0.54**	**-0.56**	**1.5**	0.1	**0.08**	2.0	-0.23	-0.38	3.5	**0.31**	**0.31**	**1.33**	0.23	**0.19**	2.5
SA/MC-TEM	-0.33	-0.3	4.83	0.13	0.14	4.0	0.21	0.1	6.0	0.41	0.44	5.83	0.18	0.08	5.83
SA/MC-TEMWL	-0.22	-0.27	5.67	0.14	0.15	5.83	-0.29	-0.3	3.5	0.37	0.4	3.5	0.22	0.15	3.33
SA/MC-LE	-0.48	-0.46	1.67	**0.09**	0.09	**1.5**	0.15	0.03	5.5	0.4	0.43	5.0	0.19	0.09	5.17
SA/MC-LEWL	-0.37	-0.38	3.5	0.12	0.11	3.67	-0.45	-0.48	2.83	0.35	0.38	3.67	0.23	0.16	2.17

Table 17: Average and median scores, as well as average ranks per decoder and variation of history encoder, for relevant marked datasets. Refer to Section 5.5 for details on the aggregation procedure. Best results are highlighted in bold.

	Marked Datasets														
	NLL-T			PCE			NLL-M			ECE			F1-score		
	Mean	Median	Rank	Mean	Median	Rank	Mean	Median	Rank	Mean	Median	Rank	Mean	Median	Rank
CONS-EC	1.74	1.34	3.0	0.3	0.35	2.83	0.63	0.56	2.67	0.48	0.49	3.0	0.14	0.06	3.0
SA-EC	0.73	0.63	2.0	0.25	0.27	2.17	0.04	-0.04	2.0	0.43	0.42	2.0	0.2	0.15	1.83
GRU-EC	**0.19**	**0.14**	**1.0**	**0.22**	**0.23**	**1.0**	**-0.17**	**-0.29**	**1.33**	**0.39**	**0.38**	**1.0**	**0.22**	**0.17**	**1.17**
CONS-LNM	-0.35	-0.44	2.83	**0.02**	0.02	2.33	0.58	0.43	3.0	0.48	0.49	3.0	0.14	0.06	3.0
SA-LNM	-0.61	-0.68	1.83	0.02	0.02	2.17	-0.63	-0.39	1.83	0.39	0.39	1.83	0.24	0.17	1.83
GRU-LNM	**-0.8**	**-0.83**	**1.33**	0.03	**0.01**	**1.5**	**-1.11**	**-0.83**	**1.17**	**0.35**	**0.37**	**1.17**	**0.26**	**0.2**	**1.17**
CONS-FNN	1.02	0.72	3.0	0.2	0.24	2.67	0.5	0.25	2.83	0.46	0.46	2.83	0.17	**0.11**	2.5
SA-FNN	0.78	0.53	1.83	0.19	0.23	2.0	0.05	0.06	2.17	0.45	0.45	1.83	**0.18**	0.11	2.0
GRU-FNN	**0.52**	**0.13**	**1.17**	**0.18**	**0.21**	**1.33**	**-0.17**	**-0.04**	**1.0**	**0.42**	**0.44**	**1.33**	0.18	0.11	**1.5**
CONS-MLP/MC	0.5	0.52	3.0	0.19	0.23	2.83	0.4	0.3	2.33	0.39	0.4	2.0	0.22	0.17	2.33
SA-MLP/MC	0.13	0.13	2.0	0.17	0.21	2.0	0.04	-0.02	2.33	0.38	0.39	2.67	0.22	0.17	2.33
GRU-MLP/MC	**-0.15**	**-0.14**	**1.0**	**0.16**	**0.18**	**1.17**	**-0.03**	**-0.26**	**1.33**	**0.35**	**0.37**	**1.33**	**0.23**	**0.18**	**1.33**
CONS-RMTPP	0.87	0.66	3.0	0.18	0.21	2.33	0.97	0.65	2.67	0.47	0.48	3.0	0.13	0.05	3.0
SA-RMTPP	0.13	0.17	1.83	0.17	0.19	2.17	-0.38	-0.36	2.17	0.38	0.39	1.83	0.24	0.18	1.83
GRU-RMTPP	**-0.15**	**-0.17**	**1.17**	**0.15**	**0.17**	**1.5**	**-0.95**	**-0.66**	**1.17**	**0.34**	**0.37**	**1.17**	**0.26**	**0.22**	**1.17**
CONS-SA/CM	0.01	-0.06	3.0	0.1	0.12	2.83	0.51	0.36	2.67	**0.44**	**0.44**	2.17	**0.18**	**0.11**	2.17
SA-SA/CM	-0.17	-0.2	1.83	0.08	**0.08**	1.83	**0.12**	0.09	**1.5**	0.44	0.44	**1.83**	0.18	0.11	**1.17**
GRU-SA/CM	**-0.22**	**-0.22**	**1.17**	**0.07**	0.08	**1.33**	0.12	**0.07**	1.83	0.44	0.44	2.0	0.18	0.11	2.67
CONS-SA/MC	0.44	0.2	3.0	0.18	0.19	2.83	0.42	0.28	2.67	0.41	**0.41**	2.33	**0.2**	**0.13**	2.0
SA-SA/MC	0.07	0.03	1.67	**0.16**	**0.16**	1.83	-0.05	**-0.16**	**1.5**	**0.39**	0.41	**1.67**	0.19	0.12	2.33
GRU-SA/MC	**0.05**	**-0.04**	**1.33**	0.16	0.16	**1.33**	**-0.1**	-0.16	1.83	0.39	0.42	2.0	0.2	0.12	**1.67**

Table 18: Average, median, and worst scores, as well as average ranks per decoder and variation of event encoding, for relevant unmarked datasets. Refer to Section 5.5 for details on the aggregation procedure. Best scores are highlighted in bold.

	Unmarked Datasets							
	NLL-T				PCE			
	Mean	Median	Worst	Rank	Mean	Median	Worst	Rank
EC-TO	0.36	0.35	0.6	3.33	0.08	0.04	0.16	2.67
EC-LTO	0.39	0.34	0.64	3.67	0.08	0.04	0.16	4.0
EC-TEM	**-0.03**	**-0.13**	**0.31**	**1.0**	**0.06**	**0.03**	**0.14**	**1.0**
EC-LE	0.17	0.04	0.46	2.0	0.07	0.03	0.15	2.33
LNM-TO	-2.19	-0.73	-0.53	3.0	**0.01**	**0.01**	**0.01**	2.67
LNM-LTO	-2.18	-0.72	-0.49	3.33	0.01	0.01	0.01	2.33
LNM-TEM	**-2.64**	**-0.82**	**-0.76**	**1.33**	0.01	0.01	0.01	**1.67**
LNM-LE	-1.55	-0.82	-0.56	2.33	0.01	0.01	0.01	3.33
FNN-TO	0.54	0.51	0.62	2.33	0.08	0.04	0.15	2.33
FNN-LTO	**-0.78**	**-0.65**	**-0.25**	**1.0**	**0.01**	**0.01**	**0.01**	**1.0**
FNN-LE	0.51	0.52	0.54	2.67	0.08	0.05	0.15	2.67
MLP/MC-TO	-0.03	0.01	0.1	3.33	0.04	0.03	0.08	3.33
MLP/MC-LTO	-0.21	-0.17	0.06	2.33	**0.02**	0.03	**0.03**	**1.33**
MLP/MC-TEM	-0.12	-0.14	-0.04	2.33	0.04	0.03	0.09	3.0
MLP/MC-LE	**-0.31**	**-0.39**	**-0.12**	**2.0**	0.03	**0.02**	0.06	2.33
RMTPP-TO	-0.11	-0.16	0.11	3.33	0.04	0.02	0.08	3.33
RMTPP-LTO	-0.12	-0.15	0.2	3.0	**0.02**	0.02	**0.03**	2.33
RMTPP-TEM	**-0.33**	**-0.29**	**-0.25**	**1.33**	0.03	**0.01**	0.07	2.33
RMTPP-LE	-0.25	-0.24	-0.14	2.33	0.03	0.01	0.08	**2.0**
SA/CM-TO	**-0.34**	-0.5	0.72	2.0	0.02	0.02	0.03	2.33
SA/CM-LTO	0.67	**-0.55**	3.38	2.33	0.04	0.02	0.1	2.67
SA/CM-LE	-0.25	-0.3	**0.19**	**1.67**	**0.01**	**0.01**	**0.01**	**1.0**
SA/MC-TO	0.76	0.72	0.96	4.0	0.08	0.07	0.15	4.0
SA/MC-LTO	0.51	0.42	0.89	3.0	0.07	0.06	0.14	3.0
SA/MC-TEM	-0.57	-0.66	-0.39	2.0	**0.01**	**0.01**	**0.02**	**1.0**
SA/MC-LE	**-0.69**	**-0.8**	**-0.43**	**1.0**	0.01	0.01	0.02	2.0

Table 19: Average, median, and worst scores, as well as average ranks per decoder and variation of history encoder, for relevant unmarked datasets. Refer to Section 5.5 for details on the aggregation procedure. Best scores are highlighted in bold.

	Unmarked Datasets							
	NLL-T				PCE			
	Mean	Median	Worst	Rank	Mean	Median	Worst	Rank
CONS-EC	1.29	1.14	2.14	3.0	0.1	0.07	0.2	3.0
SA-EC	0.61	0.55	0.75	2.0	0.09	0.05	0.17	2.0
GRU-EC	**-0.17**	**-0.27**	**0.25**	**1.0**	**0.06**	**0.02**	**0.14**	**1.0**
CONS-LNM	-1.83	-0.25	0.12	2.33	**0.01**	**0.01**	0.02	**1.67**
SA-LNM	-1.24	-0.64	-0.24	2.67	0.01	0.01	**0.01**	2.33
GRU-LNM	**-3.04**	**-0.93**	**-0.9**	**1.0**	0.01	0.01	0.01	2.0
CONS-FNN	0.61	0.37	1.26	2.67	0.06	**0.03**	0.13	2.0
SA-FNN	0.15	0.16	0.34	2.0	**0.05**	0.03	**0.1**	**1.33**
GRU-FNN	**0.03**	**0.14**	**0.17**	**1.33**	0.06	0.03	0.11	2.67
CONS-MLP/MC	0.51	0.58	0.74	2.67	0.04	0.03	0.07	2.67
SA-MLP/MC	0.1	0.23	0.33	2.33	0.04	0.03	**0.06**	2.0
GRU-MLP/MC	**-0.44**	**-0.41**	**-0.38**	**1.0**	**0.03**	**0.02**	0.06	**1.33**
CONS-RMTPP	0.45	0.6	0.79	2.67	**0.03**	0.02	**0.05**	**1.67**
SA-RMTPP	0.03	-0.04	0.29	2.33	0.03	0.02	0.07	2.67
GRU-RMTPP	**-0.43**	**-0.37**	**-0.33**	**1.0**	0.03	**0.01**	0.06	1.67
CONS-SA/CM	0.7	0.12	2.02	3.0	0.03	0.02	**0.04**	2.67
SA-SA/CM	**0.01**	-0.43	**0.99**	1.67	**0.02**	0.02	0.04	**1.33**
GRU-SA/CM	0.04	**-0.61**	1.54	**1.33**	0.03	**0.01**	0.06	2.0
CONS-SA/MC	0.54	0.73	0.83	3.0	**0.05**	0.04	0.09	2.67
SA-SA/MC	0.05	-0.06	0.27	2.0	0.05	**0.03**	**0.08**	**1.33**
GRU-SA/MC	**-0.05**	**-0.16**	**0.25**	**1.0**	0.05	0.04	0.08	2.0

Table 20: Average, median, worst scores, and average ranks of the best combinations per decoder on the NLL-T across all relevant unmarked datasets. Best results are highlighted in bold.

	Unmarked Datasets							
	NLL-T				PCE			
	Mean	Median	Worst	Rank	Mean	Median	Worst	Rank
GRU-EC-TEM + B	-0.21	-0.28	0.16	7.0	0.06	0.02	0.13	8.33
GRU-LNM-TEM	**-3.7**	**-1.03**	**-0.83**	**1.67**	**0.01**	**0.01**	**0.01**	**1.67**
GRU-LN-LE	-0.25	-0.46	0.47	6.0	0.02	0.02	0.04	6.67
GRU-FNN-LTO	-1.03	-0.79	-0.49	4.0	0.01	0.01	0.01	2.33
GRU-MLP/MC-LTO	-0.57	-0.57	-0.5	4.67	0.02	0.01	0.03	5.67
GRU-RMTPP-TEM + B	-0.51	-0.54	-0.36	5.67	0.02	0.01	0.05	5.0
GRU-SA/CM-TO	-0.71	-0.56	0.73	5.67	0.02	0.01	0.03	6.0
GRU-SA/MC-LE	-0.81	-0.87	-0.51	2.33	0.01	0.01	0.02	5.0
Hawkes	0.05	0.06	0.16	8.0	0.01	0.01	0.02	4.33
Poisson	1.54	1.32	2.14	11.0	0.13	0.12	0.2	11.0
NH	0.87	0.9	0.96	10.0	0.09	0.06	0.17	10.0

G Critical distance diagrams for event encodings and history encoders

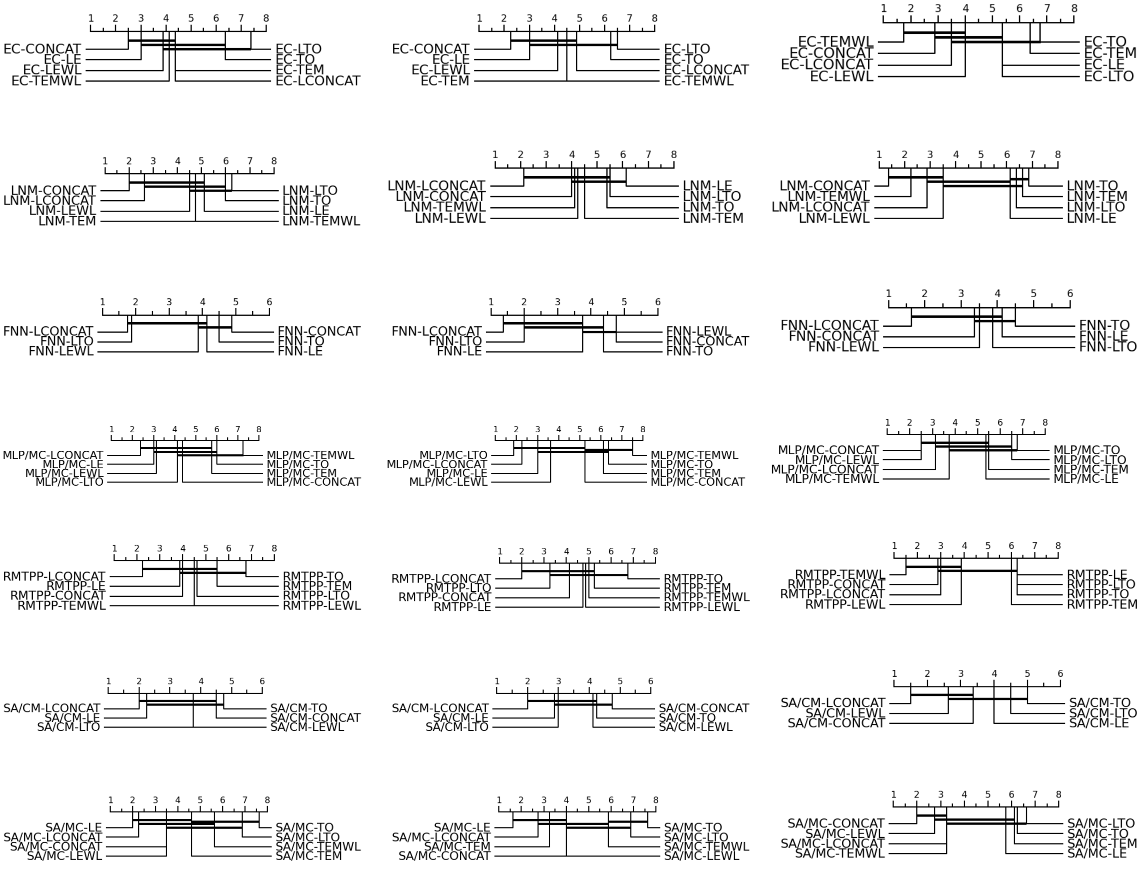

(1) NLL-T. (2) PCE. (3) NLL-M.

Figure 15: Critical Distance (CD) diagrams for the NLL-T, PCE and NLL-M at the $\alpha = 0.10$ significance level for all event encoding-decoder combinations of Table 4. The combinations' average ranks are displayed on top, and a bold line joins the combinations that are not statistically different.

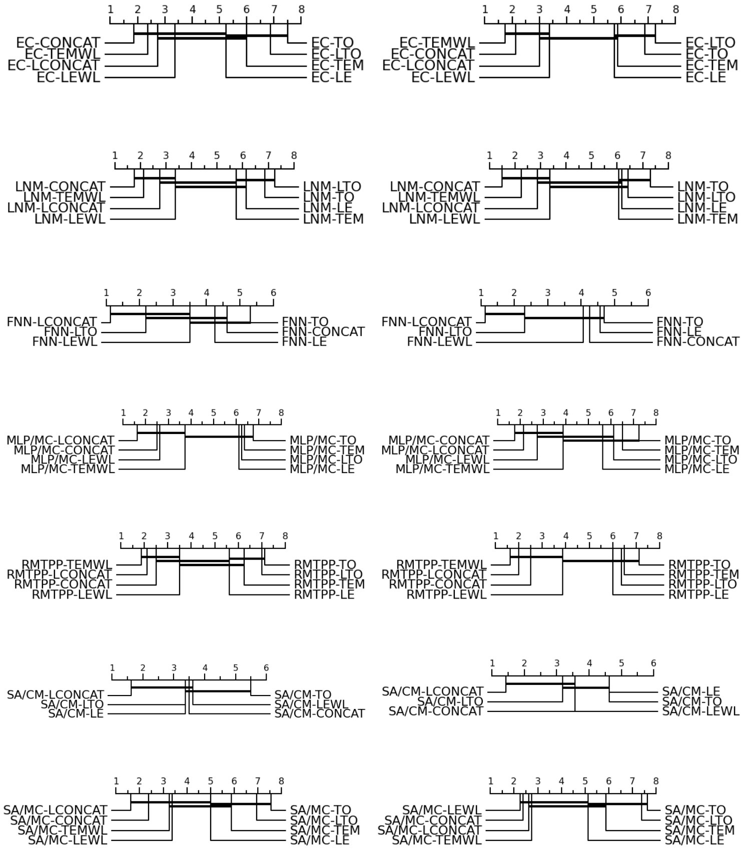

(1) ECE.

(2) F1-score.

Figure 16: Critical Distance (CD) diagrams for the ECE and F1-score at the $\alpha = 0.10$ significance level for all event encoding-decoder combinations of Table 4. The combinations' average ranks are displayed on top, and a bold line joins the combinations that are not statistically different.

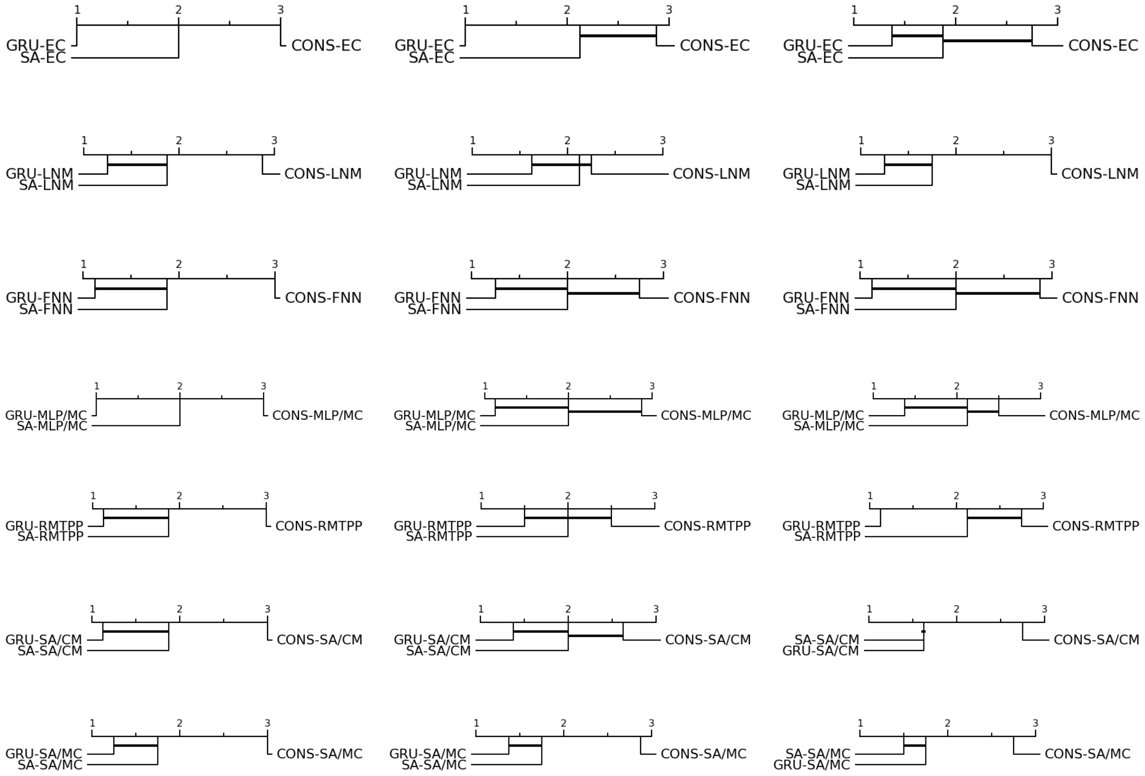

(1) NLL-T. (2) PCE. (3) NLL-M.

Figure 17: Critical Distance (CD) diagrams for the NLL-T, PCE and NLL-M at the $\alpha = 0.10$ significance level for all event history encoder-decoder combinations of Table 5. The combinations' average ranks are displayed on top, and a bold line joins the combinations that are not statistically different.

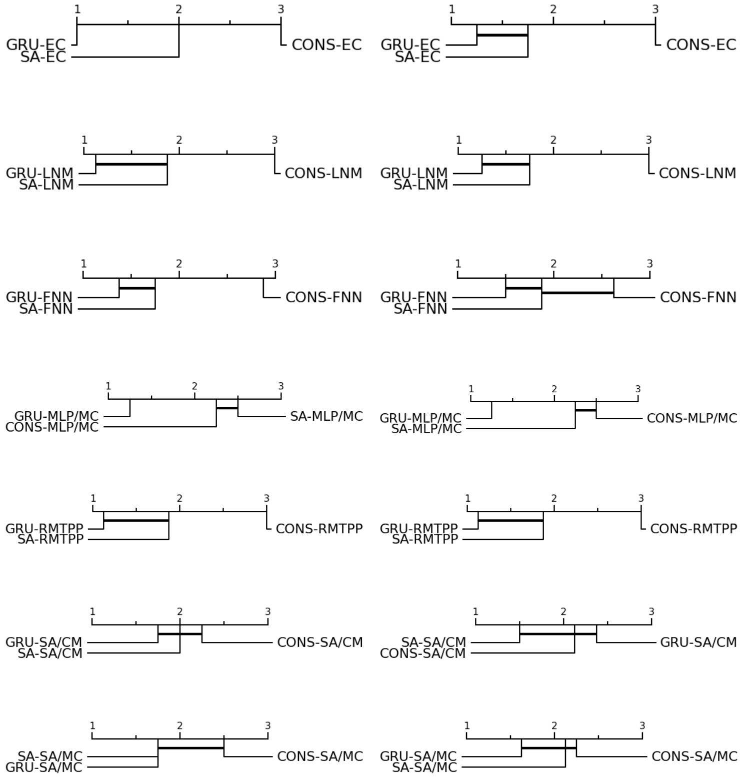

(1) ECE.   (2) F1-score.

Figure 18: Critical Distance (CD) diagrams for the ECE and F1-score at the $\alpha = 0.10$ significance level for all event history encoder-decoder combinations of Table 5. The combinations' average ranks are displayed on top, and a bold line joins the combinations that are not statistically different.

Table 21: Average and median scores, as well as average ranks per decoder and variation of event encoding, for relevant marked datasets. Refer to Section 5.5 for details on the aggregation procedure. Best results are highlighted in bold.

	Marked Datasets														
	NLL-T			PCE			NLL-M			ECE			F1-score		
	Mean	Median	Rank	Mean	Median	Rank	Mean	Median	Rank	Mean	Median	Rank	Mean	Median	Rank
EC-TO	0.59	0.56	6.5	0.2	0.23	6.25	0.19	0.21	6.5	0.44	0.44	7.12	0.19	0.17	6.88
EC-LTO	0.7	0.57	7.25	0.2	0.23	6.38	0.15	0.17	5.5	0.44	0.45	7.0	0.19	0.17	**7.25**
EC-CONCAT	0.13	0.14	**2.5**	**0.17**	**0.15**	**2.25**	-0.51	-0.75	2.75	0.34	0.31	**1.88**	**0.3**	0.28	2.12
EC-LCONCAT	0.36	0.29	4.25	0.19	0.2	4.75	-0.45	-0.66	3.5	0.34	0.3	2.75	0.28	0.27	2.88
EC-TEM	0.2	0.17	4.38	0.18	0.15	4.5	0.18	0.2	6.38	0.42	0.42	6.12	0.2	0.18	5.88
EC-TEMWL	1.48	0.3	4.25	0.19	0.17	4.88	**-0.67**	**-0.78**	**2.0**	**0.33**	**0.27**	2.38	0.3	**0.29**	1.88
EC-LE	**0.05**	**0.11**	3.0	0.18	0.15	2.88	0.15	0.15	5.38	0.41	0.42	5.38	0.2	0.18	5.75
EC-LEWL	0.17	0.19	3.88	0.18	0.15	4.12	-0.33	-0.59	4.0	0.35	0.35	3.38	0.29	0.28	3.38
LNM-TO	-0.95	-0.57	6.0	**0.02**	0.02	5.38	0.06	0.11	6.88	0.44	0.45	6.88	0.19	0.17	**7.62**
LNM-LTO	-0.58	-0.59	6.25	0.02	**0.01**	5.5	0.03	0.06	6.38	0.44	0.46	7.25	0.19	0.17	6.5
LNM-CONCAT	**-1.14**	**-0.98**	**2.0**	0.02	0.01	4.0	**-2.25**	-1.47	**1.38**	**0.25**	**0.21**	**1.75**	**0.39**	**0.35**	1.5
LNM-LCONCAT	-0.83	-0.83	2.62	0.02	0.01	**2.12**	-1.87	-1.18	2.88	0.29	0.25	2.75	0.34	0.31	2.88
LNM-TEM	-0.87	-0.79	4.75	0.02	0.01	4.5	0.03	0.05	6.62	0.42	0.44	5.75	0.2	0.18	6.0
LNM-TEMWL	-0.83	-0.87	4.75	0.03	0.02	4.12	-1.99	**-1.49**	2.25	0.28	0.25	2.12	0.36	0.32	2.25
LNM-LE	-1.11	-0.78	5.12	0.02	0.02	6.12	0.0	0.02	6.12	0.42	0.44	6.12	0.2	0.18	5.88
LNM-LEWL	-0.95	-0.92	4.5	0.02	0.01	4.25	-1.89	-1.18	3.5	0.3	0.28	3.38	0.32	0.29	3.38
FNN-TO	0.96	0.68	4.5	0.21	0.28	4.5	0.3	0.34	4.5	0.46	0.47	5.25	0.17	0.17	**5.25**
FNN-LTO	-0.32	-0.31	2.0	**0.03**	**0.02**	2.12	0.05	0.01	3.75	0.4	0.42	2.25	0.21	0.19	2.62
FNN-CONCAT	0.86	0.45	4.38	0.21	0.27	4.5	0.06	0.02	2.88	0.43	0.46	3.5	0.19	0.19	3.0
FNN-LCONCAT	**-0.57**	**-0.66**	**1.0**	0.03	0.02	**1.62**	**-0.99**	**-0.69**	**2.12**	**0.31**	**0.35**	**1.75**	**0.26**	**0.23**	1.38
FNN-LE	0.87	0.53	4.25	0.21	0.29	3.75	0.27	0.31	4.12	0.46	0.47	4.25	0.17	0.16	4.62
FNN-LEWL	0.95	0.41	4.88	0.21	0.29	4.5	0.14	0.12	3.62	0.45	0.46	4.0	0.18	0.18	4.12
MLP/MC-TO	0.11	0.22	6.0	0.16	0.16	6.38	0.36	0.33	6.75	0.41	0.4	6.75	0.2	0.18	**7.25**
MLP/MC-LTO	-0.16	-0.14	4.0	**0.09**	**0.06**	**1.88**	0.44	0.25	6.75	0.39	0.42	6.0	0.21	0.18	6.0
MLP/MC-CONCAT	0.0	0.06	4.88	0.16	0.13	5.62	-0.16	-0.26	**2.62**	0.33	0.34	3.38	0.28	**0.29**	3.12
MLP/MC-LCONCAT	**-0.34**	**-0.28**	**2.25**	0.09	0.07	2.0	-0.19	-0.42	3.25	**0.29**	0.28	**2.38**	0.28	0.28	2.88
MLP/MC-TEM	0.01	-0.01	5.5	0.15	0.13	5.75	0.26	0.23	5.5	0.4	0.41	6.38	0.2	0.18	6.5
MLP/MC-TEMWL	0.29	0.36	7.25	0.18	0.17	7.62	**-0.45**	**-0.45**	2.62	0.34	0.33	2.75	**0.3**	0.29	2.5
MLP/MC-LE	-0.2	-0.19	3.12	0.13	0.11	3.12	0.37	0.22	5.62	0.38	0.37	6.0	0.21	0.19	5.5
MLP/MC-LEWL	-0.18	-0.16	3.0	0.13	0.11	3.62	-0.42	-0.35	2.88	0.29	**0.26**	2.38	0.3	0.28	2.25
RMTPP-TO	0.15	0.23	6.75	0.16	0.16	6.75	0.11	0.12	6.25	0.42	0.43	7.12	0.19	0.18	**7.12**
RMTPP-LTO	-0.19	-0.19	4.62	0.06	0.05	3.25	0.09	0.07	6.25	0.42	0.42	7.0	0.19	0.18	6.38
RMTPP-CONCAT	-0.05	-0.05	4.0	0.15	0.12	4.12	-1.52	-1.28	2.88	0.26	0.24	2.5	0.35	0.33	2.5
RMTPP-LCONCAT	**-0.42**	**-0.34**	**2.25**	**0.04**	**0.04**	**2.0**	-1.65	**-1.51**	3.0	0.25	**0.21**	2.12	0.37	0.34	2.0
RMTPP-TEM	-0.01	0.01	5.5	0.15	0.12	5.25	0.1	0.15	6.0	0.41	0.41	6.25	0.21	0.19	6.5
RMTPP-TEMWL	0.0	0.05	4.5	0.15	0.14	5.0	**-2.1**	-1.42	**1.5**	**0.24**	0.21	**1.88**	**0.4**	**0.37**	1.62
RMTPP-LE	-0.14	0.01	3.88	0.15	0.13	4.75	0.12	0.14	6.25	0.4	0.41	5.62	0.21	0.19	6.0
RMTPP-LEWL	-0.03	-0.0	4.5	0.15	0.13	4.88	-1.19	-1.03	3.88	0.3	0.29	3.5	0.32	0.32	3.88
SA/CM-TO	10.78	0.12	4.75	0.11	0.06	4.12	1.14	0.31	4.75	0.45	0.46	5.12	0.14	0.1	**4.75**
SA/CM-LTO	20.39	-0.01	3.0	0.1	0.05	2.75	0.66	0.11	4.0	0.43	**0.44**	2.88	0.18	0.1	2.88
SA/CM-CONCAT	-0.08	-0.09	3.38	0.07	0.05	3.25	0.6	0.16	4.0	0.44	0.44	3.38	0.17	**0.17**	3.0
SA/CM-LCONCAT	20.53	0.05	4.12	0.12	0.06	3.62	0.61	0.08	**2.5**	0.43	0.45	3.25	0.18	0.11	3.0
SA/CM-LE	**-0.37**	**-0.4**	**2.0**	**0.05**	**0.04**	**2.38**	0.09	0.07	3.0	0.42	0.44	3.62	0.19	0.17	4.12
SA/CM-LEWL	2.14	-0.07	3.75	0.09	0.08	4.88	**-0.0**	**-0.01**	2.75	**0.41**	0.44	**2.75**	**0.2**	0.16	3.25
SA/MC-TO	1.22	1.0	7.38	0.23	0.31	6.75	0.24	0.31	5.12	0.47	0.47	7.12	0.17	0.16	**7.5**
SA/MC-LTO	1.07	0.82	5.75	0.22	0.29	5.88	0.28	0.4	6.25	0.46	0.47	6.0	0.17	0.16	6.38
SA/MC-CONCAT	0.64	0.85	6.5	0.19	0.17	6.25	0.1	0.2	5.0	0.44	0.47	6.25	0.2	0.17	5.88
SA/MC-LCONCAT	0.53	0.74	5.12	0.19	0.16	6.25	0.16	0.23	5.38	0.43	0.47	5.25	0.2	0.17	5.5
SA/MC-TEM	-0.42	-0.4	3.25	0.1	0.07	2.75	0.15	0.05	5.12	0.39	0.4	4.25	0.2	0.18	4.12
SA/MC-TEMWL	-0.28	-0.26	4.25	0.11	0.08	4.25	**-0.51**	**-0.34**	**1.88**	**0.32**	**0.32**	**1.88**	**0.28**	**0.25**	1.5
SA/MC-LE	**-0.76**	**-0.52**	**1.62**	**0.07**	**0.04**	**1.5**	0.11	-0.03	4.88	0.37	0.38	3.38	0.21	0.19	3.38
SA/MC-LEWL	-0.48	-0.45	2.12	0.08	0.07	2.38	-0.29	-0.23	2.38	0.34	0.32	1.88	0.25	0.24	1.75

Table 22: Average and median scores, as well as average ranks per decoder and variation of history encoder, for relevant marked datasets. Refer to Section 5.5 for details on the aggregation procedure. Best results are highlighted in bold.

	Marked Datasets														
	NLL-T			PCE			NLL-M			ECE			F1-score		
	Mean	Median	Rank	Mean	Median	Rank	Mean	Median	Rank	Mean	Median	Rank	Mean	Median	Rank
CONS-EC	1.74	1.34	3.0	0.3	0.35	2.83	0.63	0.56	2.67	0.48	0.49	3.0	0.14	0.06	3.0
SA-EC	0.73	0.63	2.0	0.25	0.27	2.17	0.04	-0.04	2.0	0.43	0.42	2.0	0.2	0.15	1.83
GRU-EC	**0.19**	**0.14**	**1.0**	**0.22**	**0.23**	**1.0**	**-0.17**	**-0.29**	**1.33**	**0.39**	**0.38**	**1.0**	**0.22**	**0.17**	**1.17**
CONS-LNM	-0.35	-0.44	2.83	**0.02**	0.02	2.33	0.58	0.43	3.0	0.48	0.49	3.0	0.14	0.06	3.0
SA-LNM	-0.61	-0.68	1.83	0.02	0.02	2.17	-0.63	-0.39	1.83	0.39	0.39	1.83	0.24	0.17	1.83
GRU-LNM	**-0.8**	**-0.83**	**1.33**	0.03	**0.01**	**1.5**	**-1.11**	**-0.83**	**1.17**	**0.35**	**0.37**	**1.17**	**0.26**	**0.2**	**1.17**
CONS-FNN	1.02	0.72	3.0	0.2	0.24	2.67	0.5	0.25	2.83	0.46	0.46	2.83	0.17	**0.11**	2.5
SA-FNN	0.78	0.53	1.83	0.19	0.23	2.0	0.05	0.06	2.17	0.45	0.45	1.83	**0.18**	0.11	2.0
GRU-FNN	**0.52**	**0.13**	**1.17**	**0.18**	**0.21**	**1.33**	**-0.17**	**-0.04**	**1.0**	**0.42**	**0.44**	**1.33**	0.18	0.11	**1.5**
CONS-MLP/MC	0.5	0.52	3.0	0.19	0.23	2.83	0.4	0.3	2.33	0.39	0.4	2.0	0.22	0.17	2.33
SA-MLP/MC	0.13	0.13	2.0	0.17	0.21	2.0	0.04	-0.02	2.33	0.38	0.39	2.67	0.22	0.17	2.33
GRU-MLP/MC	**-0.15**	**-0.14**	**1.0**	**0.16**	**0.18**	**1.17**	**-0.03**	**-0.26**	**1.33**	**0.35**	**0.37**	**1.33**	**0.23**	**0.18**	**1.33**
CONS-RMTPP	0.87	0.66	3.0	0.18	0.21	2.33	0.97	0.65	2.67	0.47	0.48	3.0	0.13	0.05	3.0
SA-RMTPP	0.13	0.17	1.83	0.17	0.19	2.17	-0.38	-0.36	2.17	0.38	0.39	1.83	0.24	0.18	1.83
GRU-RMTPP	**-0.15**	**-0.17**	**1.17**	**0.15**	**0.17**	**1.5**	**-0.95**	**-0.66**	**1.17**	**0.34**	**0.37**	**1.17**	**0.26**	**0.22**	**1.17**
CONS-SA/CM	0.01	-0.06	3.0	0.1	0.12	2.83	0.51	0.36	2.67	**0.44**	**0.44**	2.17	**0.18**	**0.11**	2.17
SA-SA/CM	-0.17	-0.2	1.83	0.08	**0.08**	1.83	**0.12**	0.09	**1.5**	0.44	0.44	**1.83**	0.18	0.11	**1.17**
GRU-SA/CM	**-0.22**	**-0.22**	**1.17**	**0.07**	0.08	**1.33**	0.12	**0.07**	1.83	0.44	0.44	2.0	0.18	0.11	2.67
CONS-SA/MC	0.44	0.2	3.0	0.18	0.19	2.83	0.42	0.28	2.67	0.41	**0.41**	2.33	**0.2**	**0.13**	2.0
SA-SA/MC	0.07	0.03	1.67	**0.16**	**0.16**	1.83	-0.05	**-0.16**	**1.5**	**0.39**	0.41	**1.67**	0.19	0.12	2.33
GRU-SA/MC	**0.05**	**-0.04**	**1.33**	0.16	0.16	**1.33**	**-0.1**	-0.16	1.83	0.39	0.42	2.0	0.2	0.12	**1.67**

Table 23: Average and median scores, and average ranks of the best combinations per decoder on the NLL-T (top rows) and NLL-M (bottom row) across all relevant marked datasets. Best results are highlighted in bold.

	Marked Datasets														
	NLL-T			PCE			NLL-M			ECE			F1-score		
	Mean	Median	Rank	Mean	Median	Rank	Mean	Median	Rank	Mean	Median	Rank	Mean	Median	Rank
GRU-EC-LE	-0.22	-0.02	7.75	0.17	0.14	9.12	-0.1	-0.03	6.5	0.39	0.41	7.0	0.21	0.18	7.38
GRU-LNM-TO	**-1.44**	**-0.93**	**1.5**	**0.02**	**0.01**	**1.88**	-0.06	-0.07	6.5	0.41	0.42	6.75	0.21	0.18	7.12
GRU-LN-LEWL	-0.54	-0.56	5.25	0.07	0.04	5.75	-1.56	-1.38	2.75	0.28	0.28	4.5	0.33	0.35	2.88
GRU-FNN-LCONCAT	-0.6	-0.71	3.38	0.02	0.02	2.25	-1.57	-1.0	3.5	0.29	0.35	4.5	0.27	0.23	4.12
GRU-MLP/MC-LCONCAT	-0.42	-0.38	5.5	0.09	0.07	6.38	-0.47	-0.47	5.62	0.26	0.26	2.88	0.28	0.28	4.38
GRU-RMTPP-LCONCAT	-0.52	-0.41	4.75	0.04	0.03	4.88	-1.88	**-1.99**	**2.38**	0.22	0.15	2.88	0.4	0.35	1.62
GRU-SA/CM-LE	-0.46	-0.42	6.12	0.05	0.03	3.75	0.1	0.07	7.75	0.43	0.45	8.12	0.19	0.18	8.75
GRU-SA/MC-LE	-0.85	-0.55	3.88	0.08	0.05	4.88	0.08	-0.04	7.62	0.35	0.37	6.5	0.21	0.2	6.62
Hawkes	1.21	-0.15	7.62	0.11	0.1	6.5	**-3.42**	-1.01	4.12	**0.15**	**0.13**	**2.12**	**0.45**	**0.43**	2.38
Poisson	1.86	1.35	10.75	0.25	0.34	10.25	2.23	1.26	10.75	0.48	0.48	10.5	0.16	0.15	10.75
NH	1.32	1.07	9.5	0.24	0.32	10.38	0.25	0.41	8.5	0.48	0.47	10.25	0.17	0.16	10.75
GRU-EC-TEMWL	0.16	0.16	8.12	0.18	0.16	8.75	-1.42	-1.1	5.12	0.29	0.24	5.88	0.3	0.3	6.12
GRU-LNM-CONCAT	**-1.41**	**-1.0**	**1.25**	**0.02**	**0.01**	**1.62**	-2.62	-1.76	2.5	0.23	0.18	4.0	0.38	0.34	3.0
GRU-LN-CONCAT	-0.51	-0.57	4.25	0.07	0.04	4.88	-2.59	-1.81	3.12	0.25	0.25	4.5	0.33	0.34	4.38
GRU-FNN-LCONCAT	-0.6	-0.71	3.0	0.02	0.02	2.25	-1.57	-1.0	5.25	0.29	0.35	4.88	0.27	0.23	5.0
GRU-MLP/MC-LEWL	-0.32	-0.28	5.25	0.13	0.11	5.62	-0.65	-0.7	7.0	0.26	0.22	5.0	0.3	0.29	5.38
GRU-RMTPP-TEMWL + B	-0.19	-0.11	6.25	0.14	0.11	6.38	-2.67	**-1.85**	**2.38**	0.2	0.16	3.0	0.42	0.42	2.62
GRU-SA/CM-LEWL	-0.23	-0.23	5.75	0.08	0.07	5.25	-0.18	-0.11	8.25	0.41	0.43	8.5	0.21	0.2	9.0
GRU-SA/MC-TEMWL	-0.29	-0.3	5.12	0.11	0.09	5.38	-0.55	-0.55	7.25	0.31	0.31	6.62	0.28	0.26	6.5
Hawkes	1.21	-0.15	6.88	0.11	0.1	5.12	**-3.42**	-1.01	5.25	**0.15**	**0.13**	**2.88**	**0.45**	**0.43**	3.12
Poisson	1.86	1.35	10.75	0.25	0.34	10.38	2.23	1.26	10.88	0.48	0.48	10.5	0.16	0.15	10.75
NH	1.32	1.07	9.38	0.24	0.32	10.38	0.25	0.41	9.0	0.48	0.47	10.25	0.17	0.16	10.88